[redacted]

[redacted]

NATIONAL ADVISORY COMMITTEE FOR AERONAUTICS

WARTIME REPORT

ORIGINALLY ISSUED
March 1946 as
Memorandum Report L6C13

TESTS OF A 1/7-SCALE POWERED MODEL OF THE KAISER TAILLESS AIRPLANE IN THE LANGLEY FULL-SCALE TUNNEL

By C. W. Brewer and E. A. Rickey

Langley Memorial Aeronautical Laboratory
Langley Field, Va.

NACA

WASHINGTON

NACA LANGLEY MEMORIAL AERONAUTICAL LABORATORY

MEMORANDUM REPORT

for the

Bureau of Aeronautics, Navy Department

MR No. L6C13

TESTS OF A 1/7-SCALE POWERED MODEL OF THE KAISER TAILLESS AIRPLANE IN THE LANGLEY FULL-SCALE TUNNEL

By G. W. Brewer and E. A. Rickey

SUMMARY

A 1/7-scale powered model of the Kaiser tailless airplane has been investigated in the Langley full-scale tunnel in order to determine its general aerodynamic characteristics and to estimate, from these results, the probable stability and control characteristics of the airplane. The results of the tests are presented in this report. The estimated flying qualities of the Kaiser tailless airplane, determined from the 1/7-scale test results, are to be presented in a separate report.

The maximum lift coefficient with the propellers windmilling and controls neutral was measured to be 1.07; this value of $C_{L_{max}}$ is decreased to 0.98 for the maximum up-elevator deflection of 30°. The wing stalls first along the trailing edge and progresses forward along a constant chord line enveloping the outer panels before the center section is materially affected. The profile drag coefficient, with propellers removed, is estimated to be 0.0130 with the model at approximately the zero-lift attitude.

The pitching-moment results indicate that, for the center-of-gravity location of 20 percent of the mean aerodynamic chord, the model is statically stable longitudinally for all power conditions except for windmilling-propeller operation at high angles of attack.

The yawing-moment test results show that the rudder effectiveness and directional stability parameters are lower for this tailless airplane than for most conventional designs.

For aileron deflections above 12° the effectiveness parameter is lower than that for the smaller deflections. The combined effects of aileron and wing stall at the high angles of attack produce a serious loss in aileron effectiveness.

INTRODUCTION

An investigation of a 1/7-scale powered model of the Kaiser tailless airplane has been conducted in the Langley full-scale tunnel at the request of the Bureau of Aeronautics, Navy Department. Previous tests made of a 1/60-scale model in the Langley free-flight tunnel indicated satisfactory stability and control characteristics. It was considered desirable, however, to determine the aerodynamic characteristics of the design with special reference to stability and control at a larger scale and to estimate from these data the flying qualities of the airplane.

This report presents the results of the tests showing the aerodynamic characteristics of the model for a wide range of propeller-operating conditions. The effects of elevator, rudder, and aileron deflection on the model forces and moments and on the control-surface hinge moments were obtained with angle of attack, angle of yaw, and power condition being the important variable parameters. Additional tests included an investigation of the progression of the stall over the wing as well as the determination of the wing profile drag by means of wake profile surveys.

On the basis of the model test results, estimates of the flying qualities of the airplane are being made, and this information is to be presented in a subsequent report.

COEFFICIENTS AND SYMBOLS

The test data are presented as standard NACA coefficients of forces and moments. All data are referred to the stability axes which are defined as a system of axes having their origin at the center of gravity. The Z axis is in the plane of symmetry and perpendicular to the relative wind, the X axis is in the plane of symmetry and perpendicular to the Z axis, and the Y axis is perpendicular to the plane of symmetry. The positive direction of forces and moments and control-surface deflections are shown in the sketch of figure 1.

C_L lift coefficient (Lift/qS)

C_X longitudinal-force coefficient (X/qS)

C_Y lateral-force coefficient (Y/qS)

C_l rolling-moment coefficient (L/qSb)

C_n yawing-moment coefficient (N/qSb)

C_m pitching-moment coefficient (M/qSc)

C_{h_a} aileron hinge-moment coefficient $\left(H_a/qb_a\bar{c}_a^{\,2}\right)$

C_{h_e} elevator hinge-moment coefficient $\left(H_e/qb_e\bar{c}_e^{\,2}\right)$

C_{h_r} rudder hinge-moment coefficient $\left(H_r/qb_r\bar{c}_r^{\,2}\right)$

c_{d_o} section profile-drag coefficient

T_c' effective-thrust coefficient $\left(T_e/qS\right)$

V/nD propeller advance-diameter ratio

$\dfrac{dC_l}{d\delta_a}$ rate of change of rolling-moment coefficient with aileron deflection

$\dfrac{dC_{h_a}}{d\delta_a}$ rate of change of aileron hinge-moment coefficient with aileron deflection

$\frac{dC_m}{d\delta_e}$ rate of change of pitching-moment coefficient with elevator deflection

$\frac{dC_{h_e}}{d\delta_e}$ rate of change of elevator hinge-moment coefficient with elevator deflection

$\frac{dC_n}{d\delta_r}$ rate of change of yawing-moment coefficient with rudder deflection

$\frac{dC_Y}{d\delta_r}$ rate of change of lateral-force coefficient with rudder deflection

$\frac{dC_{h_r}}{d\delta_r}$ rate of change of rudder hinge-moment coefficient with rudder deflection

$\frac{dC_n}{d\psi}$ rate of change of yawing-moment coefficient with angle of yaw

$\frac{dC_l}{d\psi}$ rate of change of rolling-moment coefficient with angle of yaw

$\frac{dC_Y}{d\psi}$ rate of change of lateral-force coefficient with angle of yaw

where

$\left.\begin{matrix}X\\Y\\Z\end{matrix}\right\}$ force along axes (where $Z = -\text{lift}$)

$\left.\begin{matrix}L\\M\\N\end{matrix}\right\}$ moment about axes

H_a aileron hinge moment

H_e elevator hinge moment

H_r rudder hinge moment

T_e	effective thrust of all propellers $(X - X_o)$ (subscript o refers to propellers removed)
q	dynamic pressure $\left(\frac{1}{2}\rho V^2\right)$
S	wing area (161.6 sq ft)
b	wing span (41.4 ft)
c	mean aerodynamic chord (3.9 ft)
b_a	aileron span (12.86 ft)
b_e	elevator span (6.88 ft)
b_r	rudder span (2.99 ft)
$\overline{c}_a$	root-mean-square aileron chord (0.463 ft)
$\overline{c}_e$	root-mean-square elevator chord (0.571 ft)
$\overline{c}_r$	root-mean-square rudder chord (0.432 ft)
V	free-stream velocity
W	airplane weight
ρ	mass density of air
n	propeller rotational speed
D	propeller diameter (2.167 ft)

and

α	angle of attack of the thrust axis, degrees, relative to the free-stream direction
ψ	angle of yaw, degrees
δ_a	aileron deflection, degrees
δ_e	elevator deflection, degrees
δ_r	rudder deflection, degrees

DESCRIPTION OF AIRPLANE AND MODEL

The Kaiser tailless airplane is a projected all-wing type cargo-carrying airplane. This airplane will have a span of 290 feet, a wing area of 7920 square feet, and a design gross weight of 175,000 pounds. It is to be powered with four engines of tractor installation driving 15-foot-diameter four-blade propellers. The important physical and dimensional characteristics of the airplane based on model design are presented in table I. The design of the airplane provides for distribution of the cargo spanwise in the wing along the 20-percent chord line, thus fixing the center of gravity approximately at this location for all flight conditions.

The 1/7-scale model of the Kaiser tailless airplane, as tested in the Langley full-scale tunnel, is shown in the photographs of figure 2. A three-view drawing of the model is given in figure 3. The model, which was supplied by Kaiser Cargo, Inc., is of all-wood construction. The wing and control surfaces were painted and sanded to remove as many of the contour irregularities as possible prior to the tests. The wing consists of two highly tapered outer panels attached to a constant chord, 0.21 span, center section. The airfoil sections are modified NACA 6-series type with the rear 15 percent of the trailing edge reflexed upward along the entire span. A drawing of a typical wing cross section is shown in figure 4.

The control surfaces are constructed of solid mahogany and include a constant-percent-chord aileron on the left outer panel, a constant-chord elevator at the center section, and four vertical surfaces each located on a nacelle center line with the rudder hinge line located slightly behind the elevator trailing edge. The location of the four vertical surfaces required that the elevator flap be divided into five separate sections; these sections, however, were operated in unison. The blunt-nose plain-flap type control surfaces were not sealed. The control surfaces were not equipped with trimming tabs. The general arrangement of the control surfaces are shown by the three-view drawing of figure 3 and sectional views of the surfaces are given in figure 5. The control linkages projected outside the skin line on the model, and in order to minimize the drag of these protuberances, they were covered by streamline fairings. Photographs of the fairings on the model are given in figures 6 and 7.

The model was powered by four 56-horsepower, three-phase induction motors which were located within the wing at the center section. Power to the four-blade model propellers of right-hand rotation was transmitted from these motors by direct drive through extension shafts. The model was not equipped with landing gear and the nacelles had no cowl flaps or internal ducting.

METHODS AND TESTS

The 1/7-scale model of the Kaiser tailless airplane is shown mounted for tests on the Langley full-scale tunnel balance in figure 2. The model was supported by the two main front struts and by two rear cables in tension which were the means for changing the angle of attack of the model. The full-scale tunnel and balance equipment used for the tests are described in reference 1.

To simulate the flight thrust-lift relationship in the wind tunnel, a thrust calibration of the model propellers was made at a tunnel airspeed of about 60 miles per hour with the model at the zero-lift attitude and with all controls neutral. The propeller blade angle was maintained at constant setting of 17° at the 0.75 radius. The effective thrust coefficient T_c' for the model propellers was obtained from the difference between the propellers-operating and the propellers-removed drag coefficients. The flight thrust-lift and torque-lift curves for a single propeller and for constant power operation at sea level are presented in figure 8. The thrust-lift variation was duplicated exactly by the use of the model propeller blade angle of 17°, but the torque-lift variation was not in close agreement.

The tests of the 1/7-scale model consisted primarily of elevator-, rudder-, and aileron-effectiveness tests at zero yaw. Rudder and aileron tests were also made with the model yawed to angles of approximately 3°, ±6°, ±10°, and 15°. Elevator, rudder, and aileron hinge moments were obtained at zero yaw but only rudder hinge moments were obtained for tests with the model yawed. In addition, tests were made to determine the lift, drag, and stalling characteristics of the model.

In order to facilitate the presentation of the test conditions and model configurations, the information concerning the several investigations is outlined in some detail in table II. The specific information not given in this table is included in the following discussion.

The stalling characteristics of the model were obtained by visual observation and photographic record of the behaviour of wool tufts attached to the upper skin surfaces and to vertical masts dispersed at several different chordwise stations along the span.

The wing and section profile-drag coefficients were obtained by measuring the wing wake at a distance of 0.25c behind the trailing edge at numerous stations along the span. The methods of analyzing the results of pressure surveys to obtain profile-drag coefficients are presented in reference 2.

Inasmuch as elevator deflection caused appreciable changes in lift at a given angle of attack, it was not feasible to run constant power elevator tests. The propeller-operating elevator tests were made, therefore, by the constant-thrust method in which several values of T_c' are maintained constant over the range of elevator deflections tested at a given angle of attack. A sufficient number of thrust coefficients were used to bracket the constant power thrust-lift curves given in figure 8.

The rudder tests were made for the propellers-windmilling, the normal-rated, the military-rated, and the asymmetric power conditions. Tests with asymmetric power consisted of three-engine operation at normal-power with the right outboard propeller windmilling. Since the effect of rudder deflection on the lift of the model was negligible and since the lift coefficient at a given angle of attack did not vary appreciably with angle of yaw, the constant power T_c' versus C_L curves used for zero yaw were employed for all rudder tests throughout the range of yaw angles tested.

It was assumed that the propeller slipstream did not affect the air flow in the region of the aileron. At zero angle of yaw the aileron tests were made with propellers removed, whereas for tests with the model yawed, the propellers were windmilling.

The elevator-, rudder-, and aileron-effectiveness and hinge-moment tests and most of the maximum lift tests were made at a tunnel airspeed of about 61 miles per hour, corresponding to a Reynolds number at standard conditions of about 2,230,000 based on the mean aerodynamic chord.

PRESENTATION OF RESULTS

The data are presented for the most part as variations of force, moment, and hinge-moment coefficients with control-surface deflection for a range of angle of attack at a given angle of yaw. In some instances, cross plots of the test results are given to show specific trends of the data with reference to the stability and control characteristics of the model. Tabulation of the values of force coefficients and the slopes of the force and moment coefficient curves are included for convenient summarization of the data. The results are included in the following sections: (1) lift, stall, and drag, (2) elevator effectiveness and hinge moments, (3) rudder effectiveness and hinge moments, (4) aileron effectiveness and hinge moments, and (5) aerodynamic characteristics in yaw.

All data presented in the report have been corrected for tares and for wind-tunnel blocking and jet-boundary effects by the methods presented in references 3 and 4. The pitching moments are based on the mean aerodynamic chord and all moments are computed about a center of gravity located at 20 percent of the mean aerodynamic chord and on the thrust line.

Lift, Stall, and Drag

Lift.- The aerodynamic characteristics of the model with propellers windmilling are given in figure 9 for elevator deflections of 10°, 0°, -15°, and -30°. The effects of propeller operation, Reynolds number, and angle of yaw on the aerodynamic characteristics of the model with all controls neutral are shown in figures 10, 11, and 12, respectively. For most of the conditions given above, values of the maximum lift coefficient and the slope of the lift curves are summarized in table III. The lift curve slopes were measured at lift coefficients of 0.2 and 0.6 which correspond to approximately high speed and cruising lift coefficients, respectively.

The maximum lift coefficient, controls neutral, with propellers windmilling is about 1.07. For maximum up-elevator deflection ($\delta_e = -30^\circ$) the maximum lift coefficient is decreased to approximately 0.98. The results of figure 9 show fairly large changes in lift resulting from deflection of the elevator of this tailless airplane design. Although the following condition is not a trim condition for high power at high lift, it is shown that for the normal-rated power condition $C_{L_{max}}$ is increased to about 1.20.

The slopes of the lift curve, for the propellers-windmilling and controls-neutral condition, are approximately 0.084 and 0.079 per degree for lift coefficients of 0.2 and 0.6, respectively. With the elevators deflected up 30° these values are changed to approximately 0.087 and 0.073, respectively. The combined effects of the normal force of the inclined propellers and the increase in lift resulting from the additional velocity over the center section of the wing produces an increase in the slope of the lift curve to about 0.097 at $C_L = 0.2$ and 0.098 at $C_L = 0.6$ for propeller operation at normal rated power.

For the range of airspeeds tested, the scale effect on the lift of the model is negligible for lift coefficients below 0.5. At lift coefficients greater than this, however, there is shown some increase in lift with increased Reynolds number, at least to 2,560,000 which corresponds to the test airspeed of 70 miles per hour. The effects on lift of yawing the model are not large for the yaw angle range tested except that, for an angle of yaw of 15.4°, there is shown an increase in the slope of the lift curve at high lift coefficients.

Stall.- The results of tuft tests made to determine the progression of wing stall are shown by the sketches of tuft studies in figure 13 and by the photographs in figure 14. The first departure from smooth stream flow over the wing is shown by the pronounced inflow which occurs along the trailing edge of the outer panels at an angle of attack of about 9° ($C_L \approx 0.7$). With increased angle of attack this inflow becomes more severe and disturbed with separation occurring at an angle of attack of about 13°. At this attitude, the aftmost vertical mast located about midspan at 0.75c showed very turbulent airflow extending in depth to about 5 inches above the wing skin line.

The wing stall progressed forward approximately along a constant chord line of the outer panels as the angle of attack was further increased and, when the outer panels were stalled ($\alpha = 19.5^{\circ}$), the flow at the wing center section was relatively undisturbed. The restriction of the pattern of flow breakdown primarily to the outer panels is attributed to higher velocity air flow in the region of the vertical surfaces and to the restriction of the inflow from the outer panels by the two outer vertical surfaces. Propeller operation at high thrust coefficients had little effect on the stalling characteristics of the outboard panels, but the slipstream did retard the tendency for trailing-edge separation at the center section at high angles of attack. The force test results of a maximum lift investigation (fig. 15) shows nearly a constant value of maximum lift coefficient over a range of angle of attack and then a gradual loss in lift at the angles of attack past $C_{L_{max}}$.

Profile drag.- The results of the wake-survey measurements made to obtain an estimate of the model profile-drag coefficient are presented in figure 16 as the variation of the product of the section-drag coefficient and section chord $c_{d_o}c$ with spanwise station. Similar results are given in figure 17 for the survey made behind one vertical surface. Several local increases in c_{d_o} along the wing span are shown to be produced by the wakes from the fairings used to cover the control-surface push rods and hinge brackets. There is also evidence of interference and a drag increase at the base of the vertical surface caused by the control fairing (fig. 17). The total profile-drag coefficient of the model, with propellers removed, as obtained by the momentum method is estimated to be about 0.0130. The complete influence of the nacelles on the air flow at the center section and other local disturbances are believed not to be included in this estimate.

Elevator Effectiveness and Hinge Moments

The results of tests made to determine the effectiveness of the elevator and the elevator hinge moments with the propellers windmilling and operating at various thrust conditions are shown in figures 18 through 21. These data are presented as variations of C_L, C_X, C_m, and C_{h_e} with elevator deflection for several thrust coefficients at a given angle of attack. The values of the rate of change of pitching-moment and elevator hinge-moment coefficients with elevator deflection $dC_m/d\delta_e$ and $dC_{h_e}/d\delta_e$, and elevator hinge-moment coefficient with angle of attack, $dC_{h_e}/d\alpha$ measured at $\delta_e = 0$, are given in table IV for the windmilling propeller and for the normal- and military-rated power conditions. With the propellers windmilling, $dC_m/d\delta_e$ is about -0.0025 per degree in the angle-of-attack range from 2.4° to 8.8°.

The reduction of the effectiveness parameter to -0.0016 at higher angles of attack is due mainly to separation over the region of the elevator. The elevator effectiveness is materially increased for the high power conditions. With military-rated power, $dC_m/d\delta_e$ is -0.0034 at $\alpha = 2.4°$ and -0.0060 at $\alpha = 12.7°$.

Similar effects of propeller operation are shown for the hinge-moment parameter, $dC_{h_e}/d\delta_e$, which increases from about -0.0067 to -0.0105 per degree at $\alpha = 2.4°$ and from about -0.0070 to -0.0200 at $\alpha = 16.5°$ as a result of changing from windmilling propellers to military-rated power.

With the propellers windmilling, $dC_{h_e}/d\alpha$ is negative for all angles of attack and decreases from -0.0032 per degree at $\alpha = 2.4°$ to -0.0025 at $\alpha = 16.5°$. However, for propeller operation at normal-rated power there is a marked change in the variation of $dC_{h_e}/d\alpha$ as the angle of attack is increased. The hinge-moment parameter is about -0.0040 per degree at $\alpha = 2.4°$, 0.0060 at $\alpha = 6.0°$, and zero at $\alpha = 16.5°$. The values for military-rated power are similar to the normal-rated power condition and show the same variation with angle of attack.

The test data have been cross-plotted in figures 22 and 23 to show the variation of C_m with C_L, elevator fixed and free, for the windmilling propeller and for the constant normal- and military-rated power conditions. The static longitudinal stability of the model, elevator fixed, as measured by the slope of the pitching-moment curve, dC_m/dC_L (fig. 22), is not materially affected by propeller operation at the lower lift coefficients. The average slope of the pitching-moment curve, for $\delta_e = 0^\circ$, between lift coefficients of about 0.2 and 0.8 is approximately -0.1 for all power conditions. There is a noticeable increase in the static longitudinal stability due to propeller operation at the higher lift coefficients that probably results from the improved flow conditions at the wing center section. Elevator-free static longitudinal stability is shown by the stable slope of the pitching-moment curves for $C_{h_e} = 0$ in figure 23. The reduced slope of the curve for the windmilling-propeller condition at the higher lift coefficients indicates a decrease in the stick-free stability at low flight speeds.

Rudder Effectiveness and Hinge Moments

The effects of rudder deflection at zero yaw on the aerodynamic characteristics of the model and on the rudder hinge moments are presented in figures 24 and 25 for the four power conditions listed in table II. For purposes of comparison, these data are summarized in table V by the slopes of the yawing-moment, lateral-force, and hinge-moment coefficient curves measured at $\delta_r = 0^\circ$. The results of the rudder tests made at angles of yaw of 3°, $\pm6^\circ$, $\pm10^\circ$, and 15° were found to give no appreciable variations in effectiveness from the zero-yaw data. Curves showing these test results therefore have not been presented; however, summary curves showing the variations of $dC_n/d\delta_r$, $dC_Y/d\delta_r$, and $dC_{h_r}/d\delta_r$ with angle of yaw are presented in figure 26 and the values of C_n, C_Y, and C_{h_r} measured at $\delta_r = 0^\circ$ are given in table VI.

It is shown that the effectiveness of the rudder $(dC_n/d\delta_r)$ is lower for this tailless airplane than normally found for a conventional design, but the side-force variation $(dC_Y/d\delta_r)$ is shown to be normal. The rudder parameters are increased, as expected, by propeller operation. For the condition with windmilling propellers $dC_n/d\delta_r$ is -0.00024, $dC_Y/d\delta_r$ is 0.0025, and $dC_{h_r}/d\delta_r$ is -0.0050, per degree at $\alpha = 4.2^\circ$ and these values are not materially changed throughout the angle-of-attack range. In comparison, for the normal-rated power condition, $dC_n/d\delta_r$ is -0.00030, $dC_Y/d\delta_r$ is 0.0031, and $dC_{h_r}/d\delta_r$ is -0.0054 per degree at $\alpha = 4.2^\circ$ and these values increase to -0.00043, 0.0042, and -0.0089, respectively, at an angle of attack of 12.4°. The results of figure 26 show in general relatively small changes throughout the range of yaw angles tested of these values given for zero yaw.

Aileron Effectiveness and Hinge Moments

The results of the aileron effectiveness and hinge-moment tests made for a range of angle of attack from 2.4° to 16.4° with the model at zero yaw are presented in figure 27. The data obtained at angles of yaw of about ±6°, ±10°, and 15° for angles of attack of 2.4°, 6.1°, and 12.6° are given in figure 28. The slopes of the rolling-moment and hinge-moment coefficient curves, for $\delta a_L = 0^\circ$, are presented in table VII. There is an increment of rolling-moment coefficient shown in the curves of figure 27 for zero aileron deflection with the model at zero yaw. Inasmuch as the model is considered a symmetrical configuration with the propellers removed, the increment in rolling-moment coefficient is believed caused by unsymmetrical tunnel air flow along the span of the wing, and perhaps by some dissymmetry in the model itself.

The aileron effectiveness, $dC_l/d\delta a_L$, for a single aileron, measured at $\delta a_L = 0^\circ$, is about 0.0021 per degree at $\alpha = 2.4^\circ$ and decreases to about 0.0015 at $\alpha = 16.4^\circ$. The loss in aileron effectiveness with increasing angle of attack is probably associated with the wing trailing-edge stall mentioned in an earlier section of this report. It is noted that for aileron deflections above 12° the effectiveness parameter is nearly one-half that for small aileron deflections in the low angle-of-attack range. The value of $dC_l/d\delta a_L$ for deflections greater than 12° is continuously decreased as the angles of attack are increased, such that $dC_l/d\delta a_L$ is reduced to 0 at $\alpha = 12.6^\circ$ and then becomes a negative value at greater angles of attack. This rapid loss in control effectiveness occurring at the high aileron deflections is attributed to the combined effects of control surface stall and trailing-edge separation.

The value of $dC_{h_a}/d\delta_{a_L}$ at an α of 2.4° is about -0.0100 per degree and decreases to about -0.0059 at an angle of attack of 16.4°. The effect of yawing the model to an angle of 15.4° is to reduce $dC_l/d\delta_a$ by approximately 0.0003.

The yawing-moment coefficient resulting from aileron deflection is in general small for this tailless airplane except for the maximum deflection of the ailerons at high angles of attack.

Aerodynamic Characteristics in Yaw

For the determination of the characteristics of the model in yaw, the results of the rudder tests have been cross-plotted against angle of yaw for rudder-fixed and rudder-free conditions. The variations of C_n, C_Y, and C_l with angle of yaw, measured for $\delta_r = 0^{\circ}$, are presented in figure 29 for all propeller-operating conditions. Similar data, measured at $C_{h_r} = 0$, are given in figure 30. The variation of lift coefficient with angle of yaw is shown for all conditions tested in figure 31. A summary showing the slopes of the yawing-moment, rolling-moment, and lateral-force coefficient curves, measured at $\psi = 0^{\circ}$, is presented in table VIII. The rudder-free characteristics are not summarized in table VIII, but are essentially the same as the rudder-fixed results.

The directional stability parameter $dC_n/d\psi$ is approximately -0.00045 per degree for the conditions tested which is about one-half the value generally desired for satisfactory directional stability characteristics (reference 5). There is, in general, little effect of propeller operation on the directional stability parameter except for the asymmetric power condition where there is a greater increase in $dC_n/d\psi$ with increased thrust coefficient. The dihedral effect is shown to be low in comparison with conventional airplane designs; the value of $dC_l/d\psi$, per degree, ranges from 0 to about 0.00032 for the angles of attack and power conditions tested. The effective dihedral angle, for most conditions, is estimated to be about 1°. The lateral force parameter, $dC_Y/d\psi$, per degree, is positive for all conditions tested and has values ranging from about 0.0045 for windmilling propellers at $\alpha = 6.1^{\circ}$ to about 0.0067 for normal-rated power at $\alpha = 10.6^{\circ}$.

A comparison of the yawing-moment coefficient curves of the normal-rated and the asymmetric power conditions in figure 29(b) and 29(d) shows that the reduction in power of the right outboard engine causes a considerable reduction in the negative yawing moment. The configuration of asymmetric power having the left outboard propeller windmilling and the remaining engines running at full power was not tested, but computations show that this type of propeller operation would produce about an equal amount of yawing moment in the opposite direction and therefore would be the most critical condition to trim directionally, especially at the low flight speeds.

SUMMARY OF RESULTS

The following results are summarized from the Langley full-scale tunnel tests of the 1/7-scale powered model of the Kaiser tailless airplane.

1. The maximum lift coefficient with propellers windmilling and controls neutral is about 1.07. This value of $C_{L_{max}}$ is decreased to 0.98 for the maximum up-elevator deflection of 30°.

2. Wing stall occurs first at the trailing edge of the outer panels and progresses forward approximately along a constant chord line. At an angle of attack of 19.5° the outer panels are nearly completely stalled; the flow at the center section of the wing, however, is relatively undisturbed at this angle.

3. The profile-drag coefficient of the model (propellers removed) as determined by the wake-survey momentum method, is estimated to be approximately 0.0130.

4. The elevator effectiveness, propellers windmilling, is essentially a constant value of -0.0025, per degree, at low and moderate angles of attack. At an angle of attack of 16.4° the elevator effectiveness is reduced to -0.0016. The effects of propeller operation at high thrust coefficients materially increases $dC_m/d\delta_e$ to about -0.0060 at $\alpha = 12.4°$. Similar effects of propeller operation are shown for the elevator-hinge-moment parameter, $dCh_e/d\delta_e$, which ranges from about -0.0067 (propellers windmilling at $\alpha = 2.4°$) to about -0.0200 (military-rated power at $\alpha = 16.5°$). The rate of change

of elevator hinge-moment coefficient with angle of attack (with propellers windmilling) is essentially a constant negative value averaging about -0.0028 over the range of angle of attack. A marked change in this relation is caused by high power operation, such that $dC_{h_e}/d\alpha$ changes from -0.0040 at $\alpha = 2.4^{\circ}$ to 0.0060 at $\alpha = 6.0^{\circ}$ and to about 0 at $\alpha = 16.5^{\circ}$.

5. The pitching-moment results show that (for a center of gravity located at 20 percent of the mean aerodynamic chord) the model is statically stable longitudinally, controls fixed and free except at very high angles of attack with windmilling propellers.

6. The rudder effectiveness $dC_n/d\delta_r$ for this tailless airplane is lower than normally found for a conventional design. The value for $dC_n/d\delta_r$ is about -0.00024 per degree throughout the angle-of-attack range with propellers windmilling. The effect of propeller operation at high thrust coefficients is to nearly double the rudder effectiveness parameter to a value of -0.00043 at an α of 12.4°. The value for the rudder-hinge-moment parameter $dC_{h_r}/d\delta_r$ ranged from about -0.0050 to -0.0089 per degree for the range of propeller operation tested.

7. The aileron effectiveness $dC_l/d\delta_a$ measured for a single aileron in the low-deflection range, is about 0.0021 per degree at $\alpha = 2.4^{\circ}$ and decreases to 0.0015 at $\alpha = 16.4^{\circ}$. At low angles of attack, aileron stall materially reduces the control effectiveness at deflections above about 12°. At high angles of attack, and at large aileron deflections the combined effects of aileron stall and separation along the wing trailing edge produces a reversal in the slope of the rolling-moment coefficient curves. The aileron hinge moments also reflect the undesirable flow characteristics over the ailerons for large aileron deflections at high angles of attack.

8. The aerodynamic characteristics of the model in yaw show that the average values of the directional stability parameter $\frac{dC_n}{d\psi} \cong 0.00045$, for the large range of angle of attack and power conditions tested, are comparatively lower than those for conventional airplane designs. The dihedral effect is small and corresponds approximately to an angle of 1° for most conditions investigated. The

lateral-force parameter $dC_Y/d\psi$ has a positive value for all conditions tested.

Langley Memorial Aeronautical Laboratory
National Advisory Committee for Aeronautics
Langley Field, Va.

REFERENCES

1. DeFrance, Smith J.: The N.A.C.A. Full-Scale Wind Tunnel. NACA Rep. No. 459, 1933.

2. Goett, Harry J.: Experimental Investigation of the Momentum Method for Determining Profile Drag. NACA Rep. No. 660, 1939.

3. Silverstein, Abe, and Katzoff, S.: Experimental Investigation of Wind-Tunnel Interference on the Downwash behind an Airfoil. NACA Rep. No. 609, 1937.

4. Theodorsen, Theodore, and Silverstein, Abe: Experimental Verification of the Theory of Wind-Tunnel Boundary Interference. NACA Rep. No. 478, 1934.

5. Stability Research Division: An Interim Report on the Stability and Control of Tailless Airplanes. NACA ACR No. L4H19, 1944.

TABLE I

PHYSICAL AND DIMENSIONAL CHARACTERISTICS OF THE KAISER TAILLESS AIRPLANE BASED ON THE 1/7-SCALE MODEL - Concluded

Vertical tail:	
Total area, square feet	820
Rudder area aft of hinge line, square feet, total	267
Rudder balance, percent	12.5
Vertical tail height above wing trailing edge, feet	19.82
Root-mean-square rudder chord, feet	3.02
Hinge line, percent of fin chord	70
Maximum deflection, degrees	±30
Propeller:	
Designation	Hamilton Standard 6491A-0
Diameter, feet	15.167
Number of blades	4
Propeller gear ratio	0.45

NATIONAL ADVISORY
COMMITTEE FOR AERONAUTICS

TABLE I

PHYSICAL AND DIMENSIONAL CHARACTERISTICS OF THE

KAISER TAILLESS AIRPLANE BASED ON THE

1/7-SCALE MODEL

Design gross weight, pounds	175,000
Wing:	
Area, square feet	7920
Span, feet	290
Mean aerodynamic chord, feet	27.3
Location aft of root chord leading edge, feet	1.74
Aspect ratio	10.6
Taper ratio	0.20
Root section } modified with trailing	NACA 63,4-020
Tip section } edge reflexed upward	NACA 65,3-018
Dihedral, outer panel, degrees	1.7
Wing twist, degrees	0
Sweepback of 20-percent chord line, degrees	0
Wing loading, pounds per square foot	22.1
Aileron:	
Area aft of hinge line, each, square feet	277
Aileron balance, percent	15.4
Span, feet	90
Root-mean-square chord, feet	3.24
Hinge line, percent of wing chord	85
Maximum deflection, degrees	10, -30
Elevator:	
Area aft of hinge line, square feet	193
Elevator balance, percent	12.7
Span, feet	48.2
Root-mean-square chord, feet	4
Hinge line, percent wing chord	90
Maximum deflections, degrees	10, -30

NATIONAL ADVISORY
COMMITTEE FOR AERONAUTICS

Table II

General Outline of Tests

No.	Tests	α deg	ψ deg	Propeller Operation	Test airspeed m.p.h. approx.	δ_e deg	δ_r deg	δ_a deg	Remarks
1	Lift and Drag (a) Effect of elevator deflection	Varied −4°→stall	0	W.P.	60	10, 0, −15, −30	0	0	Force tests
	(b) Effect of Reynold's Number	"	"	Props. removed	44, 60, 71, 84	0	"	"	"
	(c) Effect of yaw	"	±6, 10, 15	W.P.	60	"	"	"	"
2	Stall tests	Varied 0→20	0	Props. removed	"	"	"	"	Visual and photographic record of tuft motion.
3	Wake surveys	α for C_L=0	"	Props. removed	84	"	"	"	Pressure measurements of the wing wakes.
4	Thrust calibration	"	"	Rpm range	60	"	"	"	Force tests
5	Elevator tests	Varied 3°→19°	"	W.P. and varied T_c'	"	Range from +10→−30	"	"	Force tests and Hinge moment measurements
6	Rudder tests	"	0, ±3, ±6, 10, 15	Constant power (See Note*)	"	0	Range from +30→−30	"	"
7	Aileron tests	"	0, ±6, ±10, 15	W.P.	"	"	0	Range from +10→−30	Force tests for all ψ's. Hinge moments for ψ=0, only

*Constant power tests included: (1) windmilling propellers (W.P.), (2) normal rated-, (3) military rated-, and (4) asymmetric power conditions.

NATIONAL ADVISORY COMMITTEE FOR AERONAUTICS

Table III

Summary of $C_{L_{max}}$ and $dC_L/d\alpha$

Propeller operation	δ_e (deg)	ψ (deg)	$C_{L_{max}}$	$dC_L/d\alpha$ (deg)	
				C_L=0.2	C_L=0.6
Propellers windmilling	10	0	1.12	0.084	0.084
"	0	"	1.08	.084	.079
"	-15	"	1.01	.085	.075
"	-30	"	0.98	.087	.073
"	0	6.3	1.08	.086	.080
"	"	15.4	-	.088	.072
"	"	-6.4	1.08	.087	.077
"	"	-10.6	1.08	.084	.080
Normal rated power	"	0	-	.097	.098
Military rated power	"	"	-	.097	.098

NATIONAL ADVISORY COMMITTEE FOR AERONAUTICS

MR No. L6C13

TABLE IV

Summary of $\left[\frac{dC_m}{d\delta_e}, \frac{dC_{h_e}}{d\delta_e}, \text{and } \frac{dC_{h_e}}{d\alpha}\right]_{\delta_e=0}$

α (deg)	$dC_m/d\delta_e$ (per deg)			$dC_{h_e}/d\delta_e$ (per deg)			$dC_{h_e}/d\alpha$ (per deg)		
	P.W.*	N.R.P.	M.R.P.	P.W.	N.R.P.	M.R.P.	P.W.	N.R.P.	M.R.P.
2.4	-0.0024	-0.0033	-0.0034	-0.0067	-0.0103	-0.0105	-0.0032	-0.0040	-0.0035
3.3	-.0025	-.0034	-.0035	-.0064	-.0107	-.0113	-.0032	-.0030	-.0035
4.2	-.0025	-.0036	-.0038	-.0062	-.0124	-.0130	-.0030	.0025	.0010
6.0	-.0027	-.0044	-.0045	-.0059	-.0140	-.0147	-.0030	.0060	.0070
8.8	-.0024	-.0047	-.0049	-.0064	-.0165	-.0175	-.0030	.0010	.0025
12.7	-.0016	-.0054	-.0060	-.0078	-.0186	-.0200	-.0025	0	.0025
16.5	-.0016	-.0052	-.0052	-.0070	-.0190	-.0200	-.0025	0	0

*P.W. = Propellers windmilling, N.R.P. = Normal rated power, M.R.P. = Military rated power.

NATIONAL ADVISORY
COMMITTEE FOR AERONAUTICS

L-5-31

TABLE V

Summary of $\left[\frac{dC_n}{d\delta_r}, \frac{dC_Y}{d\delta_r}, \frac{dC_{h_r}}{d\delta_r}\right]_{\delta_r, \psi=0}$

Test condition	α deg	$dC_n/d\delta_r$ per deg	$dC_Y/d\delta_r$ per deg	$dC_{h_r}/d\delta_r$ per deg
Propeller Windmilling	4.2	-0.00024	0.0025	-0.0050
	5.6	-.00022	.0024	-.0055
	7.9	-.00020	.0023	-.0055
	10.7	-.00021	.0023	-.0060
	16.4	-.00021	.0020	-.0060
Normal Rated Power	2.4	-0.00027	0.0027	-0.0045
	4.2	-.00030	.0031	-.0054
	5.1	-.00032	.0033	-.0060
	7.8	-.00038	.0039	-.0072
	12.4	-.00043	.0042	-.0089
Military Rated Power	8.7	-0.00039	0.0039	-0.0079
	12.4	-.00044	.0044	-.0092
Asymmetric Power	4.2	-0.00028	0.0027	-0.0052
	6.0	-.00030	.0029	-.0057
	12.5	-.00033	.0034	-.0070

NATIONAL ADVISORY COMMITTEE FOR AERONAUTICS

TABLE VI

Summary of $[C_n, C_Y, \text{and } C_{h_r}]_{\delta_r=0}$

Power Condition	α (deg)	$\psi = -10.6°$ C_n	C_Y	C_{h_r}	$\psi = -6.4°$ C_n	C_Y	C_{h_r}	$\psi = 3.3°$ C_n	C_Y	C_{h_r}
P.W.*	6.1	0.0040	-0.0480	0.0020	0.0022	-0.0280	-0.0020	-0.0017	0.0140	-0.0020
↓	8.8	.0043	-.0485	.0030	.0025	-.0300	0	-.0013	.0120	-.0050
↓	14.5	.0048	-.0475	.0050	.0027	-.0330	0	-.0013	.0100	-.0070
N.R.P.	2.4	.0032	-.0485	0	.0015	-.0280	—	-.0020	.0190	-.0080
↓	5.1	.0030	-.0540	.0040	.0012	-.0300	—	-.0026	.0197	-.0075
↓	10.6	.0028	-.0700	.0150	-.0002	-.0475	—	-.0045	.0110	-.0130
M.R.P.	6.9	.0032	-.0650	.0050	.0010	-.0390	—	-.0035	.0200	-.0075
↓	12.4	.0025	-.0750	.0130	-.0003	-.0540	—	-.0055	.0120	-.0110
A.P.	4.2	.0043	-.0405	-.0070	.0023	-.0290	-.0070	-.0012	.0190	-.0090
↓	6.0	.0050	-.0525	-.0050	.0032	-.0380	-.0030	-.0014	.0190	-.0120
↓	12.5	.0058	-.0700	.0030	.0042	-.0530	.0020	-.0010	.0070	-.0150

*P.W. = Propellers windmilling; N.R.P. = Normal rated power; M.R.P. = Military rated power; A.P. = Asymmetric power.

NATIONAL ADVISORY COMMITTEE FOR AERONAUTICS

TABLE VI - CONCLUDED

Power Condition	α (deg)	ψ = 6.3°			ψ = 10.6°			ψ = 15.4°		
		C_n	C_Y	C_{h_r}	C_n	C_Y	C_{h_r}	C_n	C_Y	C_{h_r}
P.W.	6.1	-0.0030	0.0310	-0.0150	-0.0043	0.0485	-0.0170	-0.0070	0.0760	-0.0300
↓	8.8	-.0030	.0260	-.0120	-.0045	.0480	-.0170	-.0063	.0710	-.0290
	14.5	-.0025	.0250	-.0130	-.0050	.0420	-.0170	-.0073	.0610	-.0260
N.R.P.	2.4	-.0035	.0355	-.0170	-.0049	.0575	-.0210	-.0072	.0840	-.0270
↓	5.1	-.0040	.0370	-.0180	-.0052	.0560	-.0200	-.0085	.0960	-.0380
	10.6	-.0063	.0370	-.0250	-.0074	.0580	-.0260	-.0095	.1080	-.0530
M.R.P.	6.9	-.0045	.0365	-.0070	-.0065	.0610	-.0200	-.0085	.0900	-.0500
↓	12.4	-.0065	.0270	-.0180	-.0085	.0580	-.0300	-.0107	.0890	-.0650
A.P.	4.2	-.0023	.0335	-.0130	-.0040	.0570	-.0220	—	—	-.0370
↓	6.0	-.0025	.0340	-.0120	-.0040	.0570	-.0200	-.0066	.0880	-.0370
	12.5	-.0025	.0215	-.0100	-.0045	.0525	-.0190	-.0074	.0835	-.0580

NATIONAL ADVISORY
COMMITTEE FOR AERONAUTICS

TABLE VII

Summary of $\left[\frac{dC_l}{d\delta_{a_L}} \text{ and } \frac{dC_{h_a}}{d\delta_{a_L}}\right]_{\delta_{a_L}=0}$

[Results given for one aileron]

Test Condition		$dC_l/d\delta_{a_L}$ (per deg.)						$dC_{h_a}/d\delta_{a_L}$
	ψ deg / α deg	0	6.3	10.6	15.4	-6.4	-10.6	0
Propellers	2.4	0.0021	0.0022	0.0020	0.0018	0.0022	0.0020	-0.0100
removed at $\psi=0°$	4.2	.0022	—	—	—	—	—	-.0099
and	6.1	.0020	.0021	.0020	.0016	.0021	.0020	-.0096
Propellers wind-	8.9	.0017	—	—	—	—	—	-.0081
milling at $\psi=\pm6°$	12.6	.0018	.0018	.0016	.0015	.0018	.0017	-.0065
$\pm10°$ and $15°$	16.4	.0015	—	—	—	—	—	-.0059

NATIONAL ADVISORY
COMMITTEE FOR AERONAUTICS

TABLE VIII

Summary of $\left[\frac{dC_n}{d\psi}, \frac{dC_l}{d\psi}, \text{and } \frac{dC_Y}{d\psi}\right]_{\psi, \delta_r = 0}$

Test Condition	α (deg)	$dC_n/d\psi$ (per deg)	$dC_l/d\psi$ (per deg)	$dC_Y/d\psi$ (per deg)
Propellers windmilling	6.1	-0.00040	0.00022	0.0045
	8.8	-.00040	00022	.0045
	14.5	-.00042	00030	.0046
Normal rated power	2.4	-0.00040	0.00027	0.0049
	5.1	-.00042	.00017	.0054
	10.6	-.00045	.00032	.0067
Military rated power	6.9	-0.00043	0.00027	0.0060
	12.4	-.00048	.00032	.0064
Asymmetric power	4.2	-0.00035	0.00015	0.0054
	6.0	-.00045	.00008	.0057
	12.5	-.00052	0	.0062

NATIONAL ADVISORY
COMMITTEE FOR AERONAUTICS

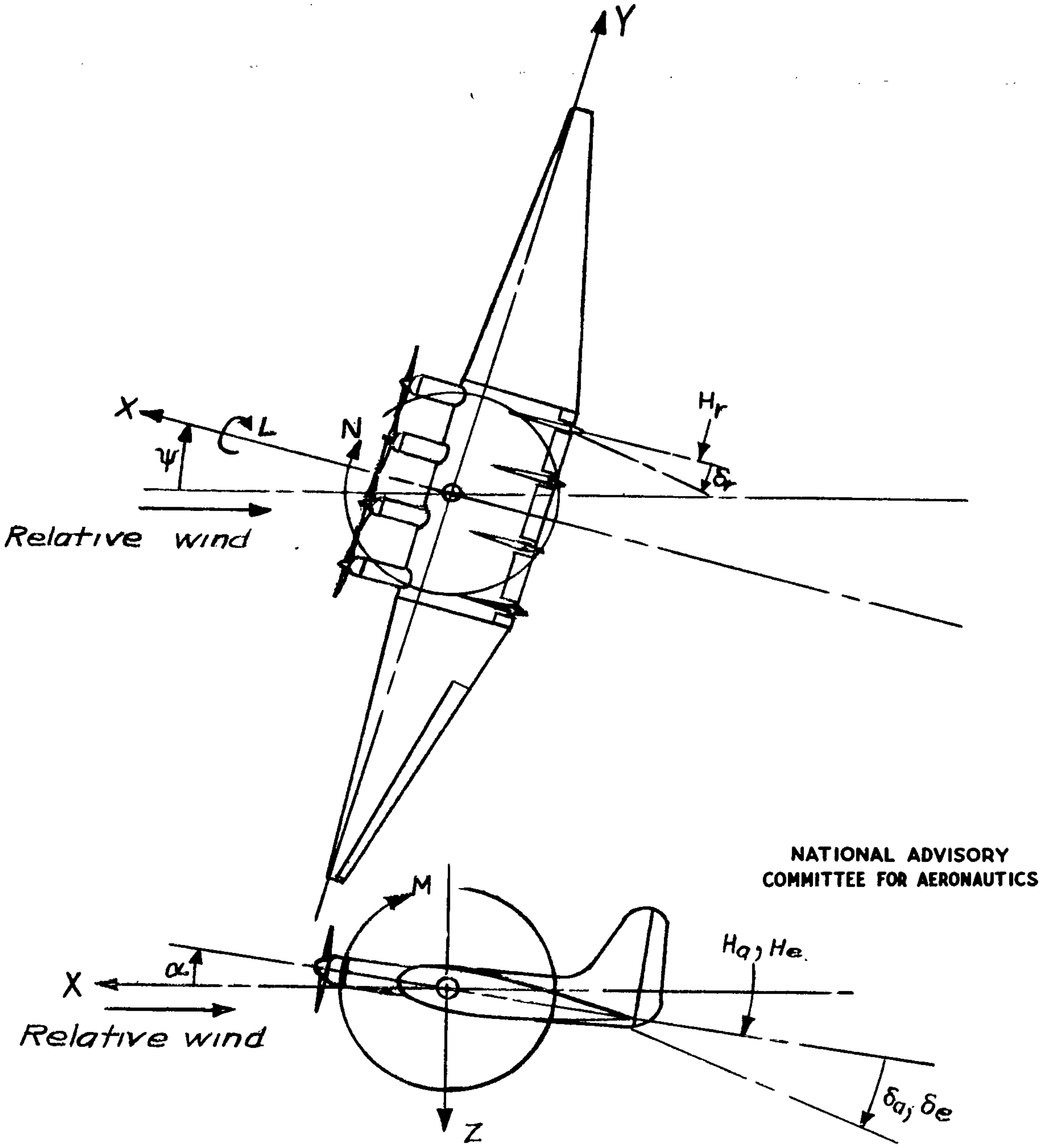

Figure 1.- System of axes and control-surface hinge moments and deflections. Positive direction of forces, moments, and angles are indicated by arrows.

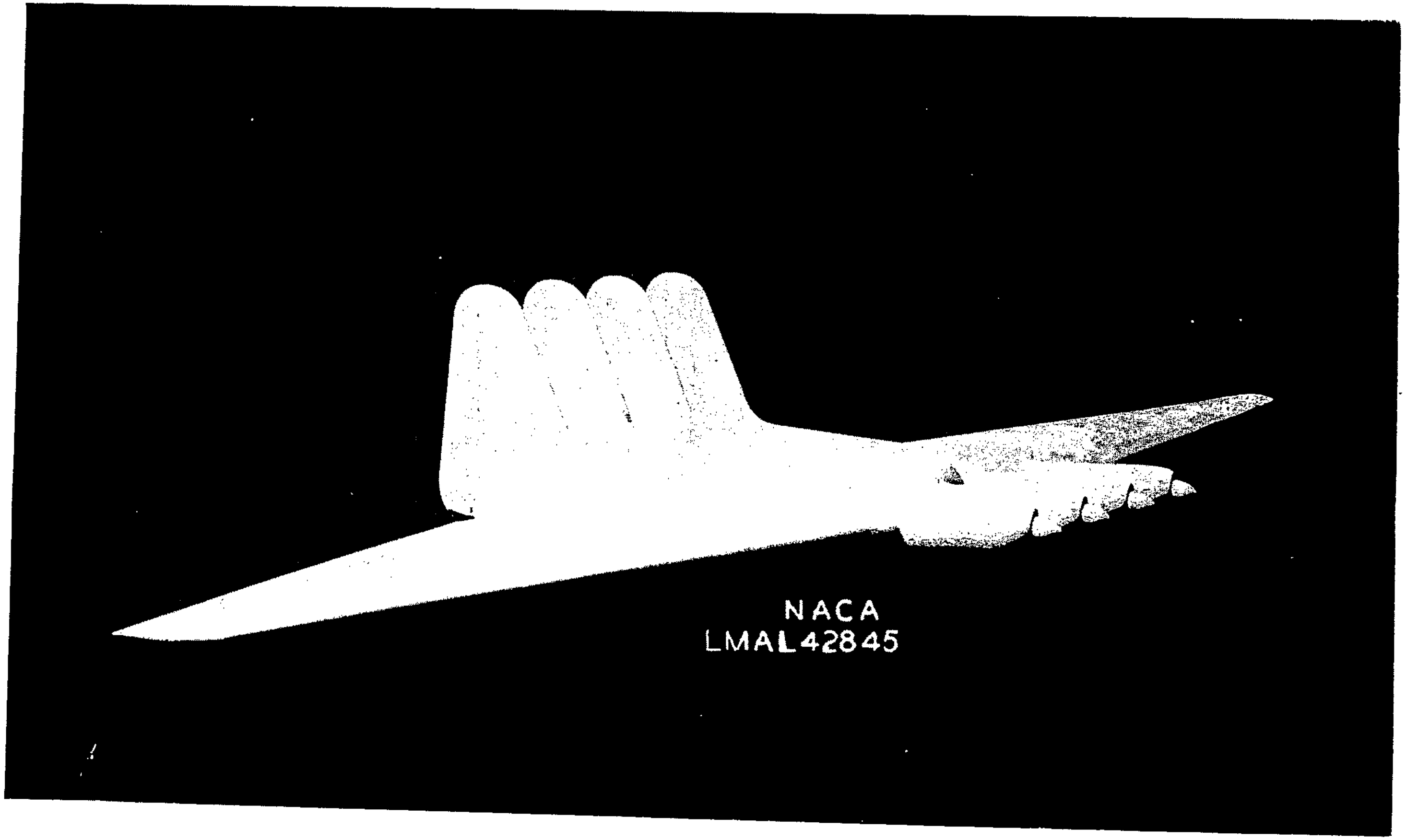

(a) Three-quarter front view.

Figure 2.- The $\frac{1}{7}$-scale model of the Kaiser tailless airplane mounted for tests in the Langley full-scale tunnel.

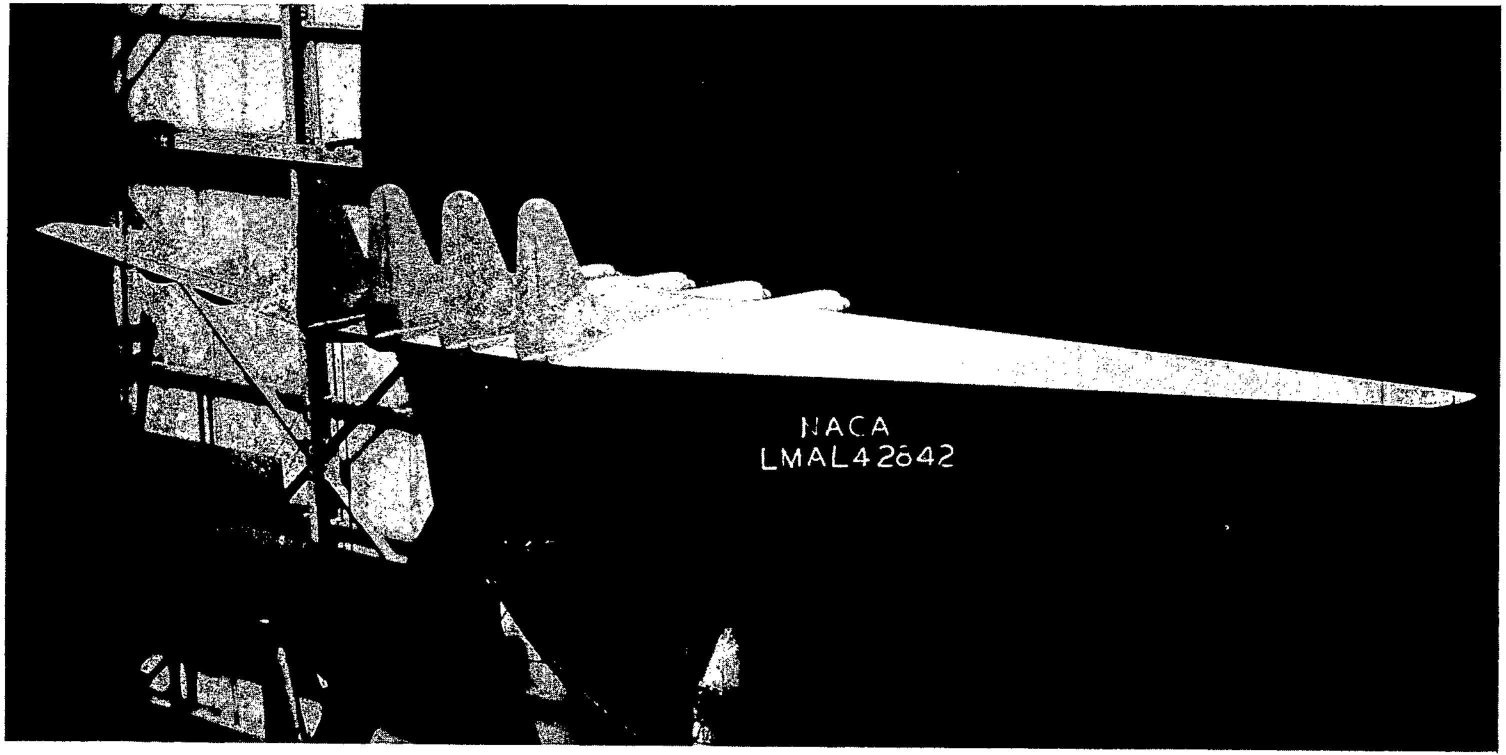

(b) Three-quarter rear view.

Figure 2.- Continued.

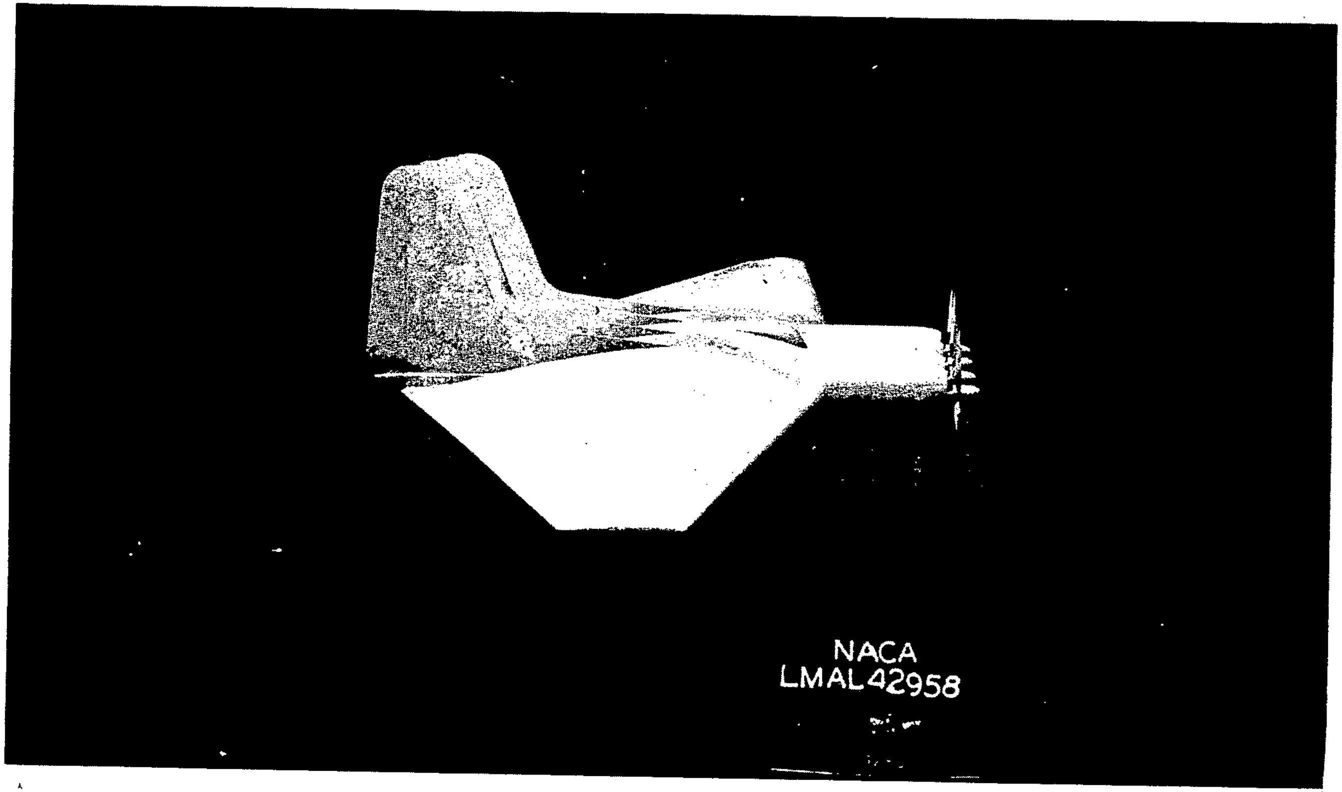

(c) Side view.

Figure 2.- Concluded.

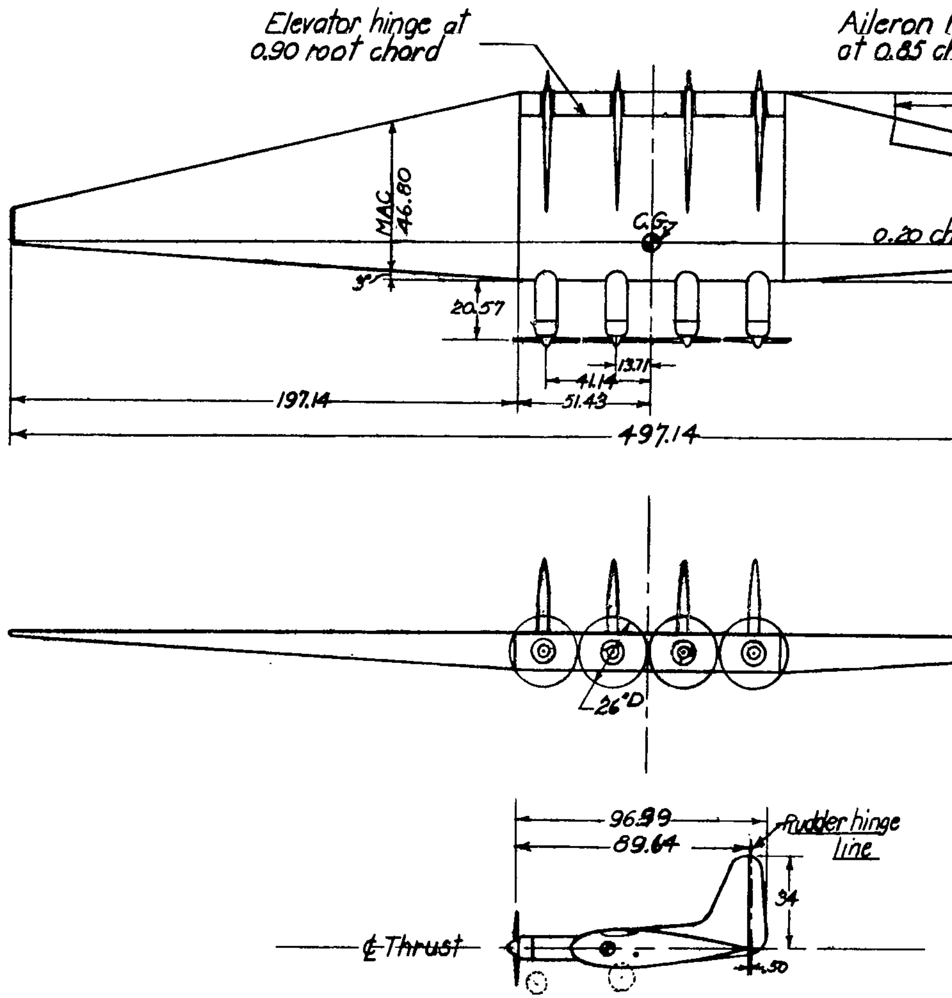

Wing area, sq.ft.	161.6
Elevator area, sq.ft.	3.93
Aileron area, sq.ft.,(one)	5.66
Vertical area, sq.ft.,(total)	16.71
Rudder area, sq.ft.,(total)	5.44
Dihedral angle, outer panel	1.7°
Wing section	
Root: NACA 65,4-020	Modified
Tip: NACA 65,3-018	Mean Line

Note: All dimensions in inches.

Figure 3 - Three-view drawing of the 1/4-scale model of the Kaiser tailless airplane.

NATIONAL ADVISORY
COMMITTEE FOR AERONAUTICS

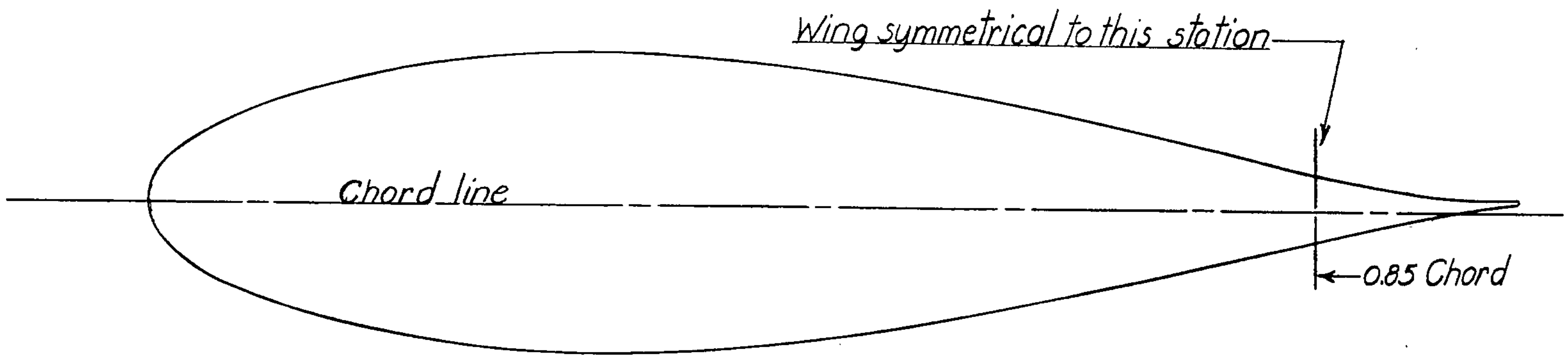

NATIONAL ADVISORY
COMMITTEE FOR AERONAUTICS

Figure 4.- A typical cross-sectional view of the wing of the 1/7-scale model of the Kaiser tailless airplane. NACA 6-series airfoil with modified mean line.

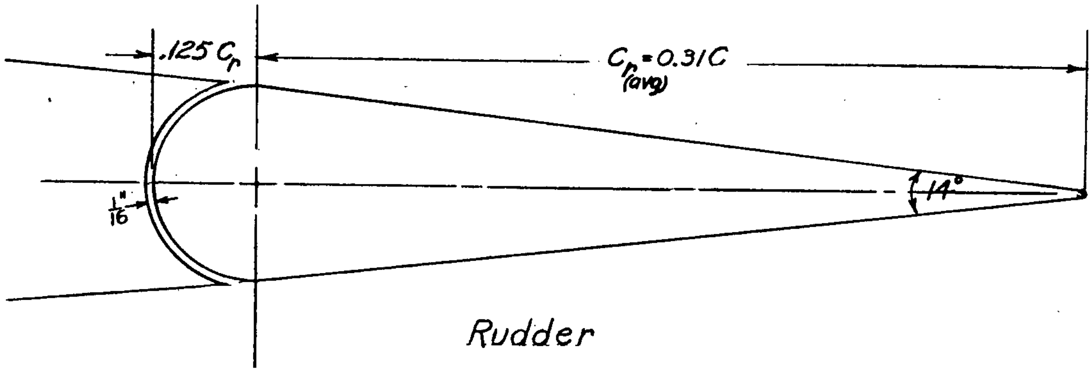

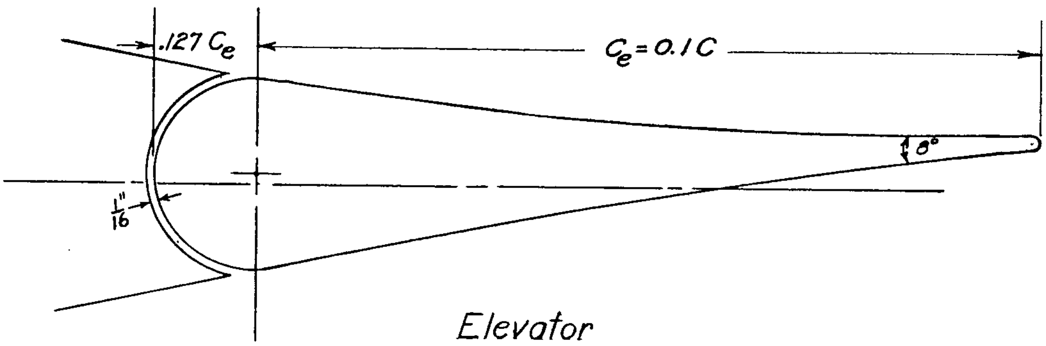

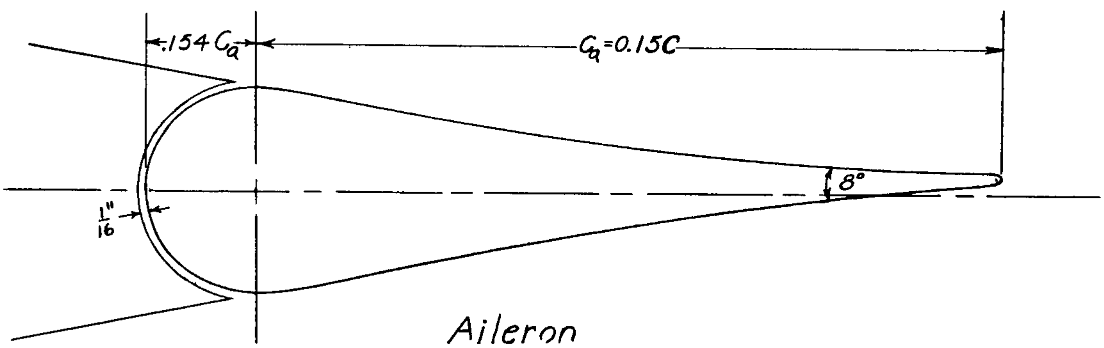

NATIONAL ADVISORY
COMMITTEE FOR AERONAUTICS

Figure 5.- Typical cross-sectional views of the control surfaces installed on the 1/7-scale model of the Kaiser tailless airplane.

L-531

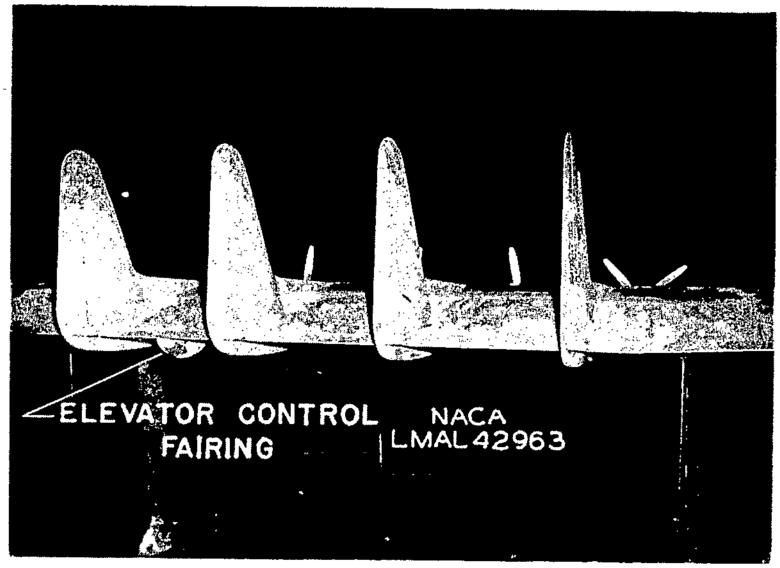

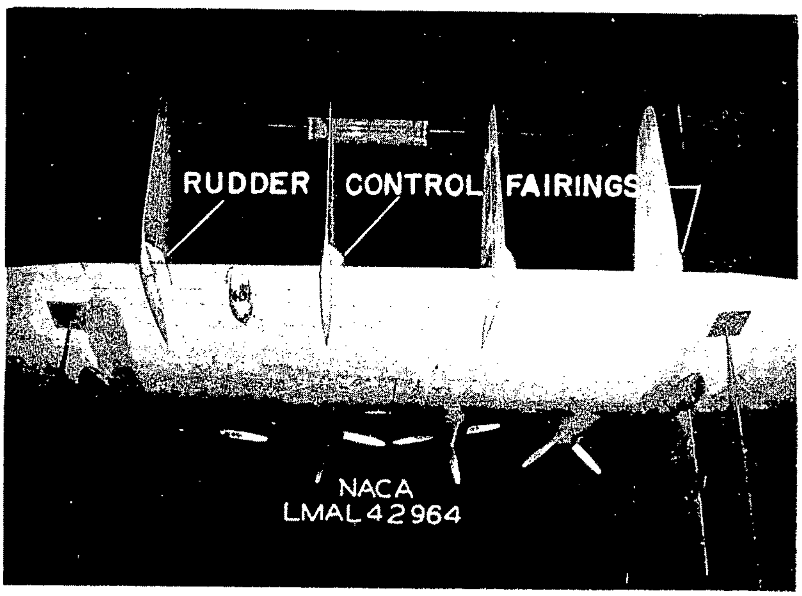

Figure 6.- Rear view of the model showing the fairings used to cover the elevator and rudder controls.

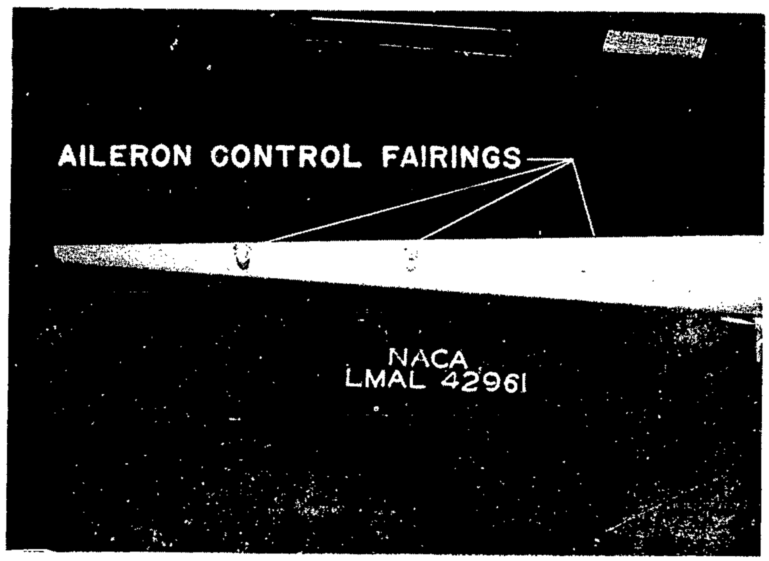

Figure 7.- Detail view of the wing showing the fairings used to cover the aileron controls.

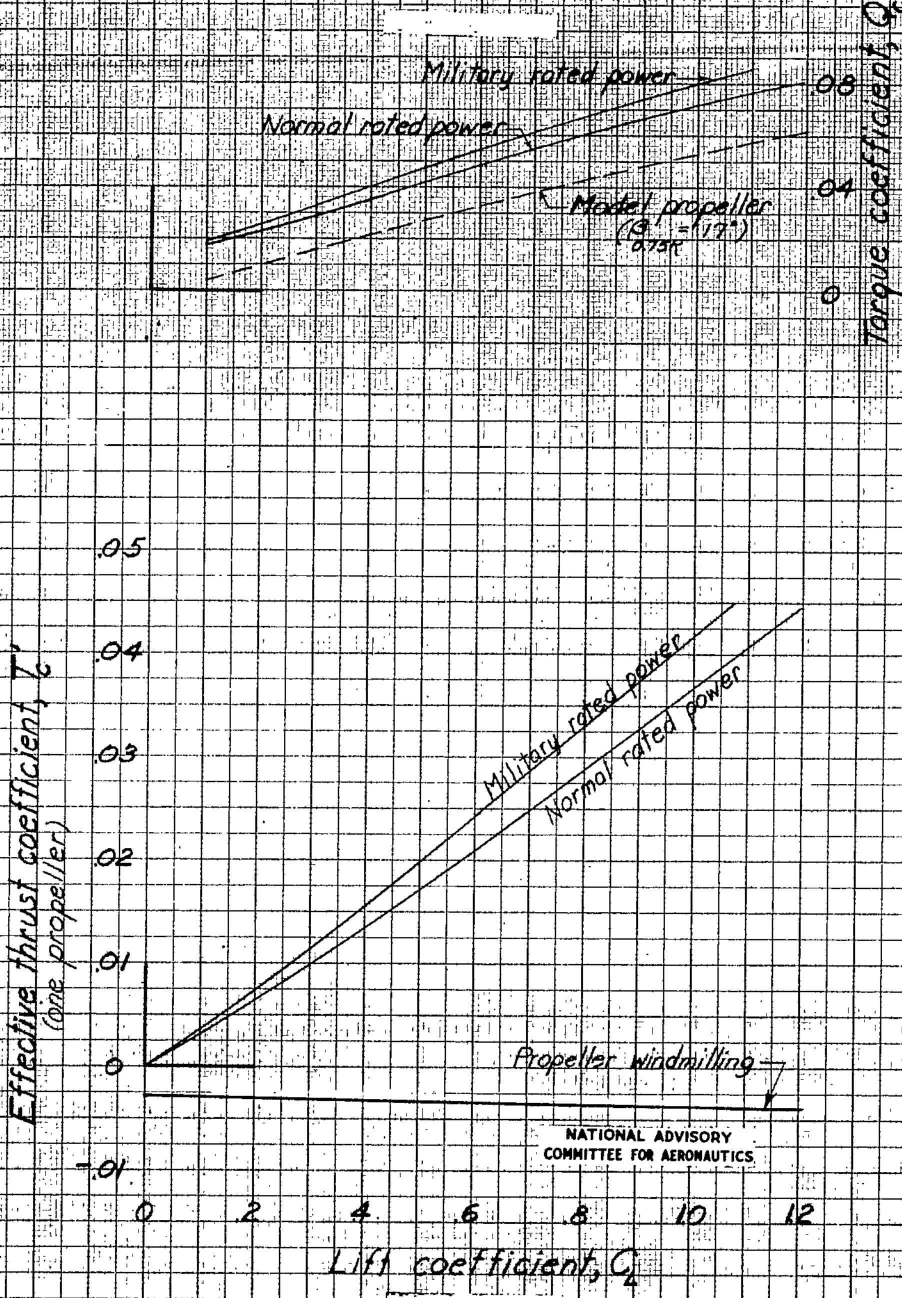

Figure 8.- Variation of effective thrust coefficient and torque coefficient with lift coefficient for a single propeller. Sea-level operation; W/S = 22.1 pounds per square foot.

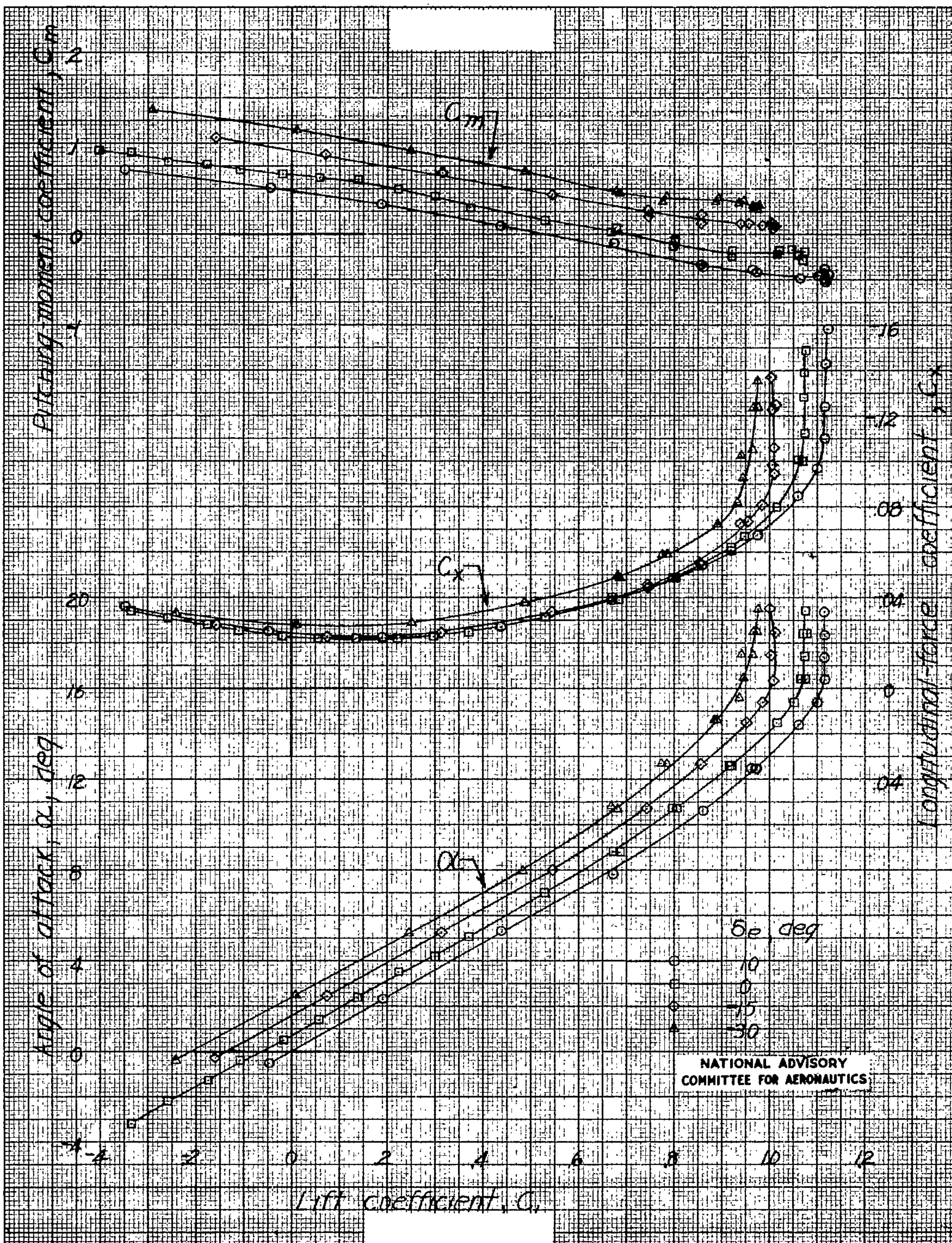

Figure 9.- Effect of elevator deflection on the aerodynamic characteristics of the model. Propellers windmilling; δ_a, 0°; δ_r, 0°; V, approximately 61 mph.

L-531

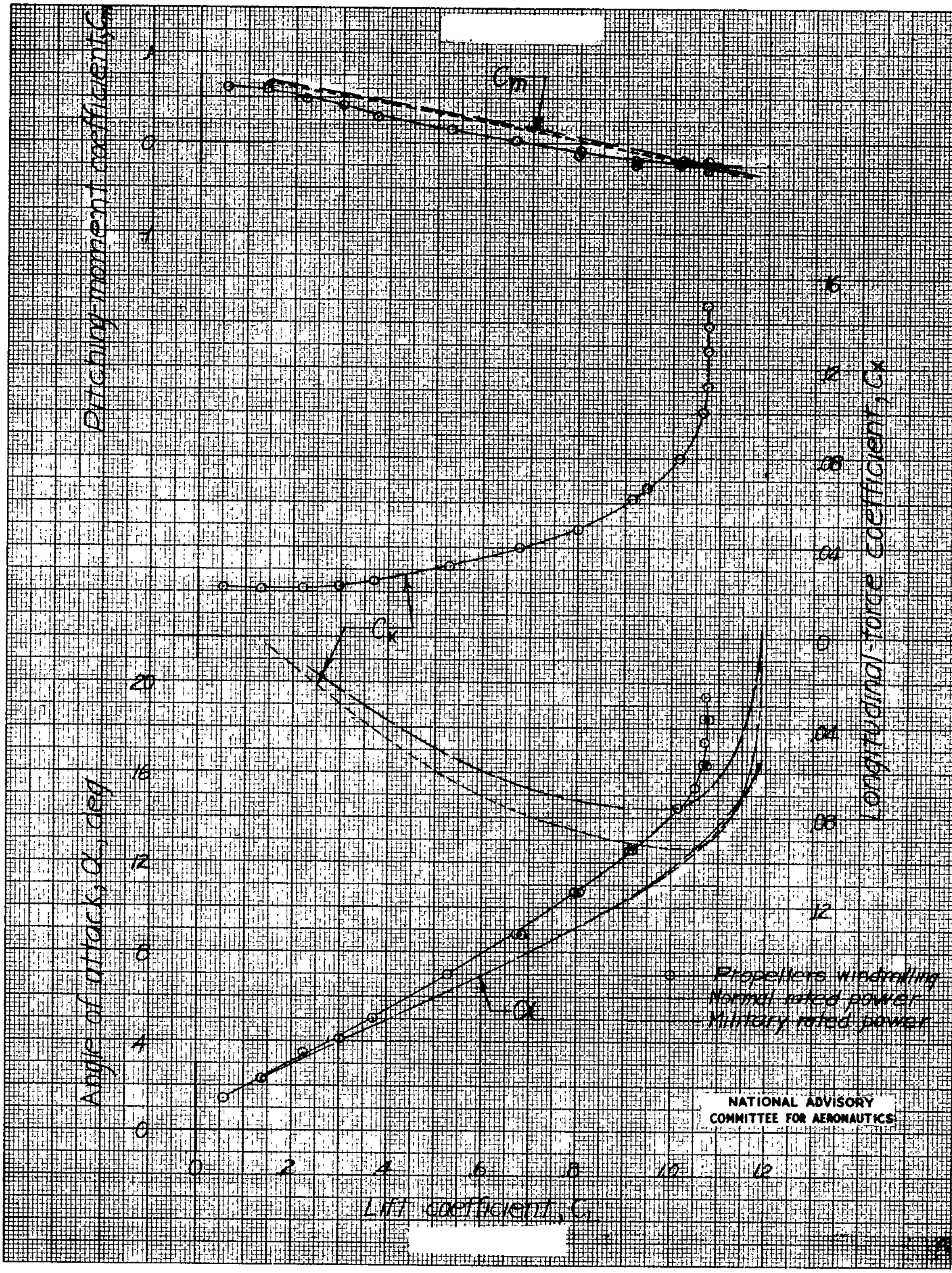

Figure 10.- Effect of propeller operation on the aerodynamic characteristics of the model. Controls neutral.

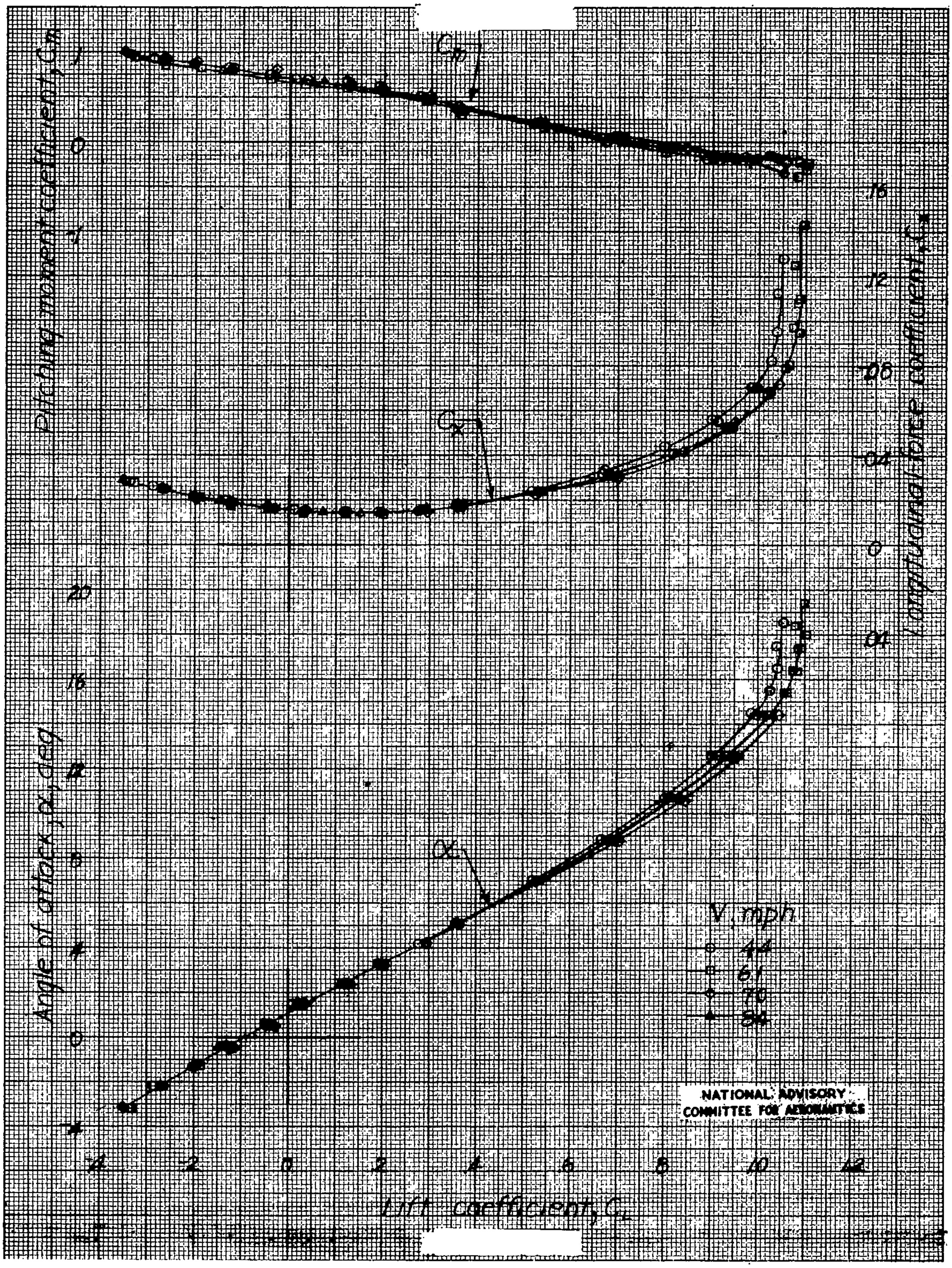

Figure 11.- Effect of test airspeed on the aerodynamic characteristics of the model. Propellers removed; controls neutral.

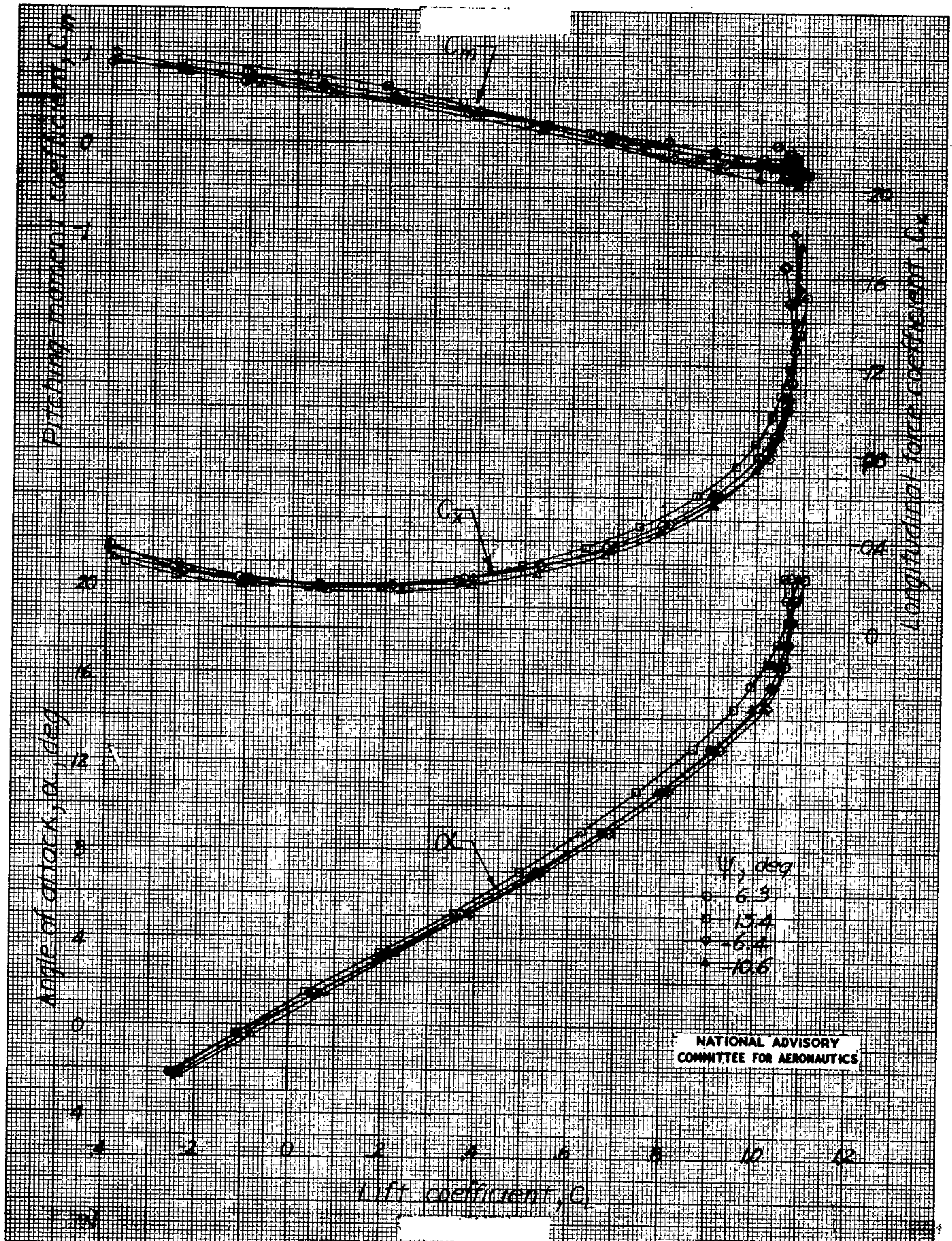

Figure 12.- Effect of angle of yaw on the aerodynamic characteristics of the model. Propellers windmilling; controls neutral; V, approximately 61 mph.

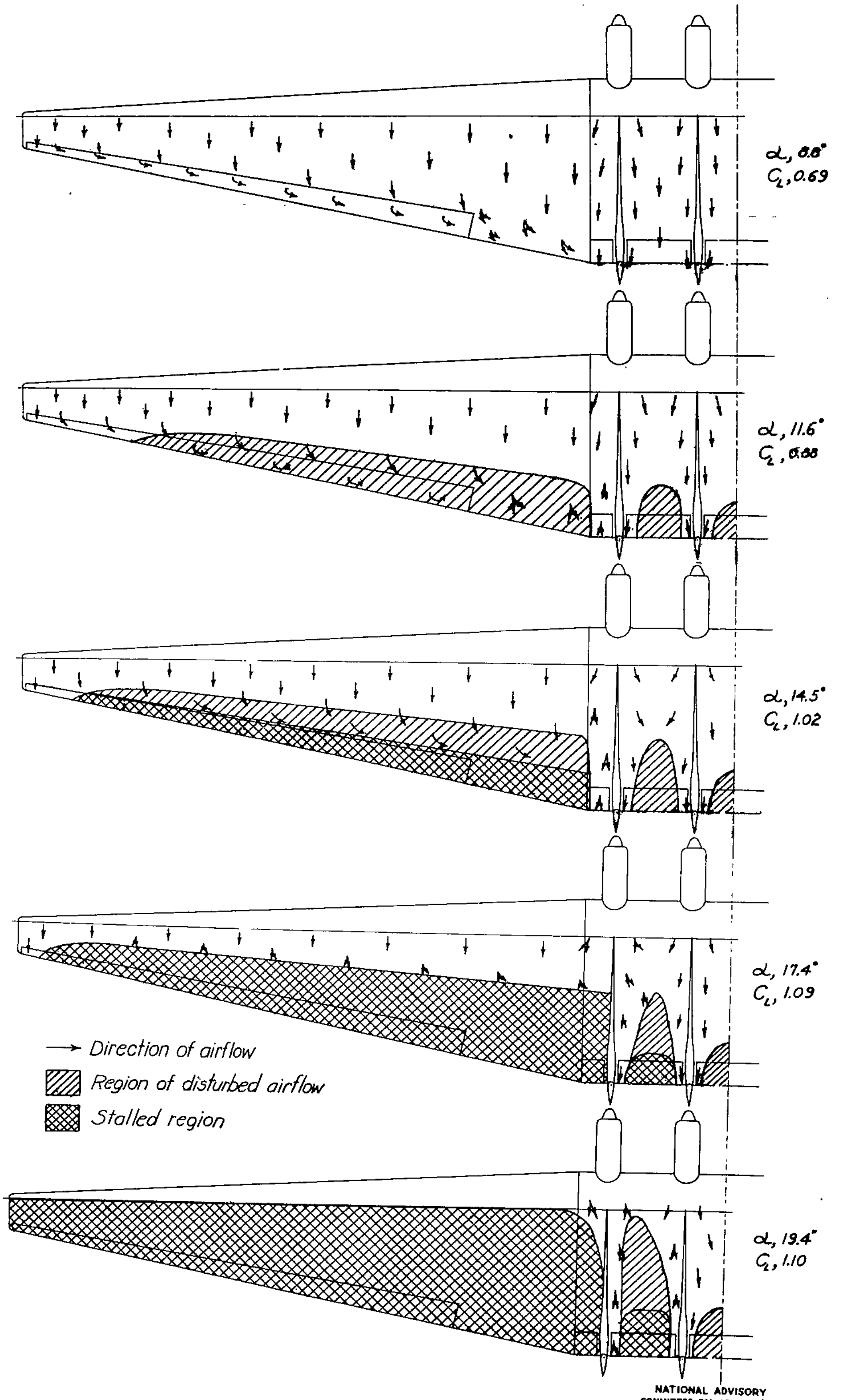

Figure 13.- Progression of the stall on the semi-span of the $\frac{1}{7}$-scale model of the Kaiser tailless airplane. Propellers removed; controls neutral, V, 61 mph.

Figure 14.- Photographs of the progression of stall over the semi-span of the $\frac{1}{7}$-scale model of the Kaiser tailless airplane. Propellers removed; controls neutral; V, 61 mph.

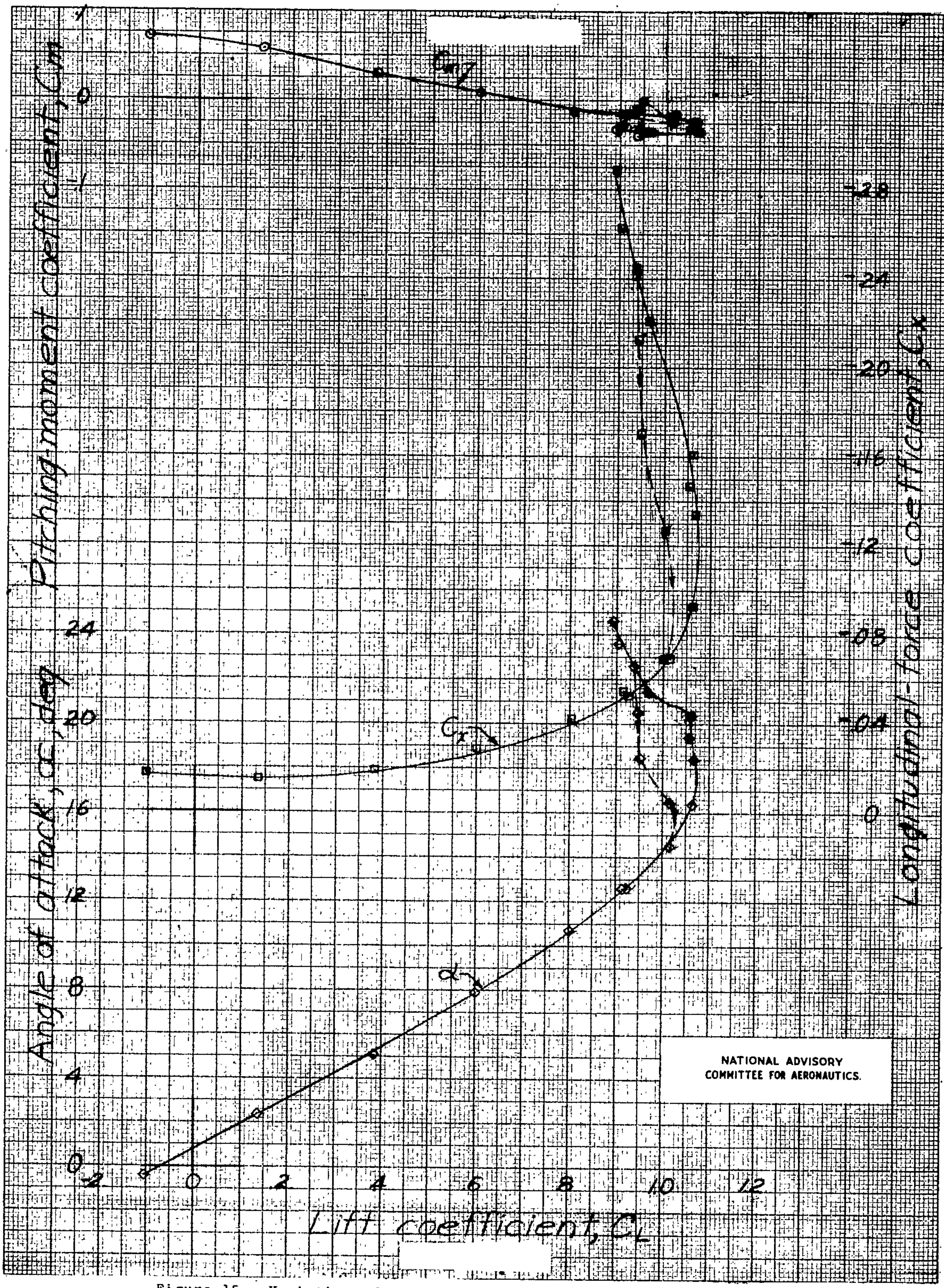

Figure 15.- Variation of α, C_X, and C_m with C_L. Propellers removed; controls neutral; V, approximately 61 mph.

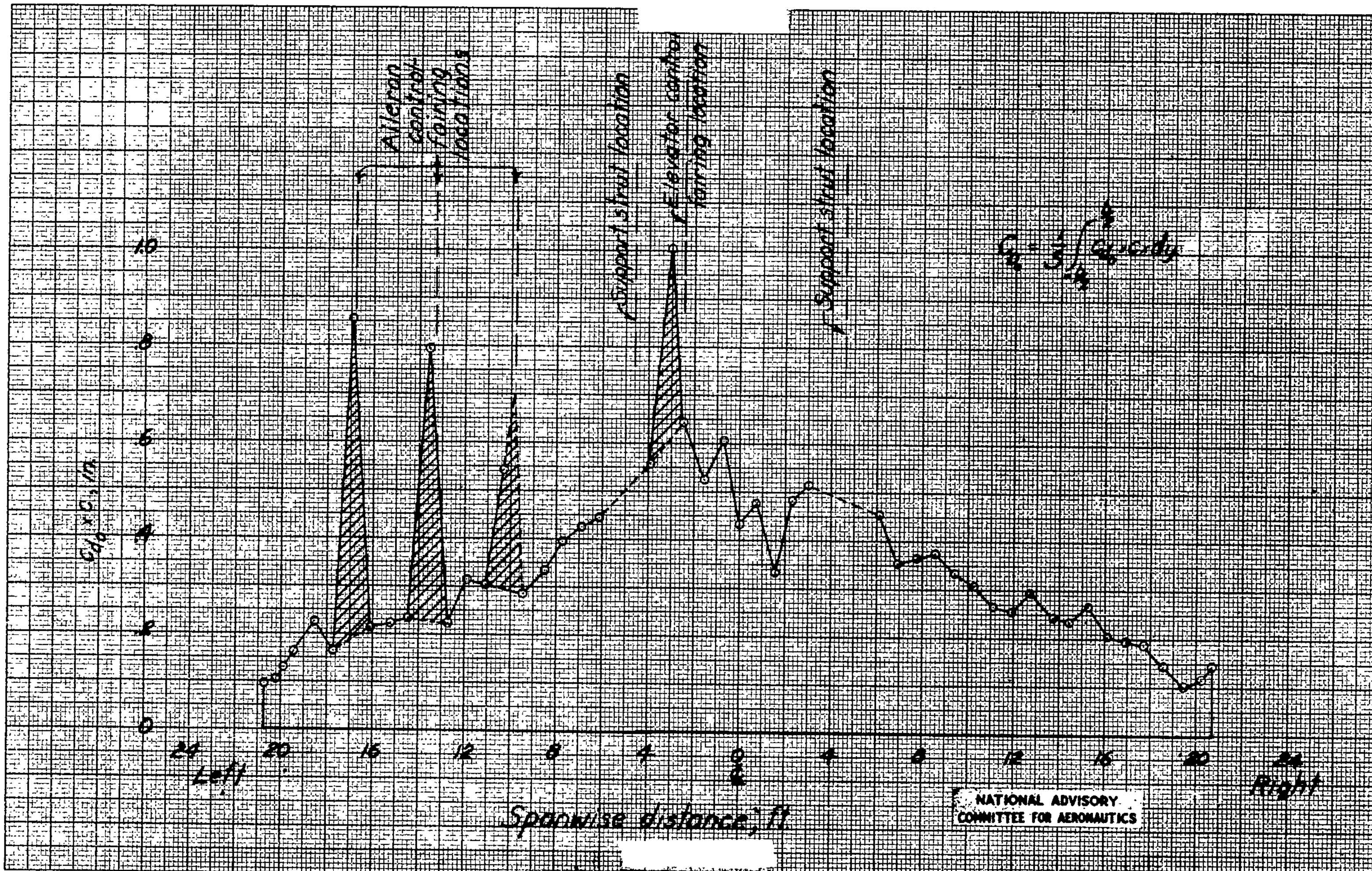

Figure 16.- Variation of $c_{d_0}c$ along the span of the model. Propellers removed; V, approximately 84 mph; C_L, 0.02.

MR No. L6C13

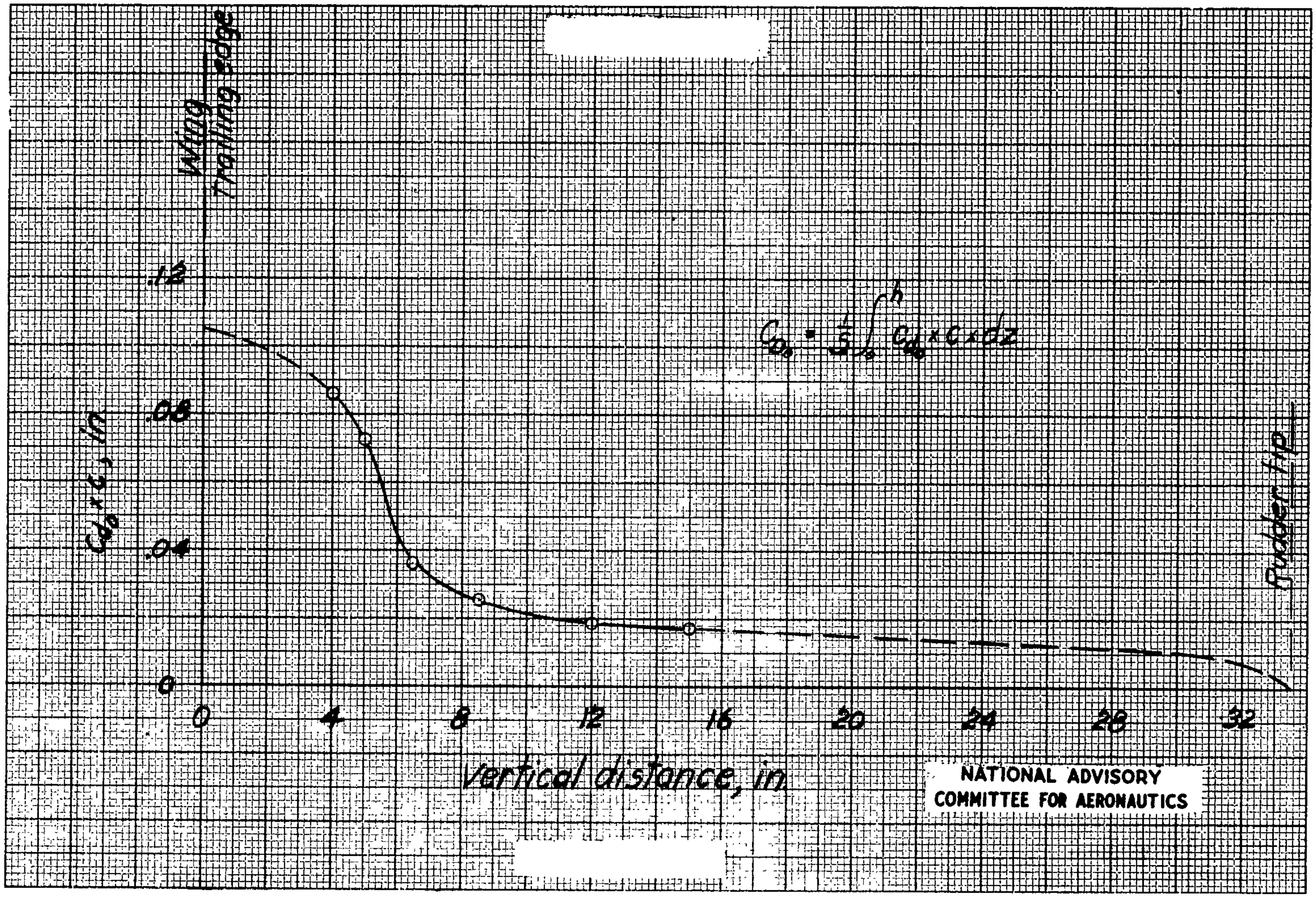

Figure 17.- Variation of $c_{d_o}c$ along the span of a vertical surface. Propellers removed; V, approximately 84 mph; C_L, 0.02.

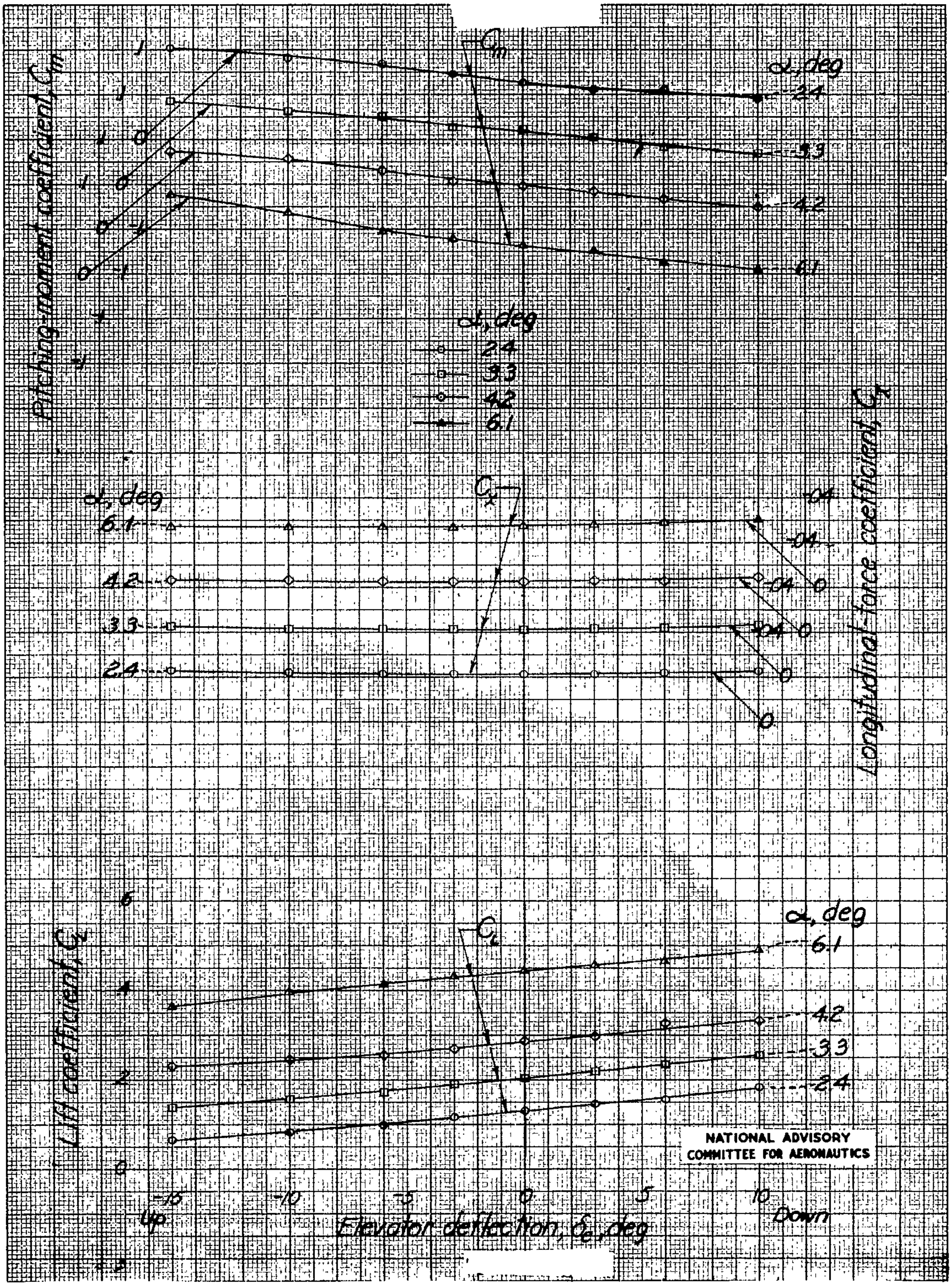

Figure 18.- Variation of C_L, C_X, and C_m with elevator deflection. Propellers windmilling: δ_a, 0°; δ_r, 0°; T_c', approximately -0.01.

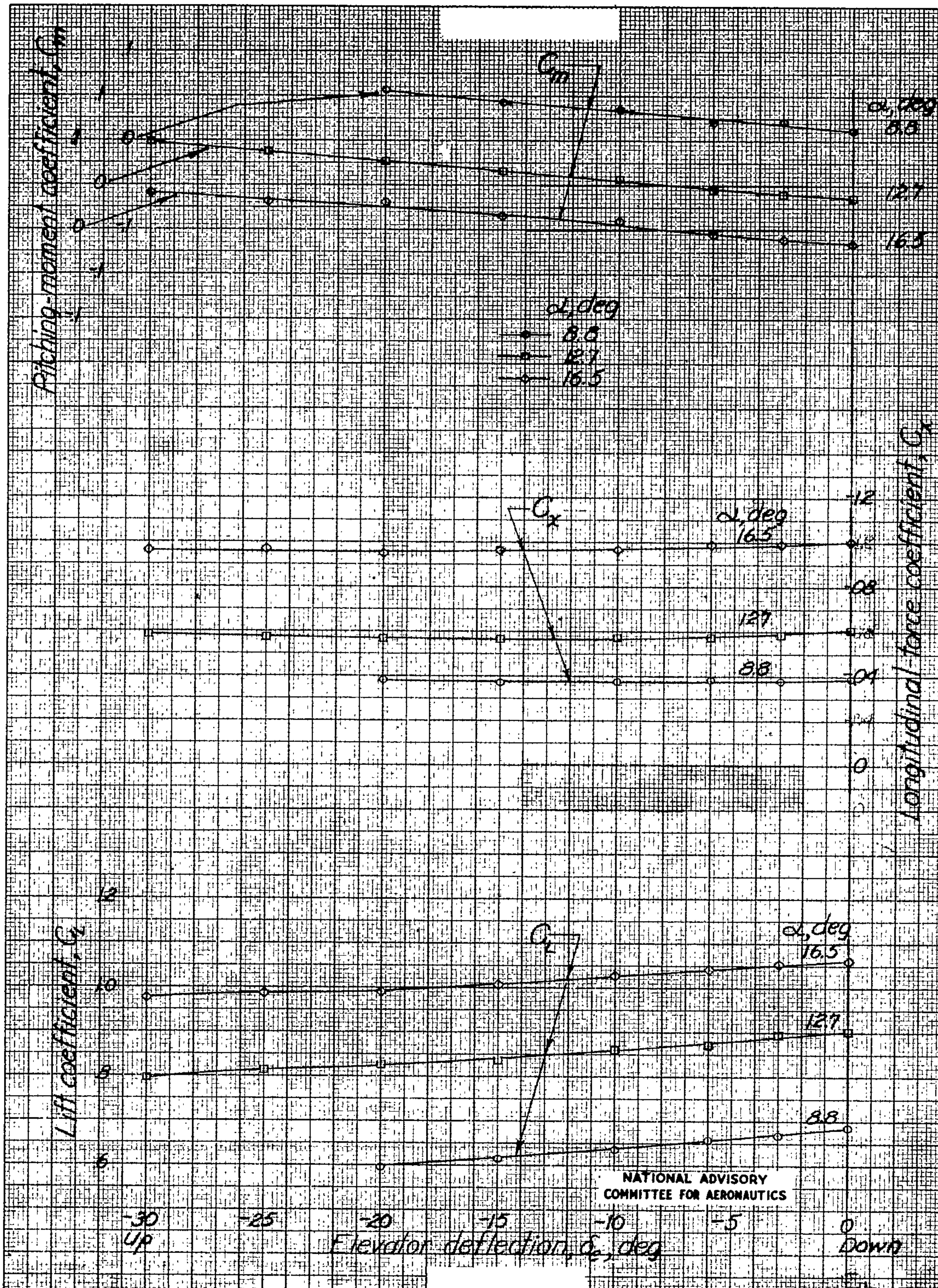

Figure 18.- Concluded.

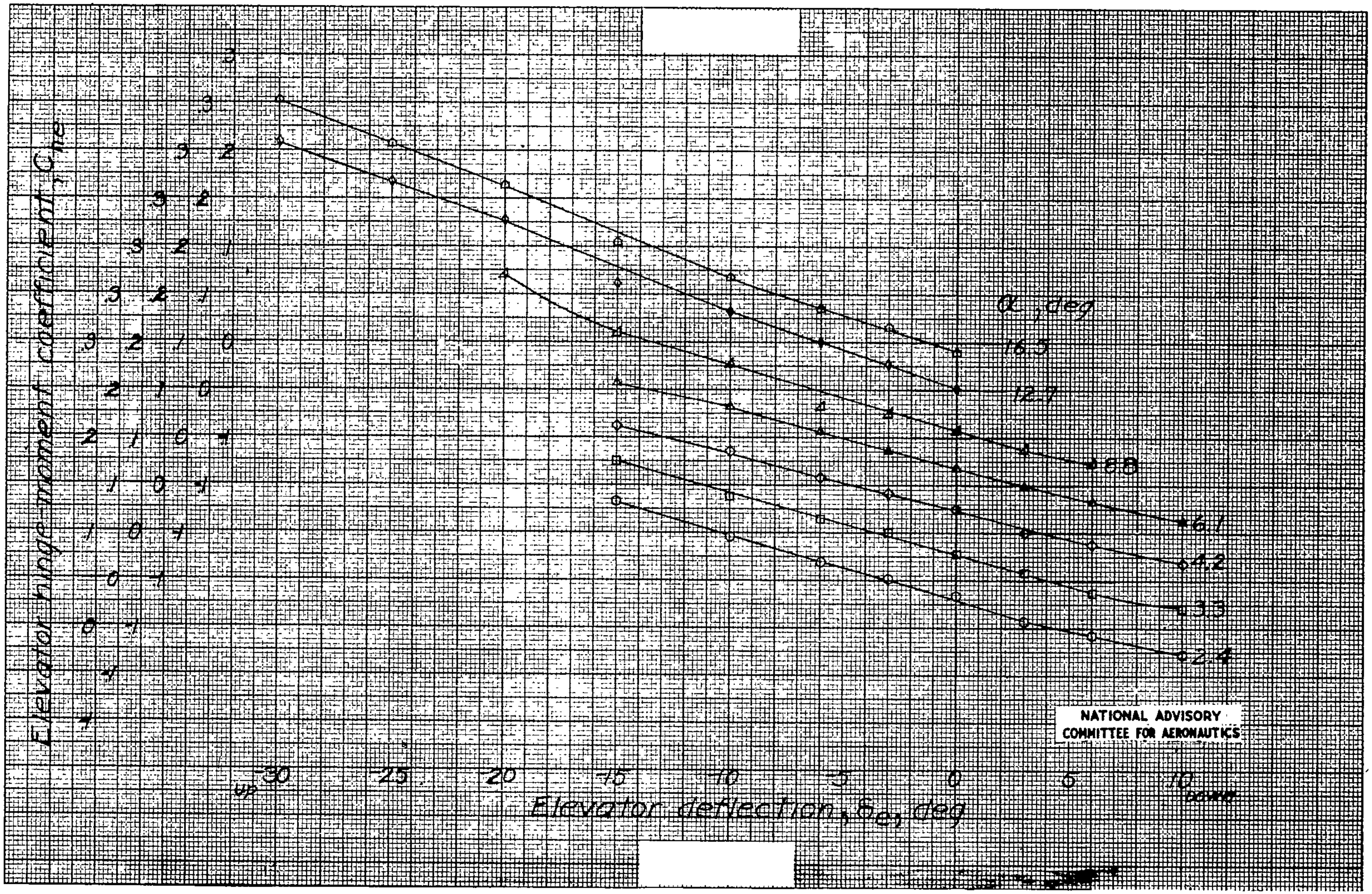

Figure 19.- Variation of C_{h_e} with elevator deflection. Propellers windmilling; δ_a, 0°; δ_r, 0°; T_c', approximately -0.01.

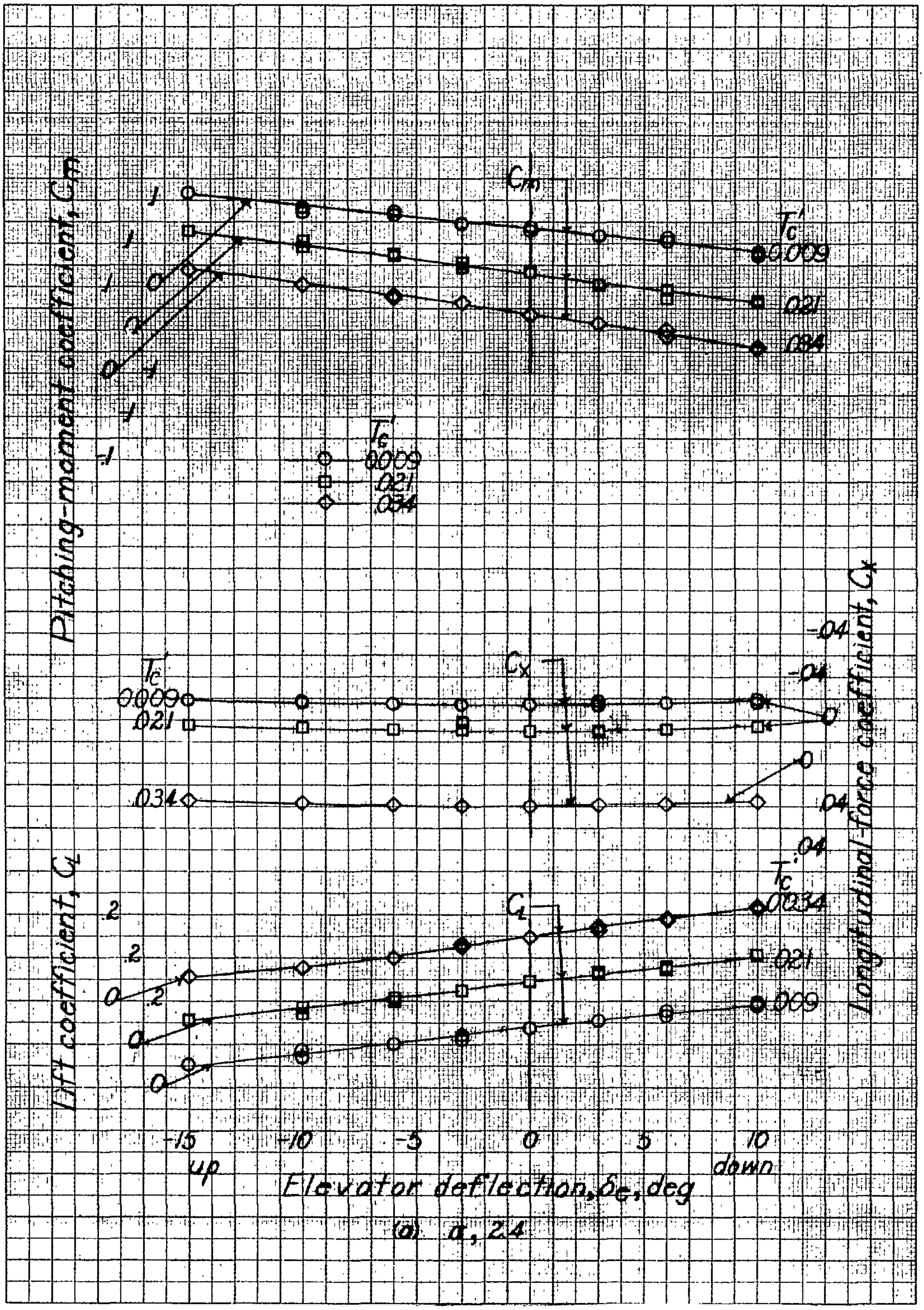

Figure 20.- Variation of C_L, C_X, and C_m with elevator deflection for a range of thrust coefficients and angles of attack. δ_a, 0°; δ_r, 0°.

L-534

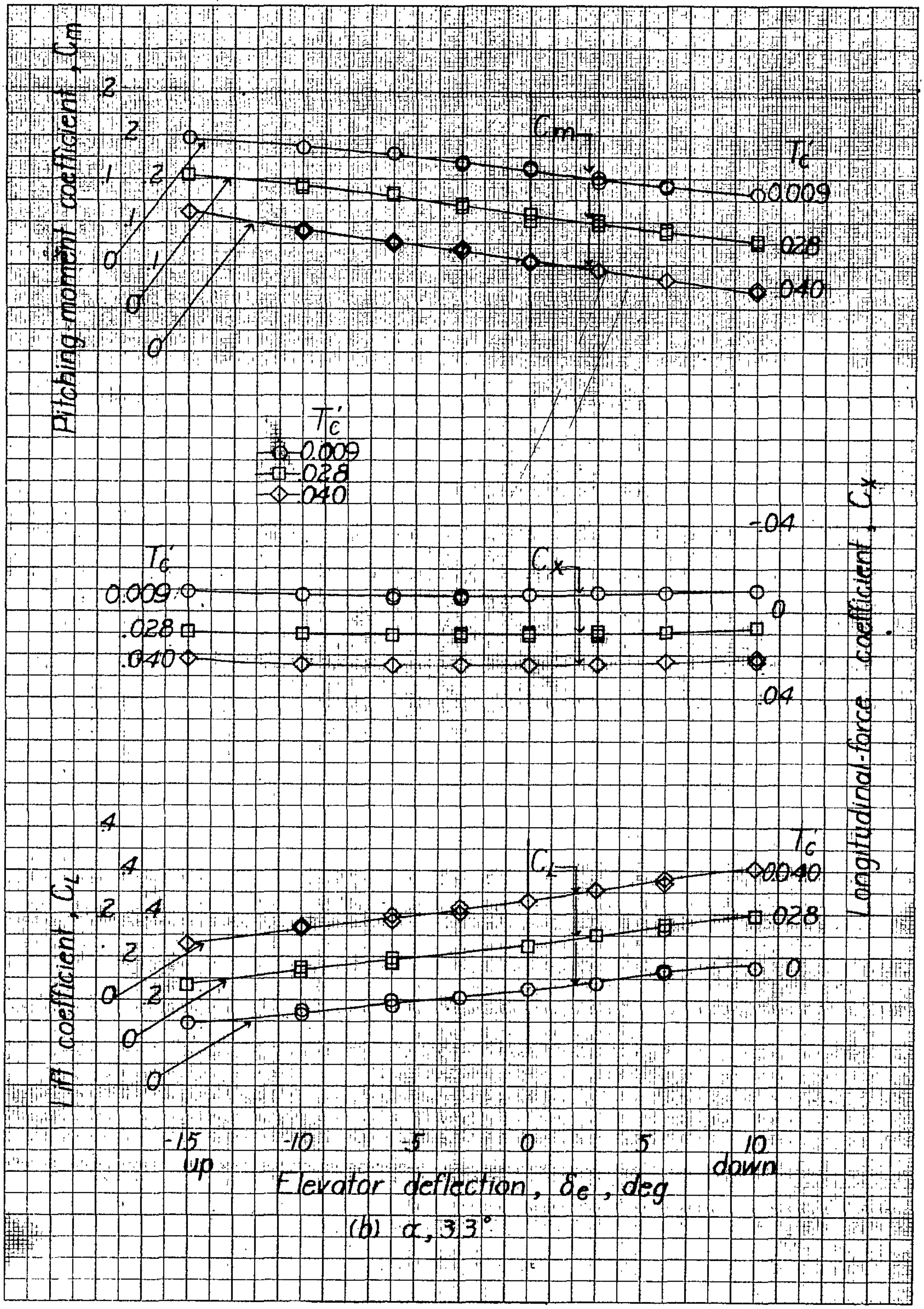

Figure 20.- Continued.

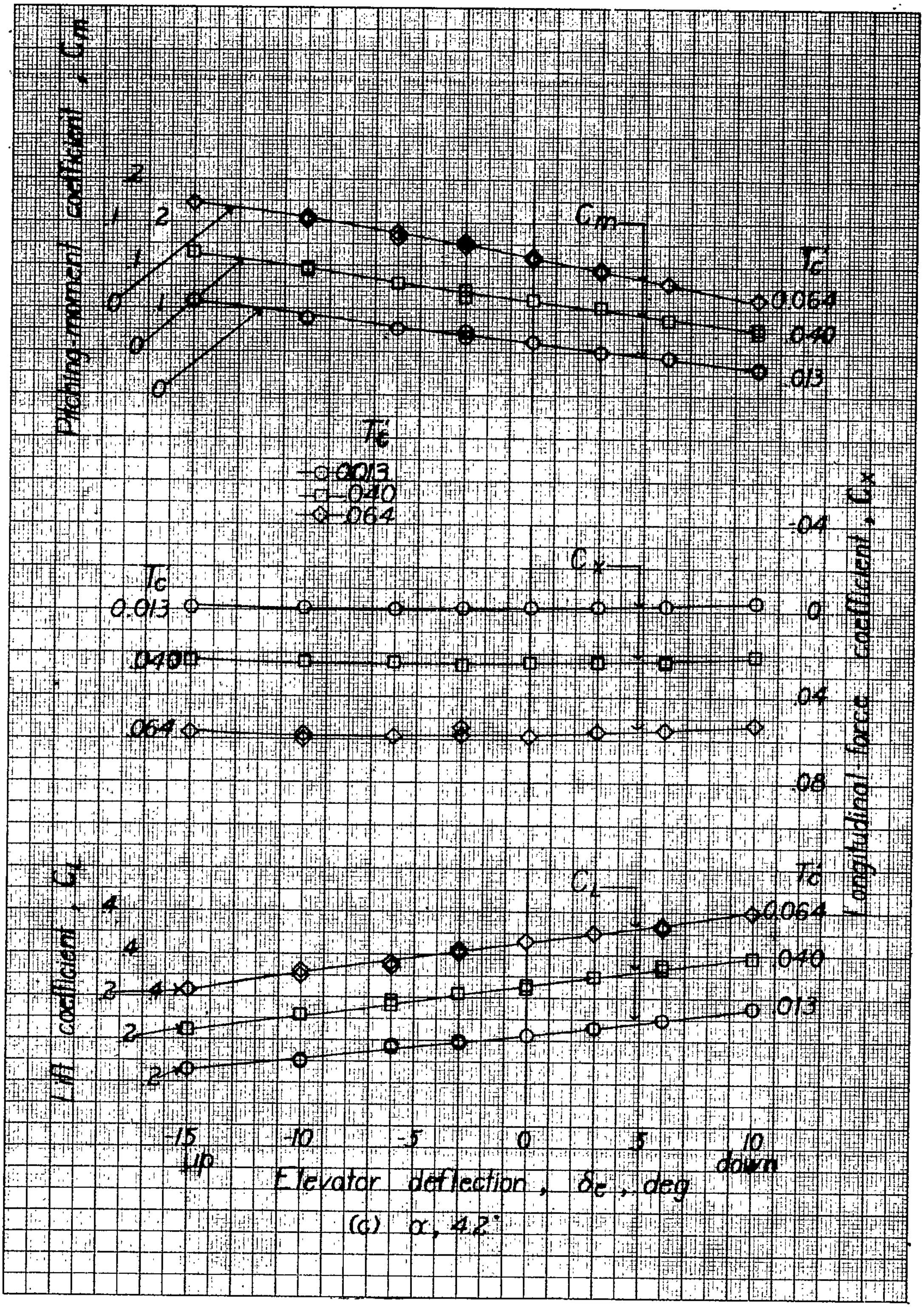

Figure 20.- Continued.

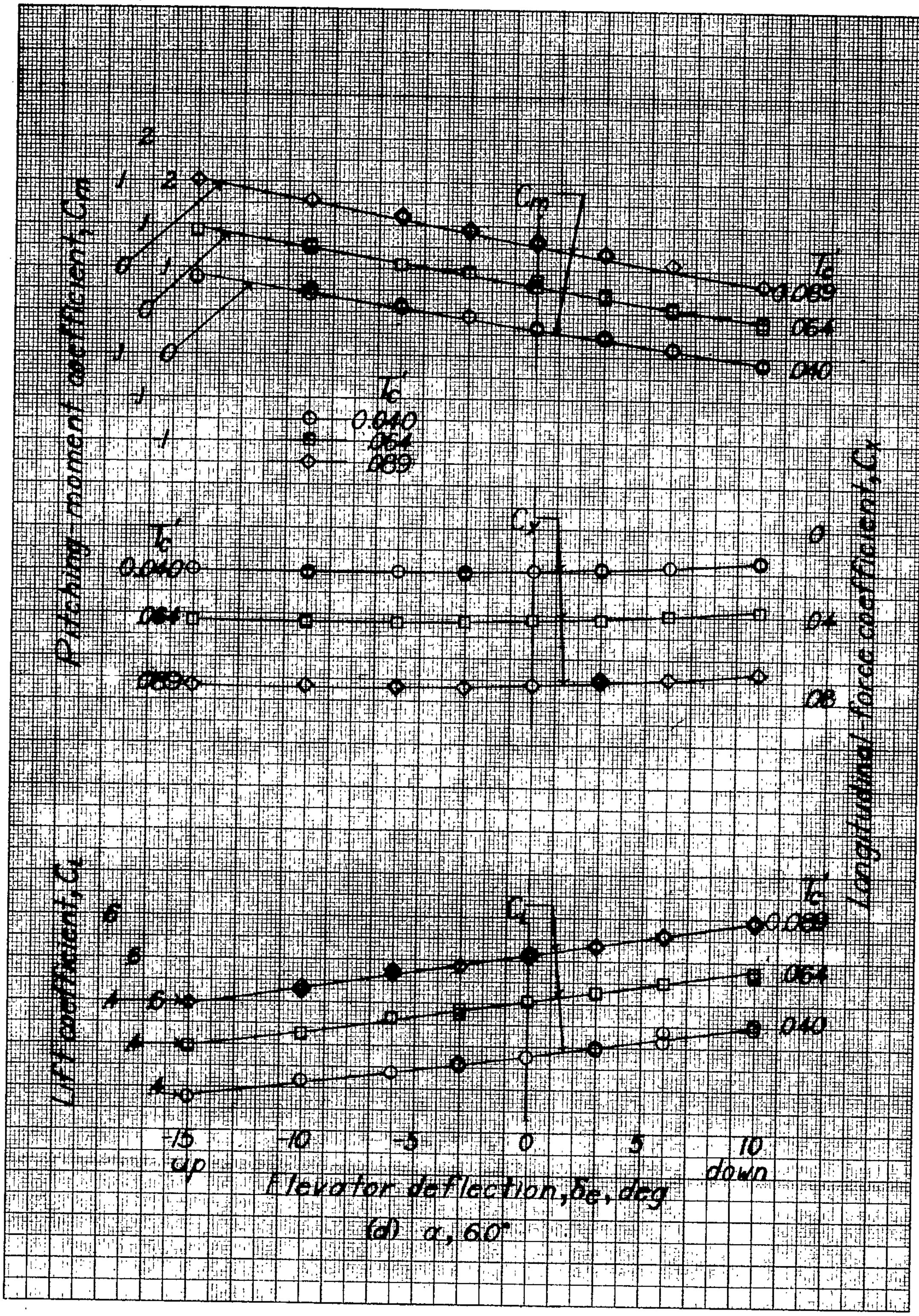

Figure 20.- Continued.

L-531

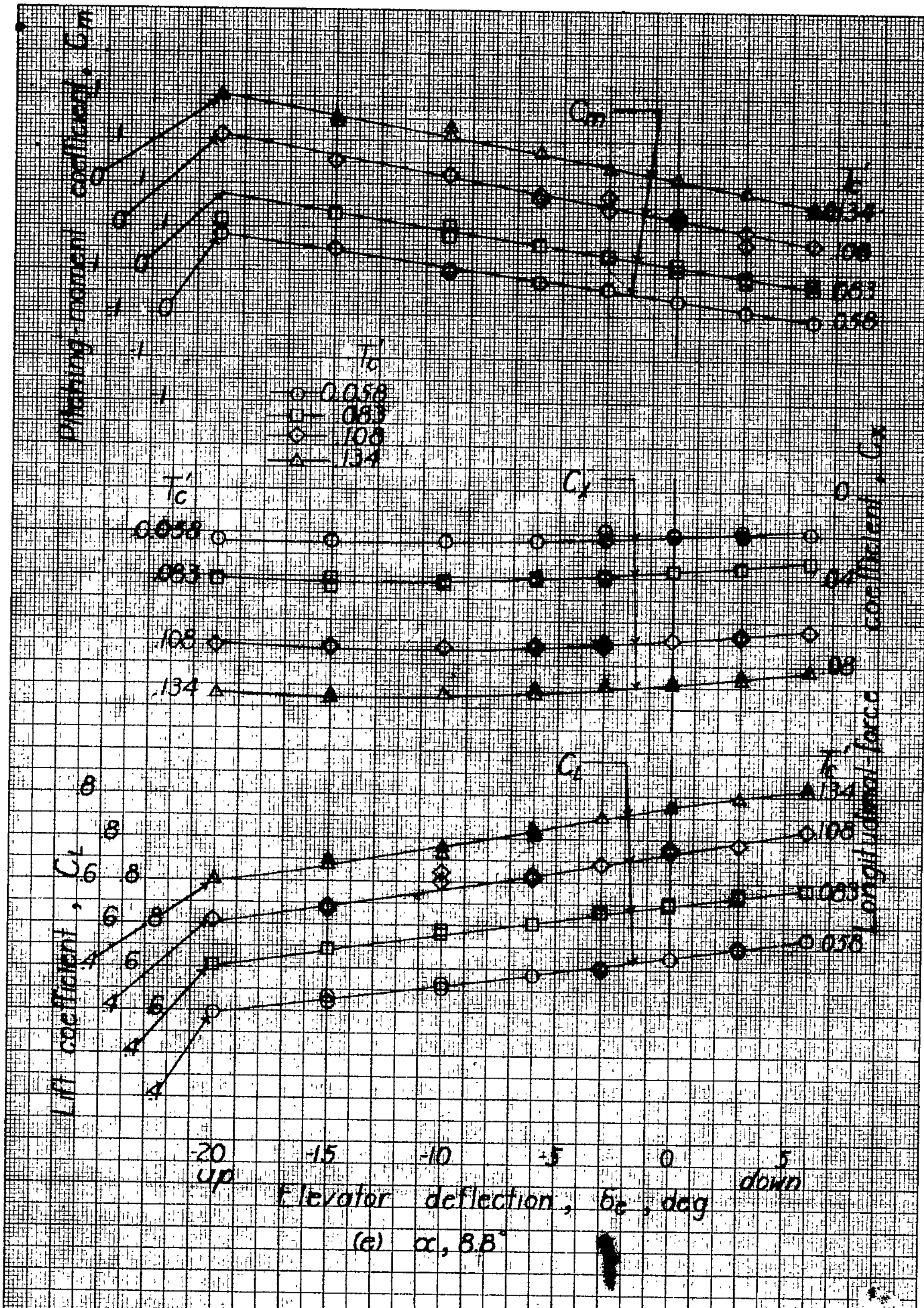

Figure 20.- Continued.

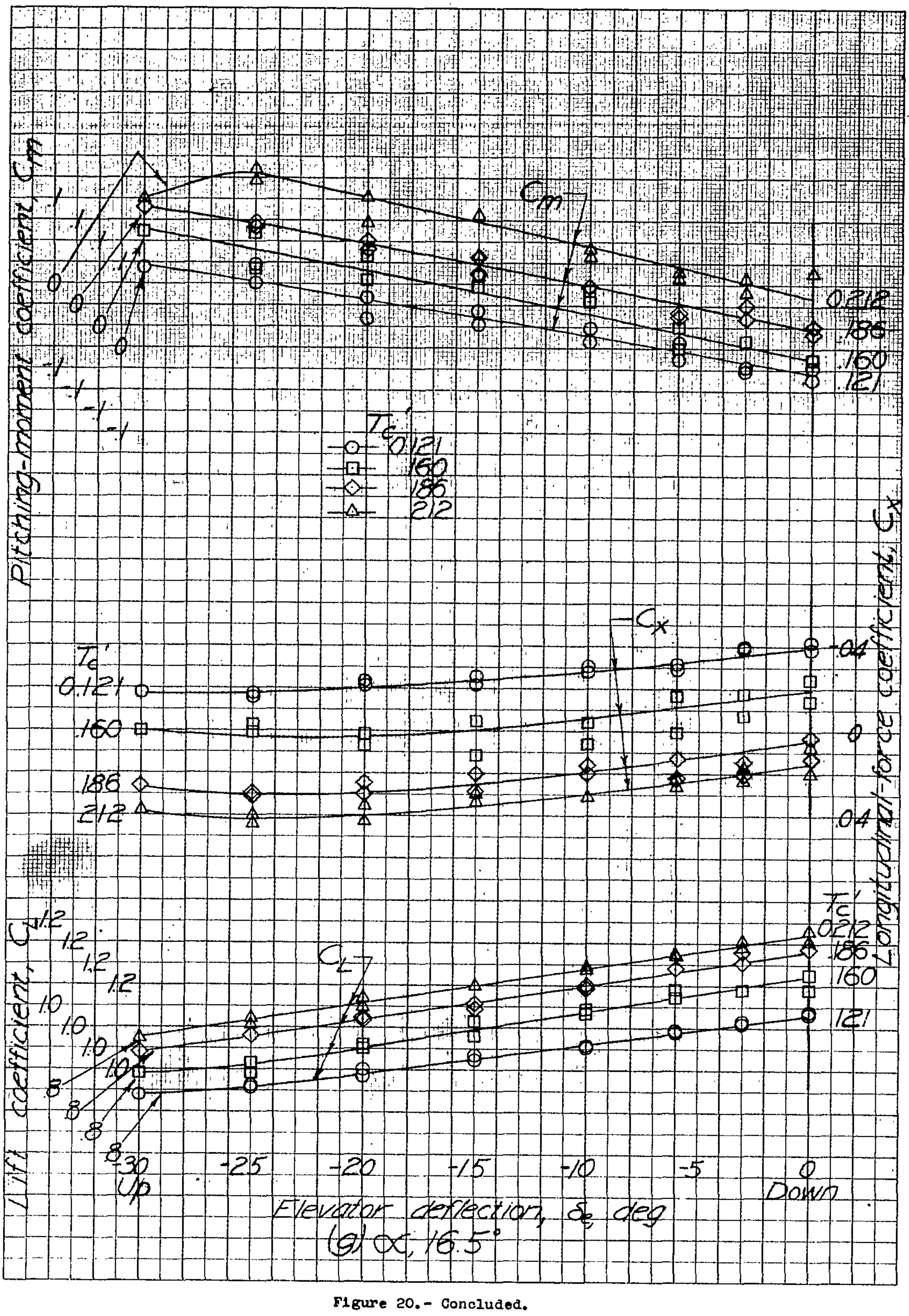

Figure 20.- Concluded.

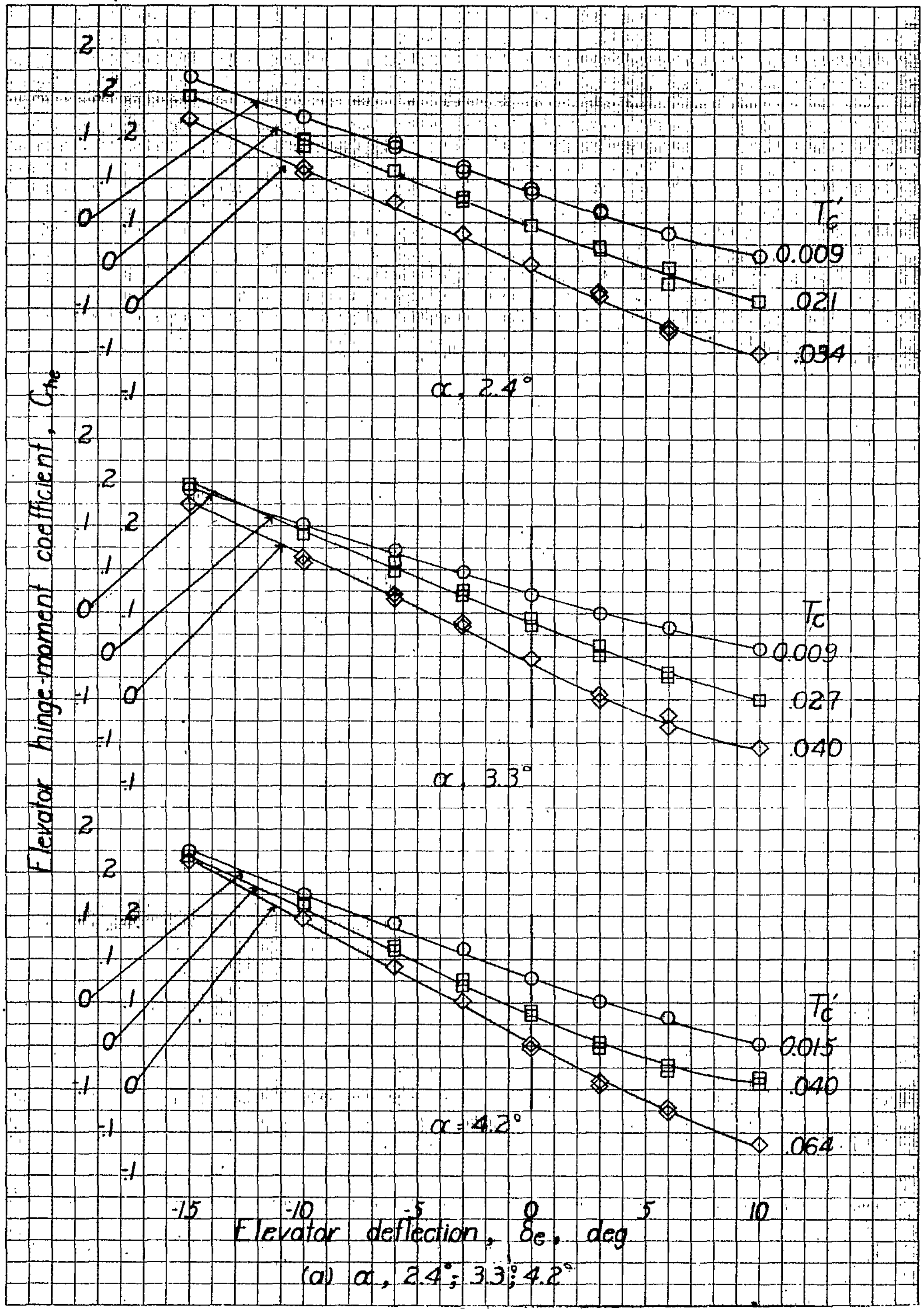

Figure 21.- Variation of C_{h_e} with elevator deflection for a range of thrust coefficients and angles of attack. δ_a, 0°; δ_r, 0°.

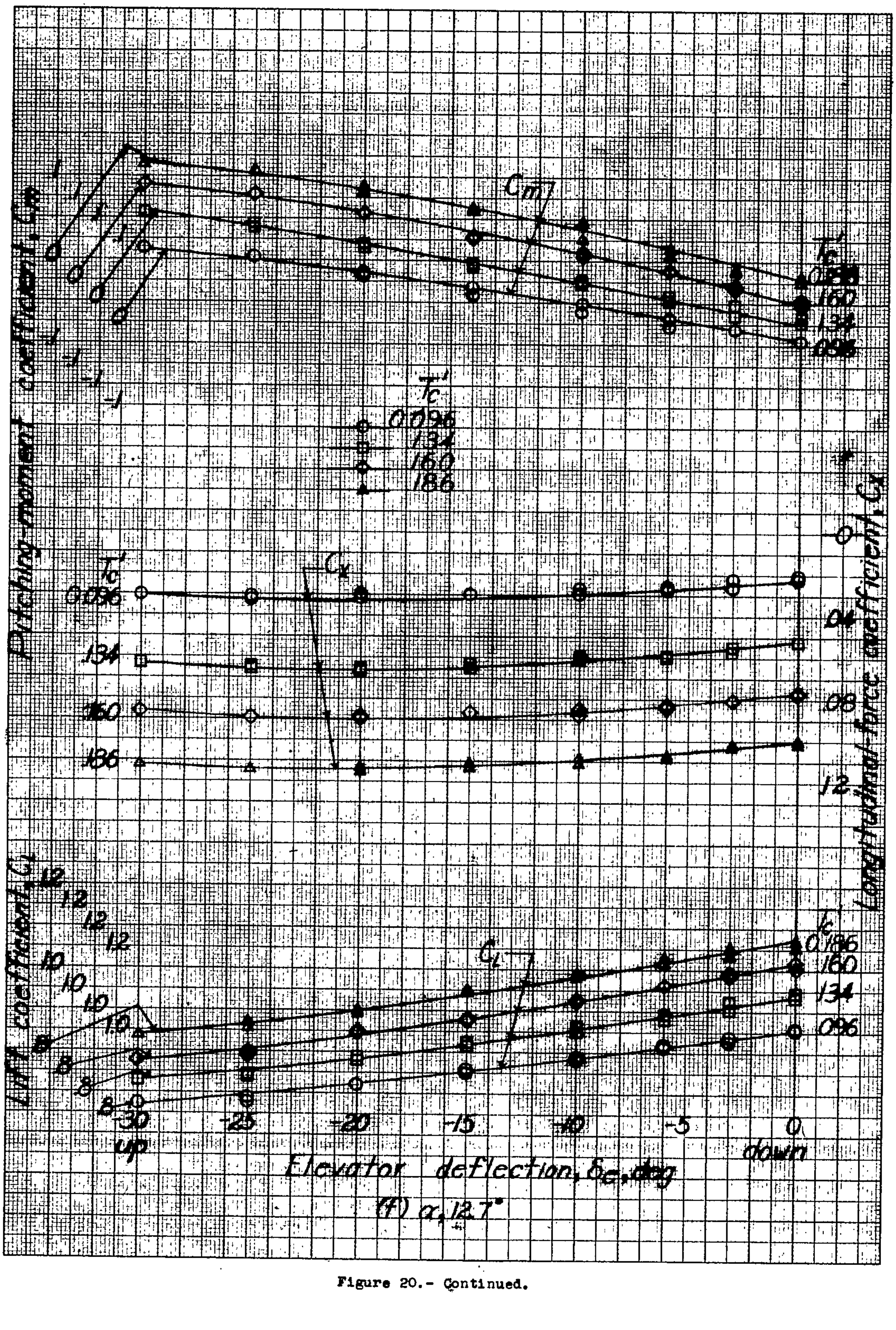

Figure 20.- Continued.

L-531

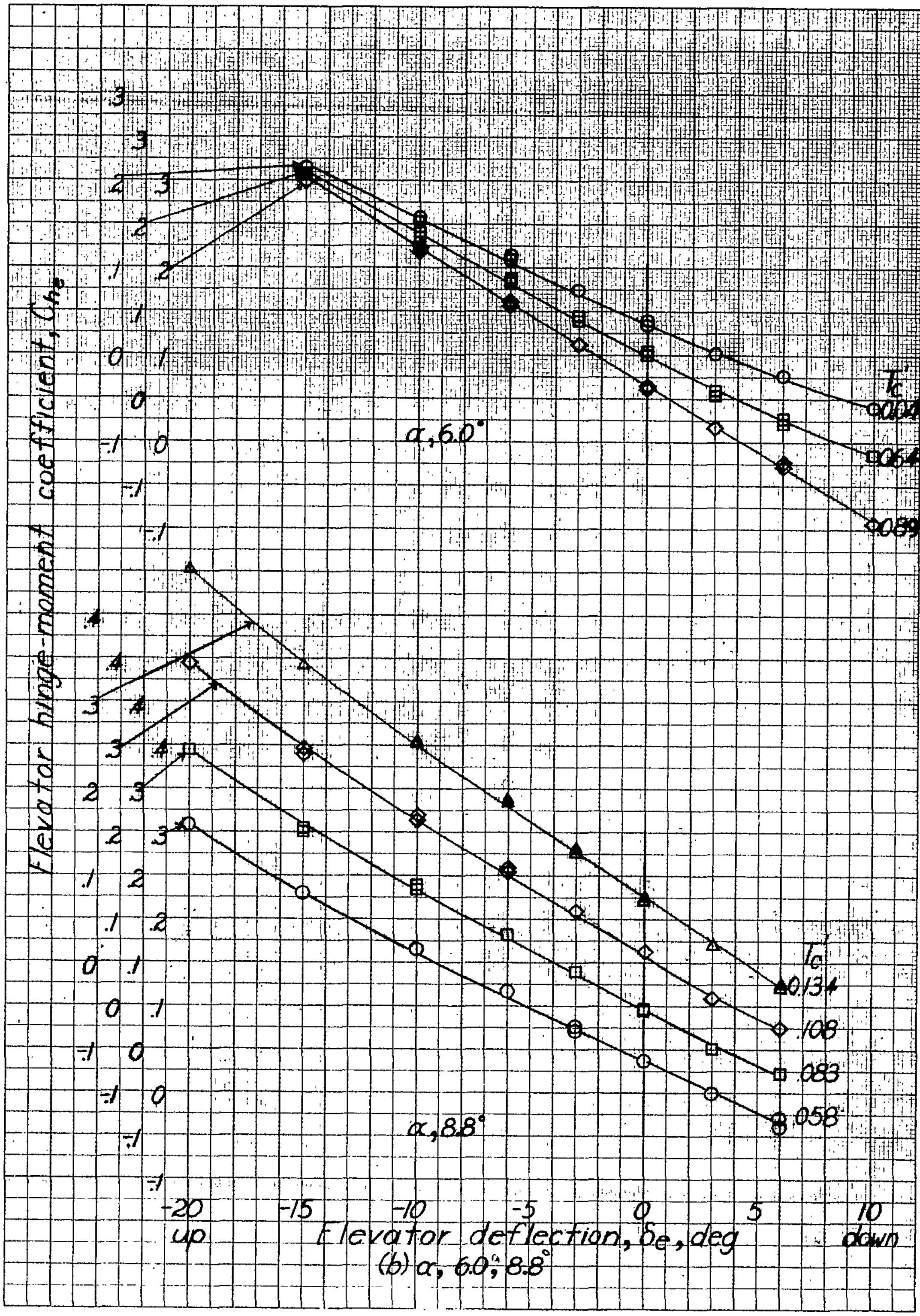

Figure 21.- Continued.

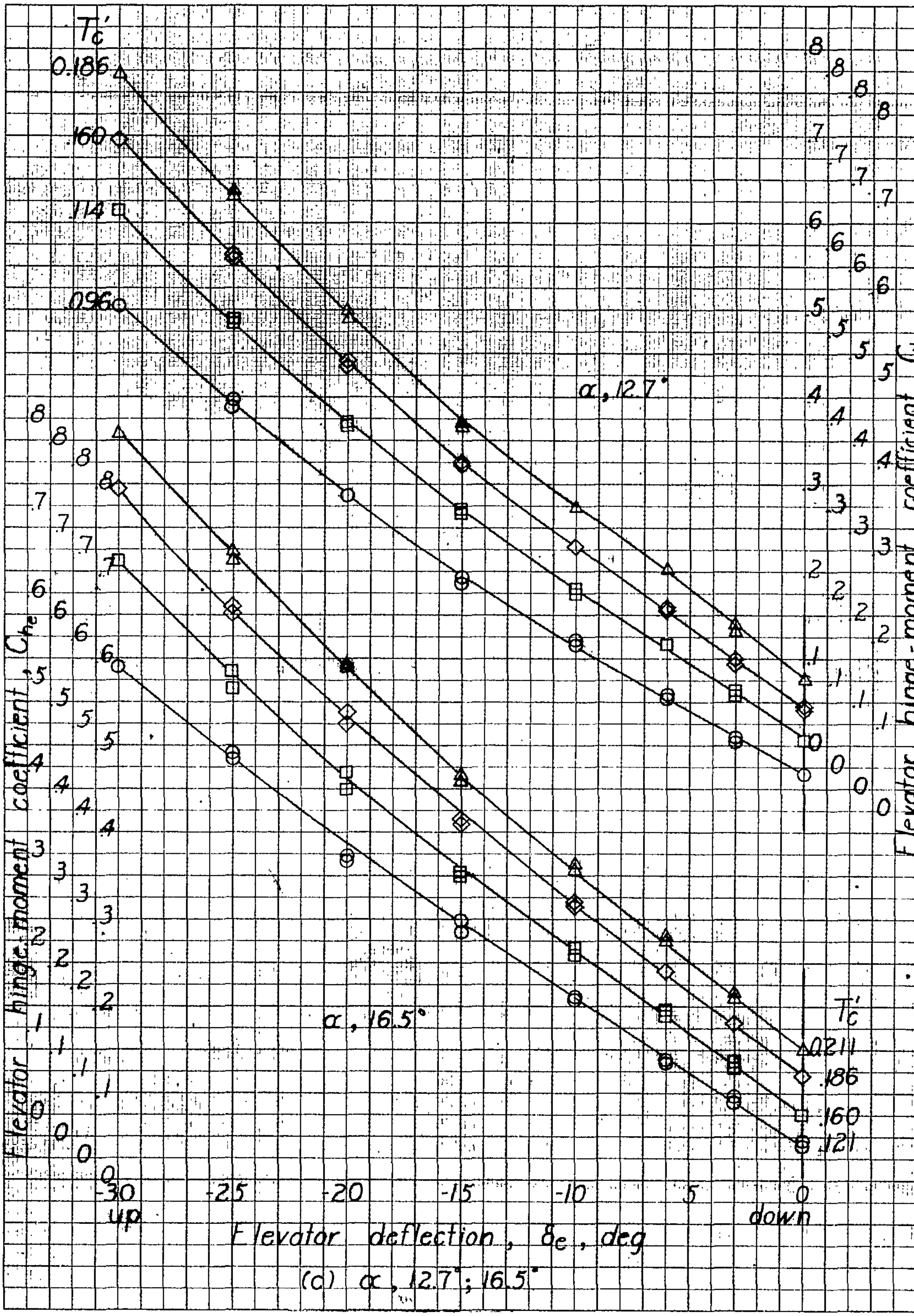

Figure 21.- Concluded.

L-531

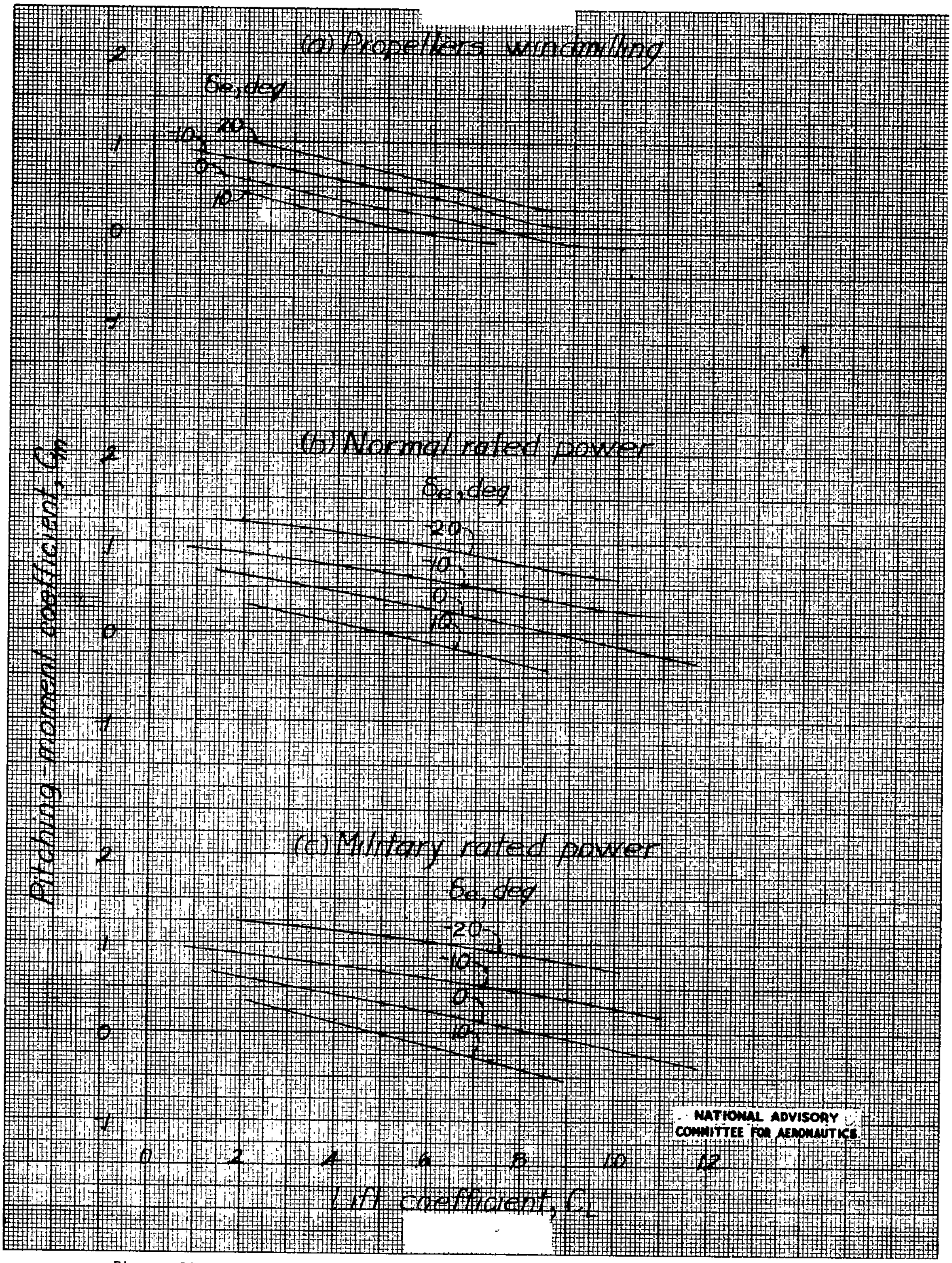

Figure 22.- Variation of C_m with C_L for a range of elevator deflections and power conditions. δ_a, 0°; δ_r, 0°. Elevators fixed.

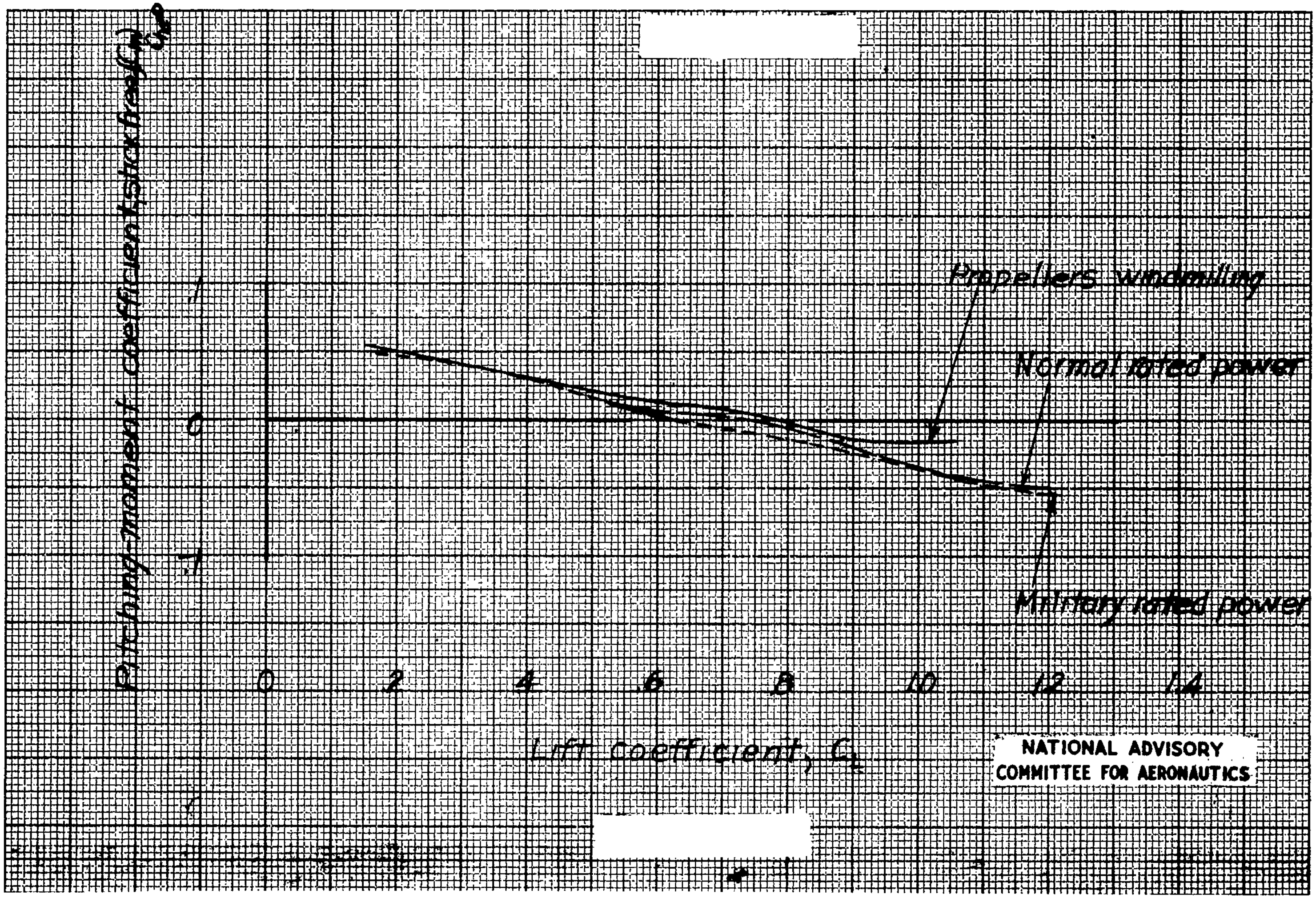

Figure 23.- Variation of C_m with C_L for a range of power conditions. Elevator free.

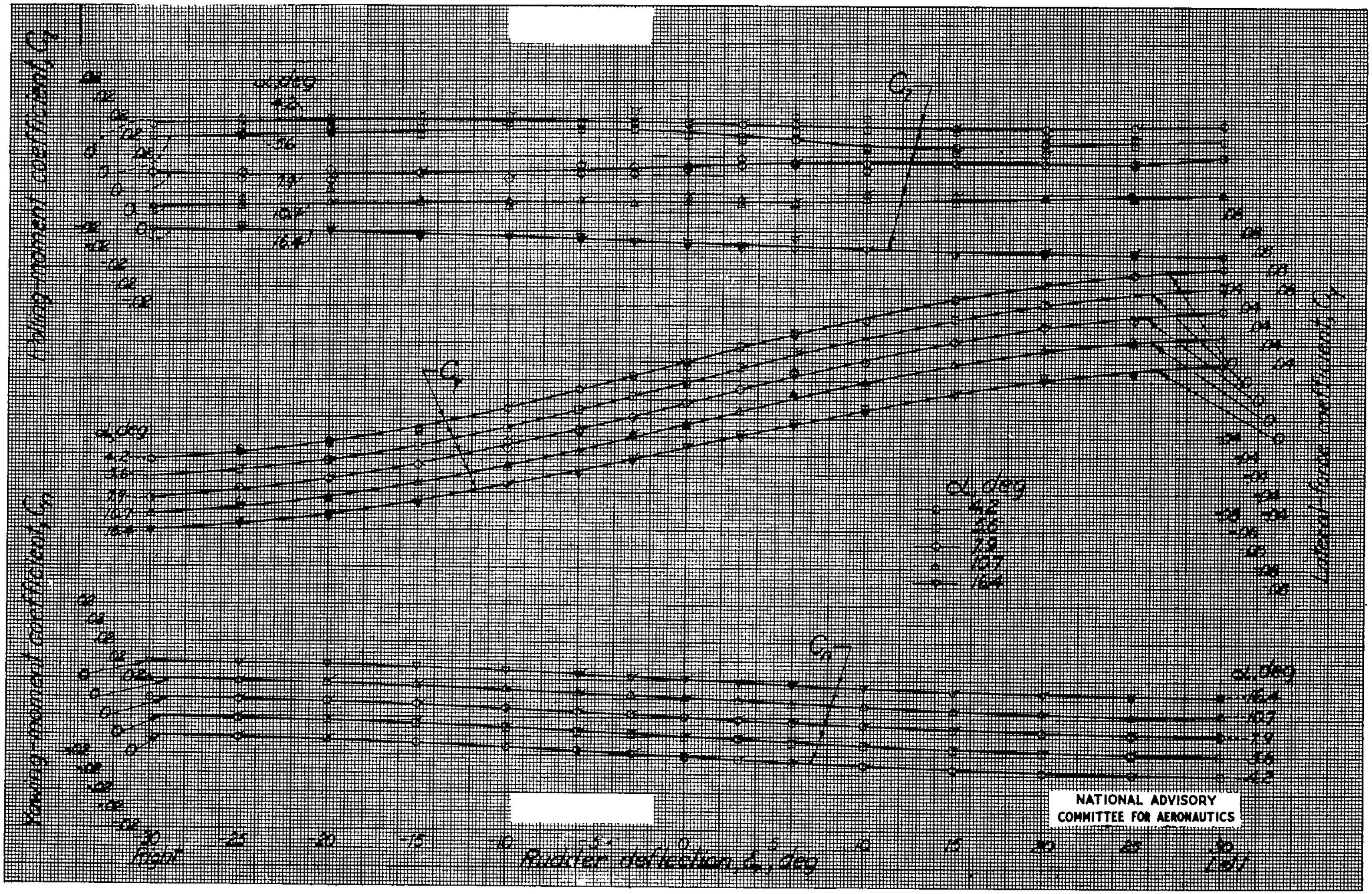

(a) Propellers windmilling.

Figure 24.- Effect of rudder deflection on the aerodynamic characteristics of the model for varied power conditions. ψ, 0°; δ_a, 0°; δ_e, 0°.

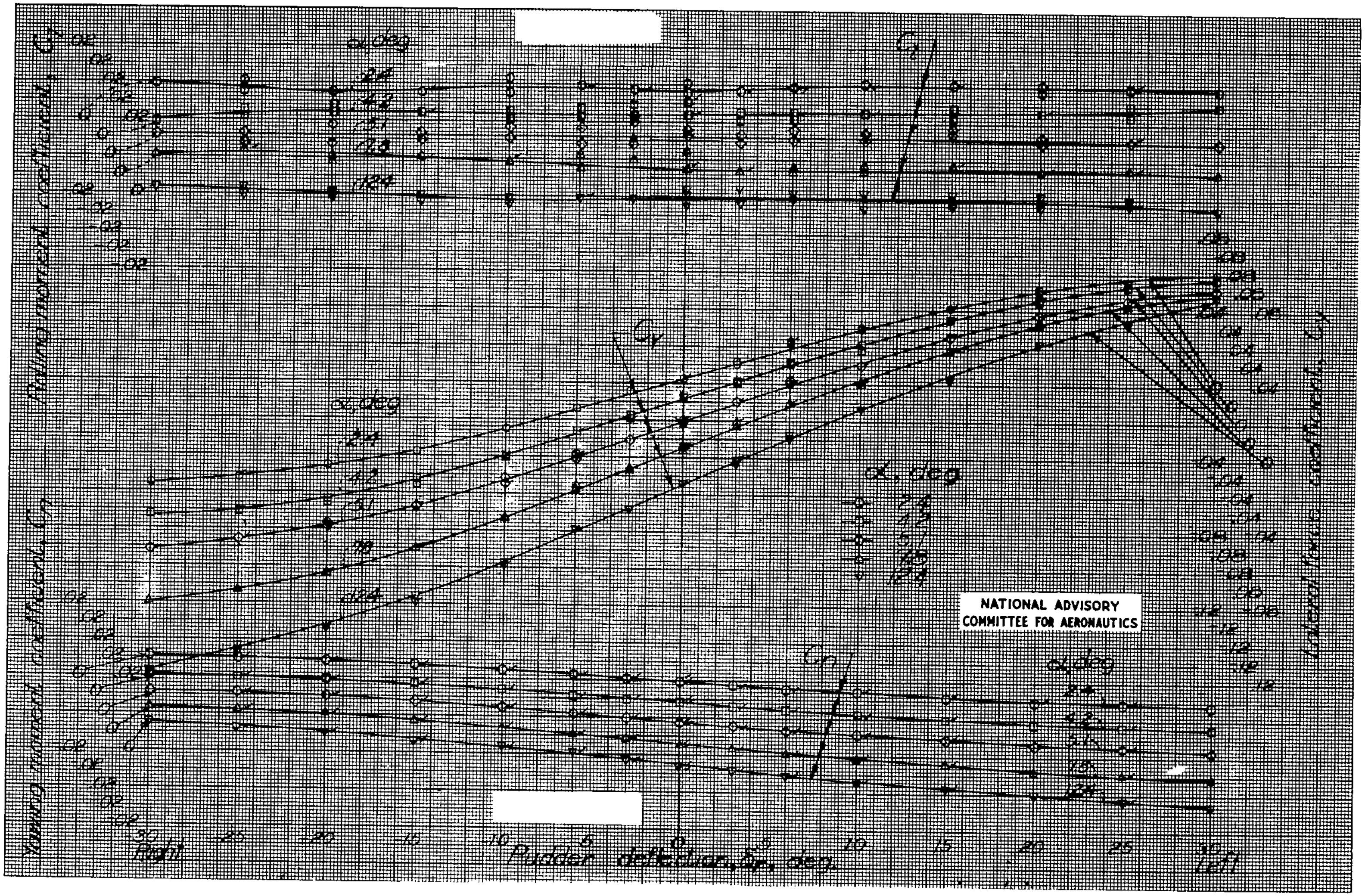

(b) Normal-rated power.

Figure 24.- Continued.

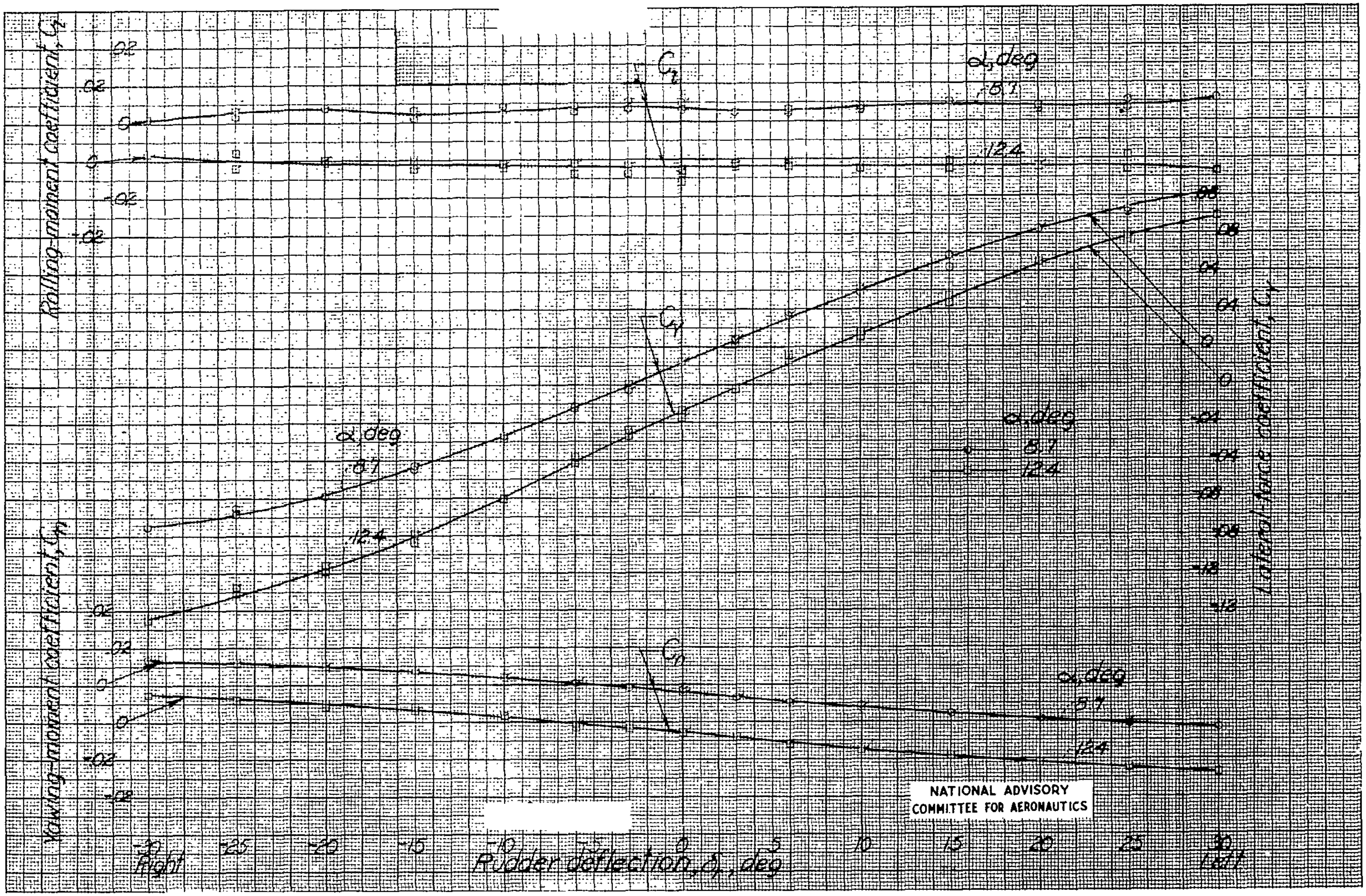

(c) Military-rated power.

Figure 24.- Continued.

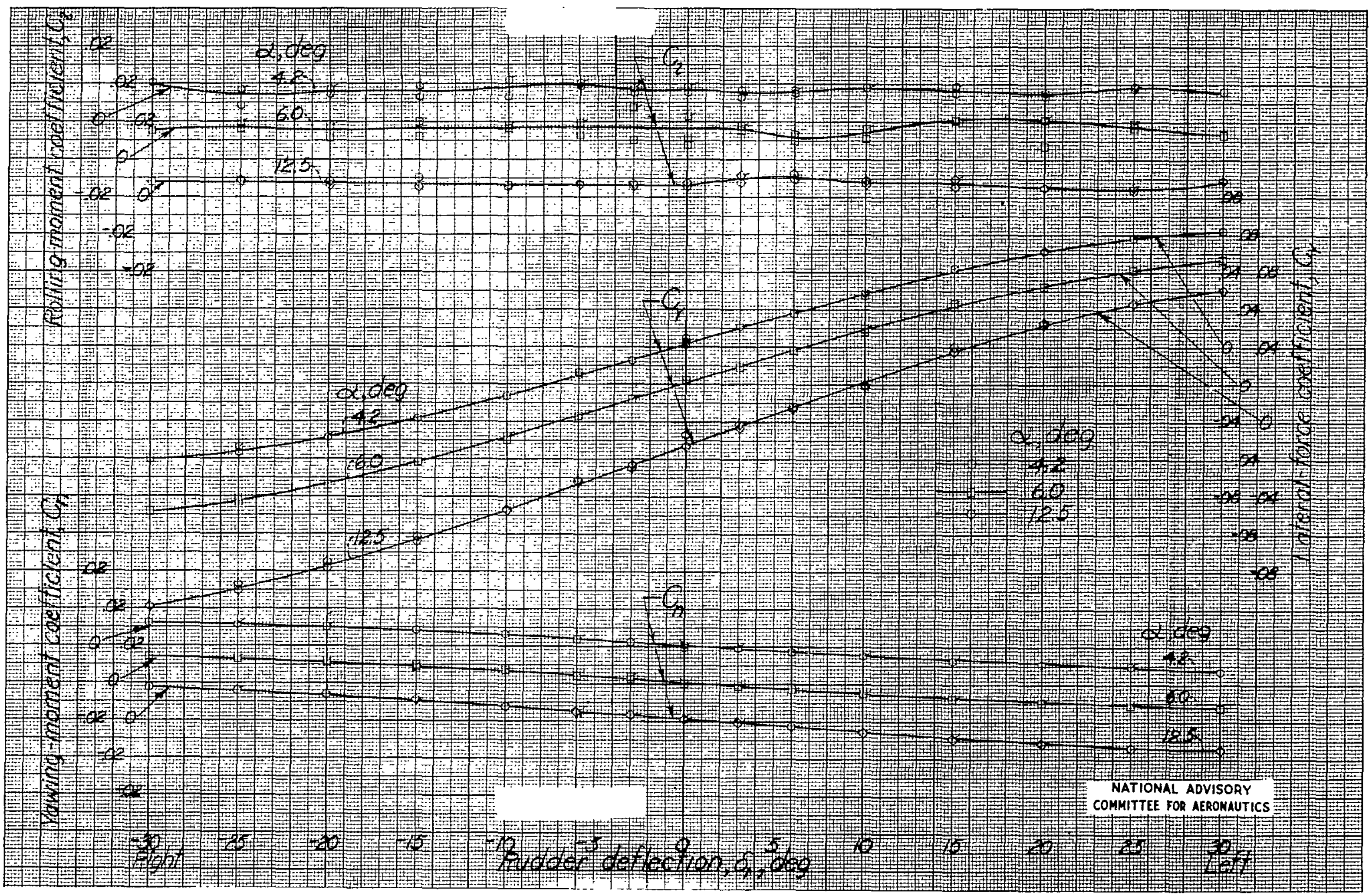

(d) Asymmetric power.

Figure 24.- Concluded.

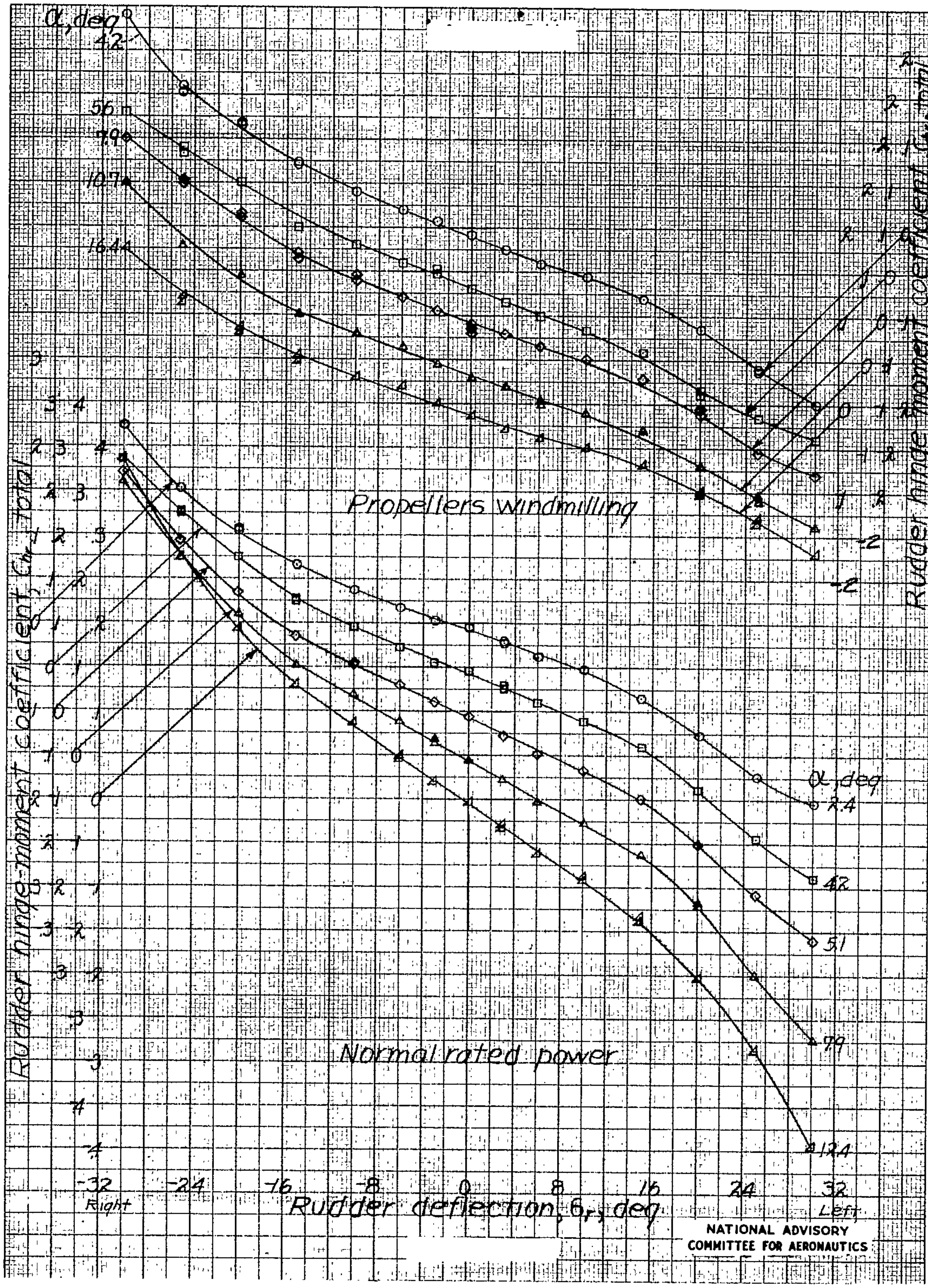

Figure 25.- Effect of rudder deflection on the rudder hinge-moment coefficients for varied power conditions. ψ, 0°; δ_a, 0°; δ_e, 0°.

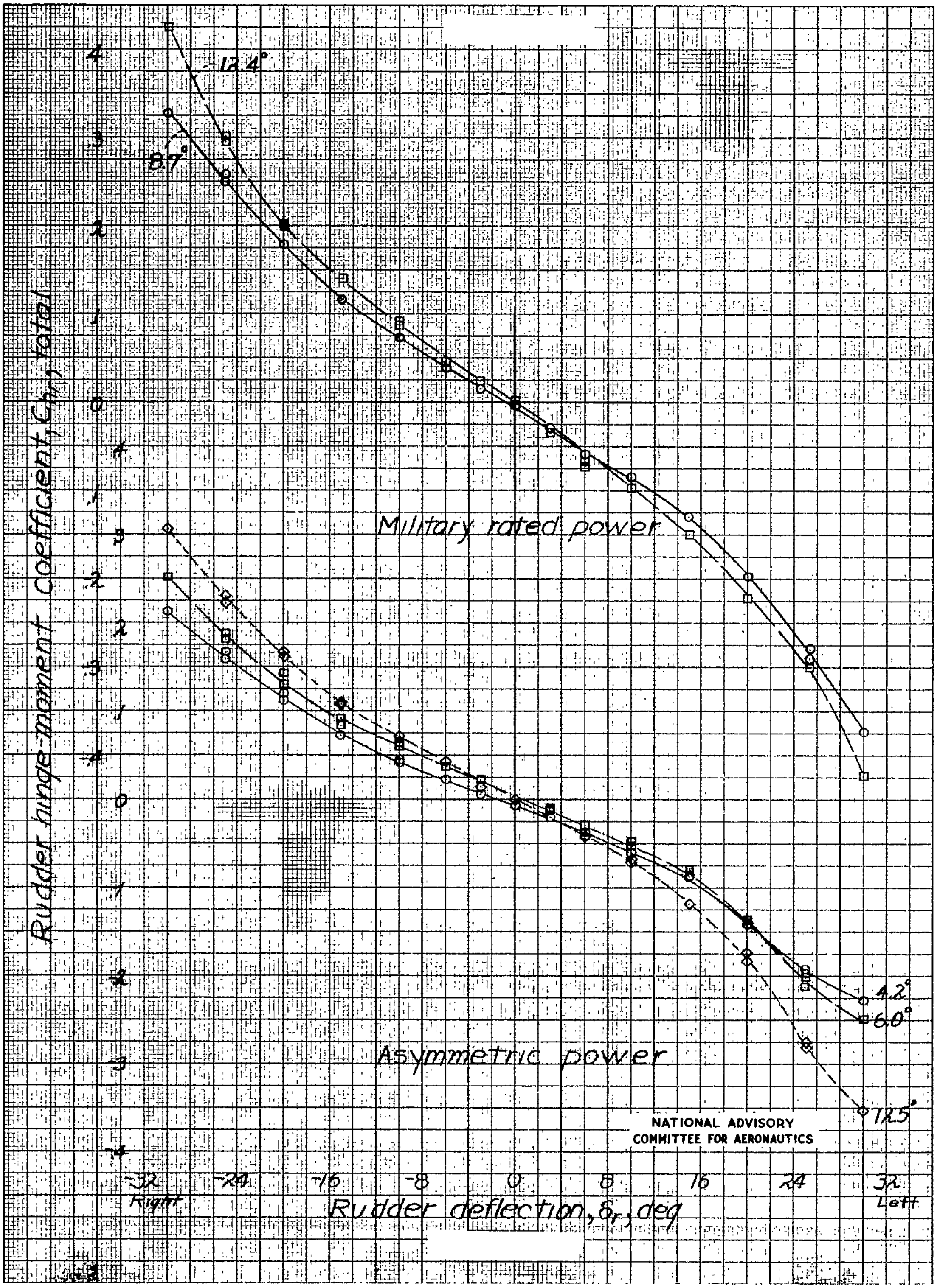

Figure 25.- Concluded.

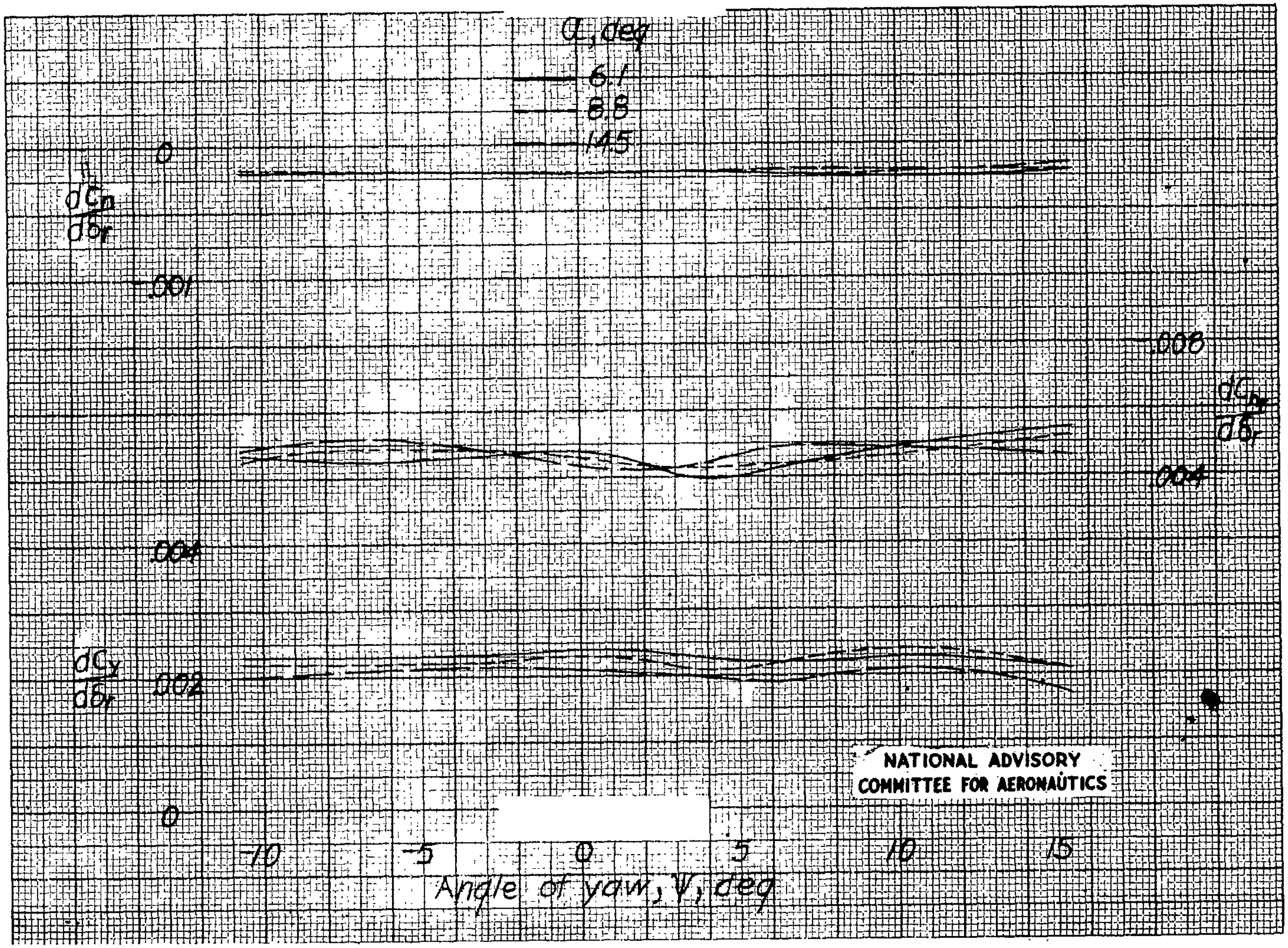

(a) Propellers windmilling.

Figure 26.- Effect of angle of attack and propeller operation on the variations of $\frac{dC_n}{d\delta_r}$, $\frac{dC_{h_r}}{d\delta_r}$, and $\frac{dC_Y}{d\delta_r}$, with angle of yaw.

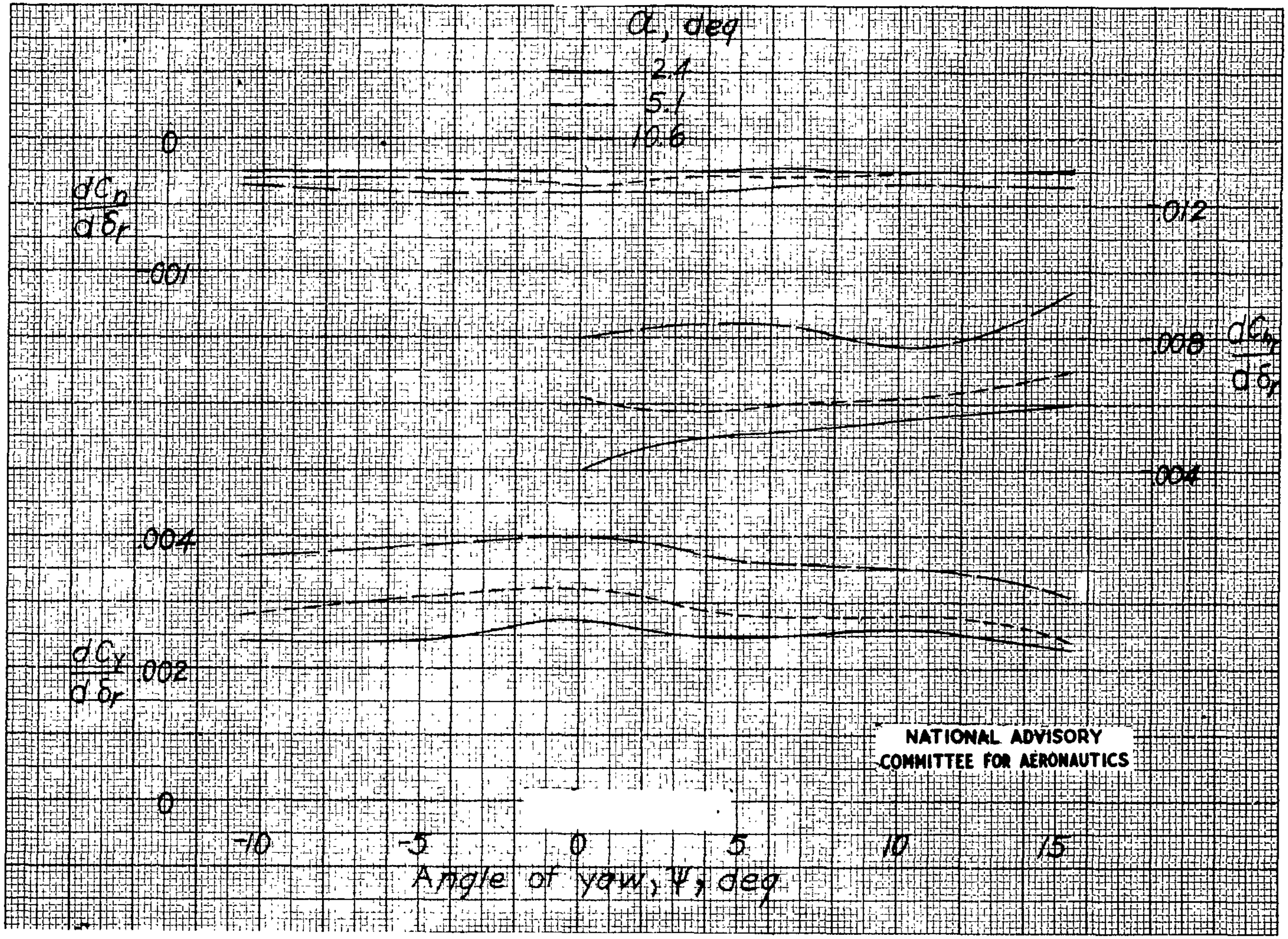

(b) Normal-rated power.

Figure 26.- Continued.

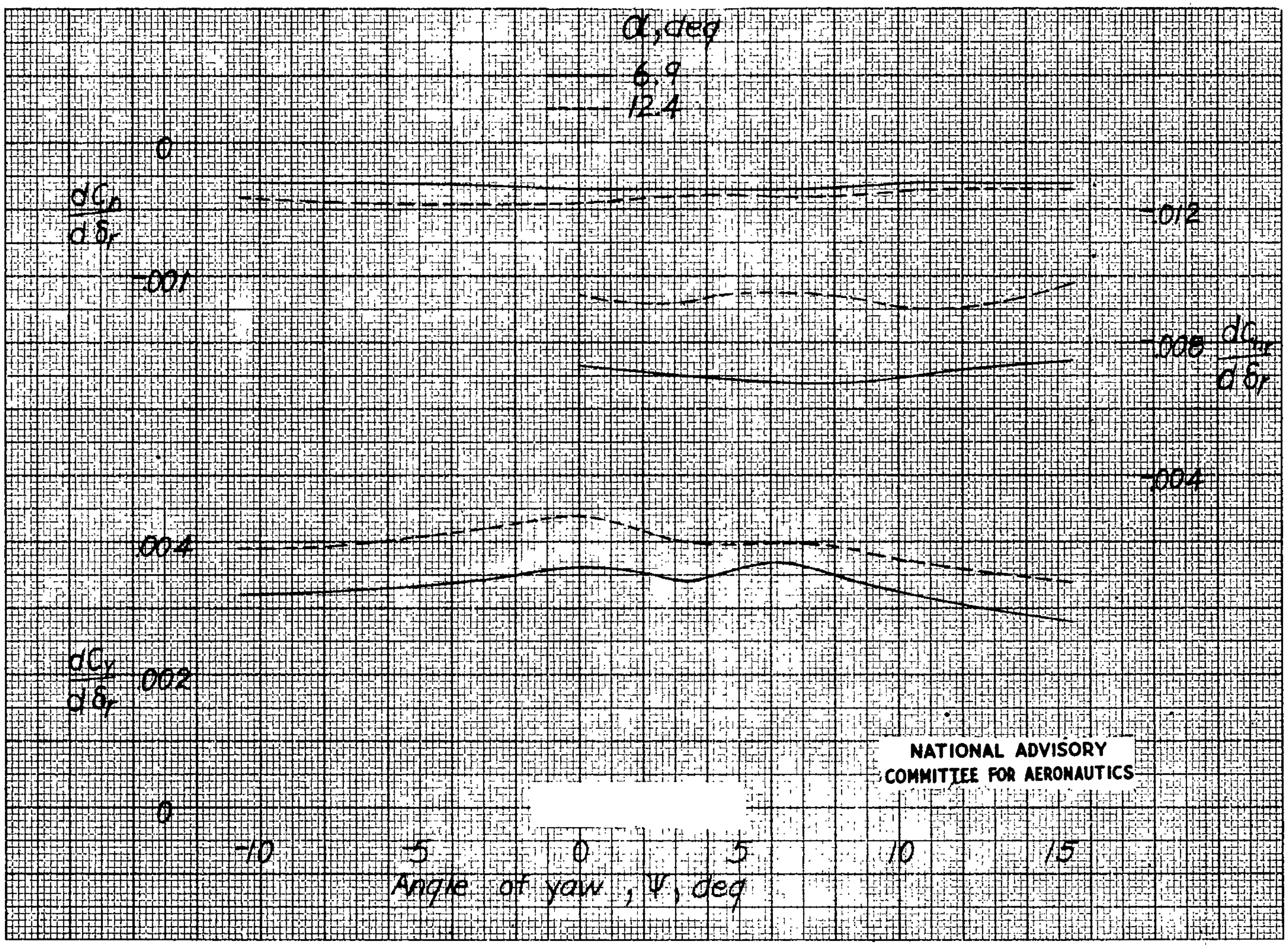

(c) Military-rated power.

Figure 26.- Continued.

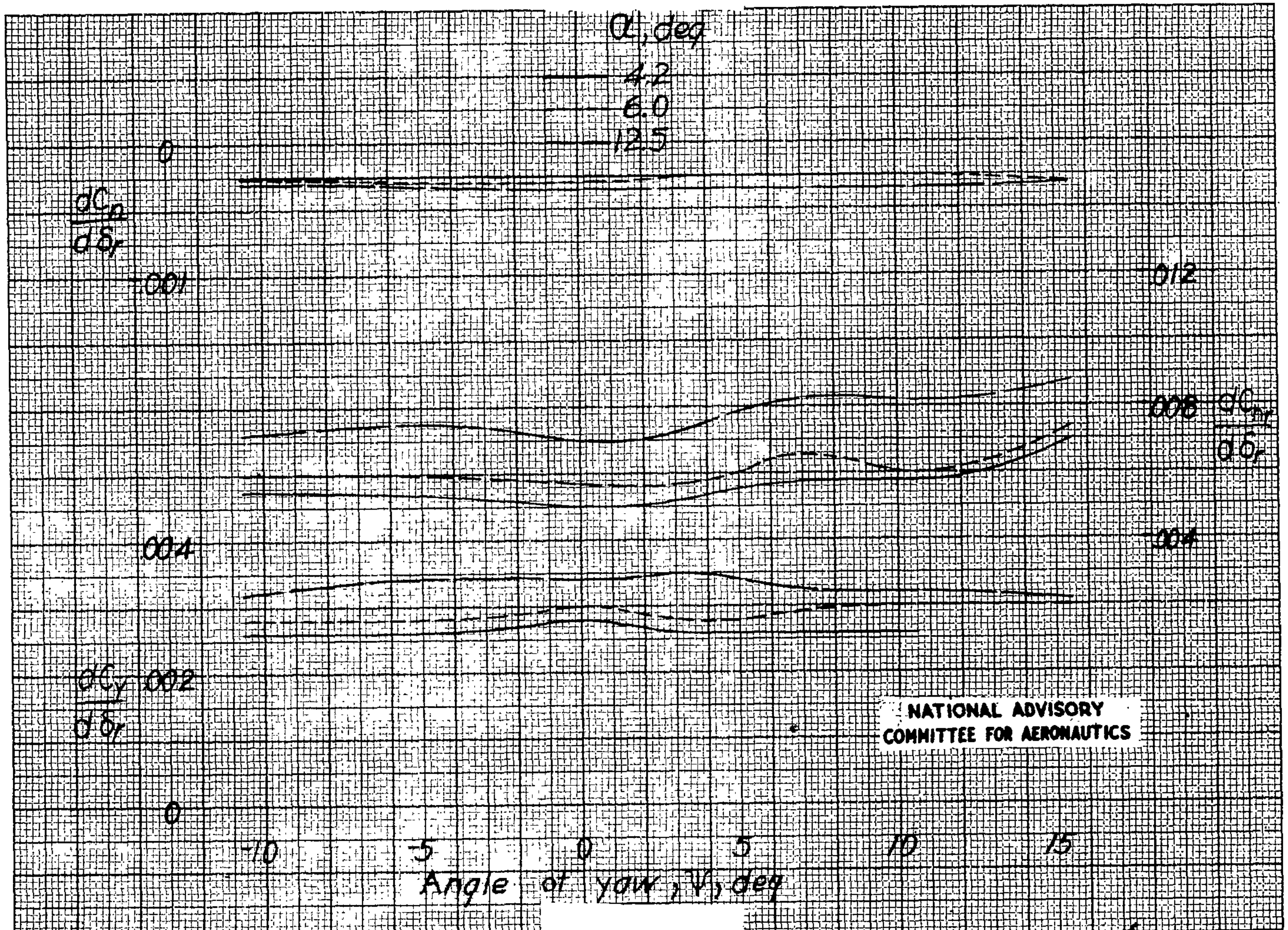

(d) Asymmetric power.

Figure 26.- Concluded.

CONFIDENTIAL

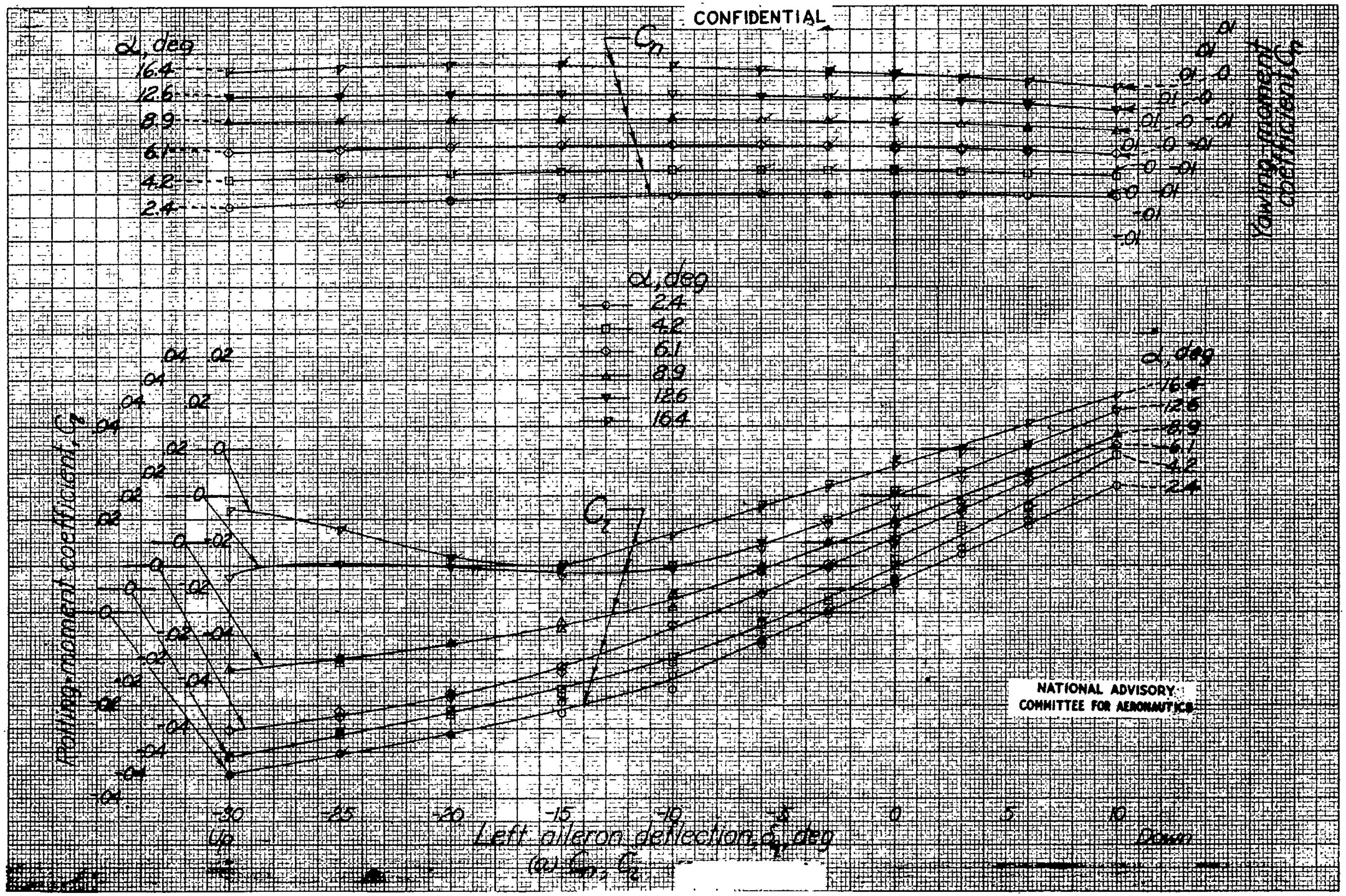

Figure 27.- Effect of aileron deflection on the aerodynamic characteristics of the model. Propellers removed; ψ, 0°; δ_e, 0°; δ_r, 0°.

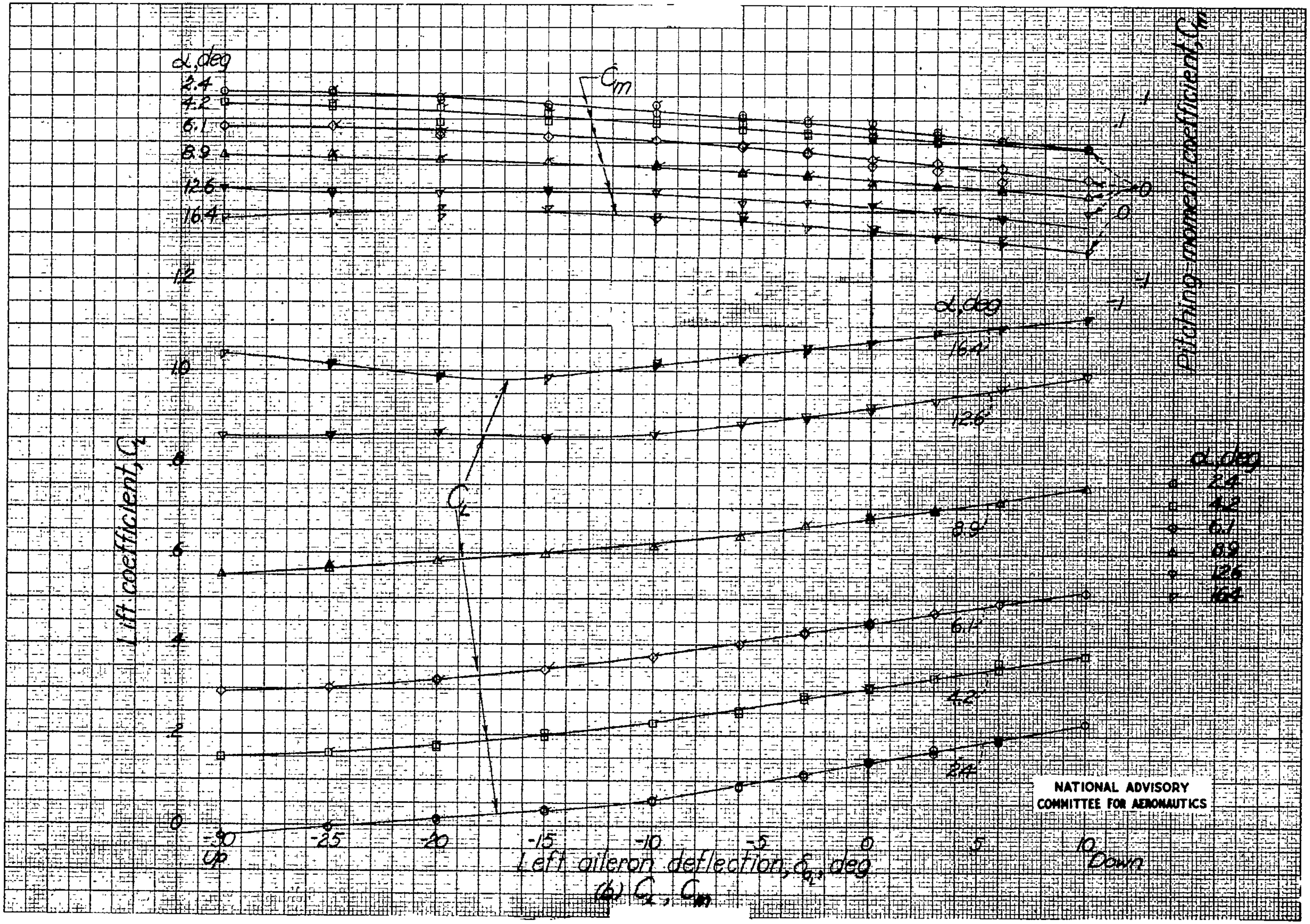

Figure 27.- Continued.

MR No. L6C13

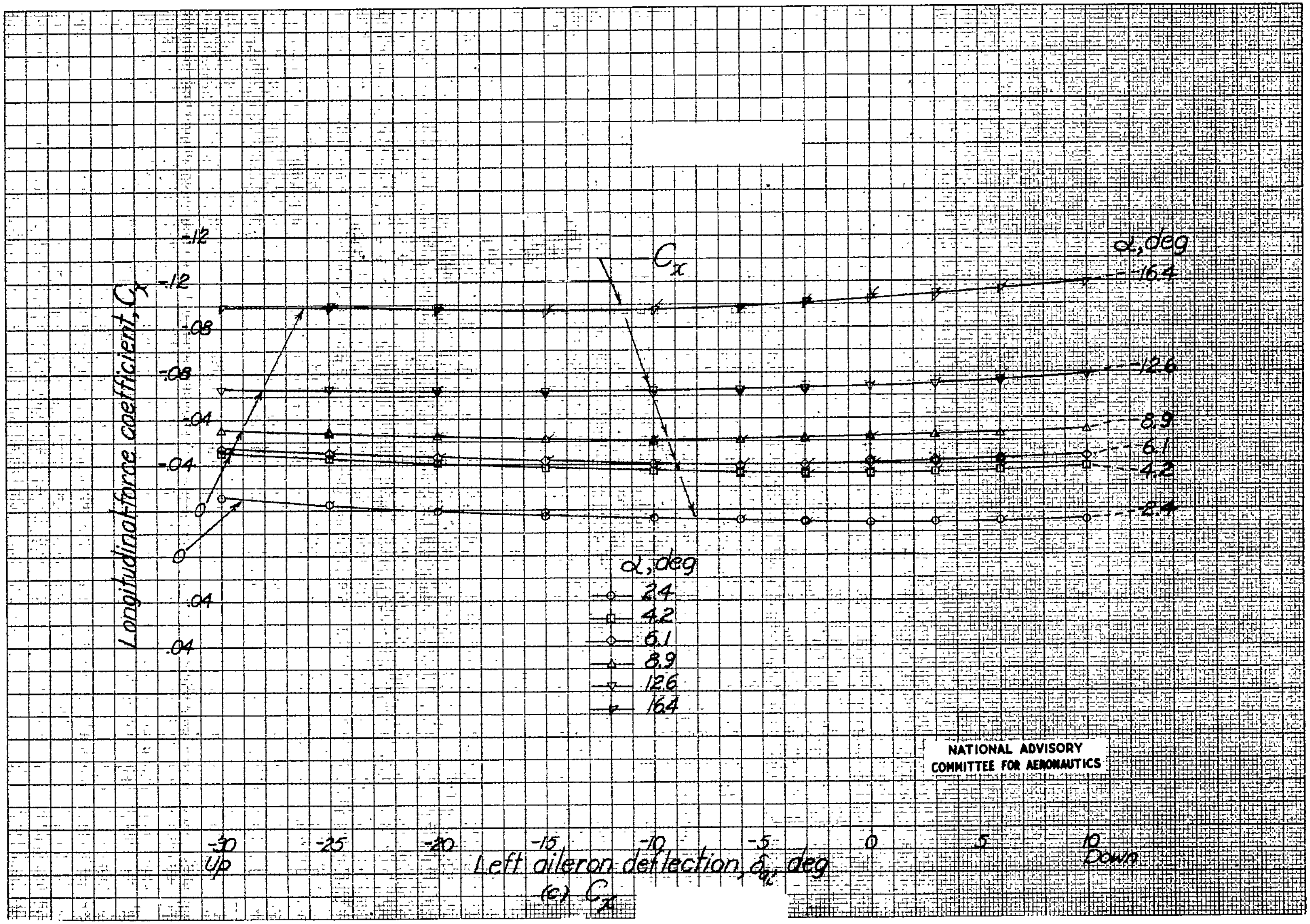

(c) C_X

Figure 27.- Continued.

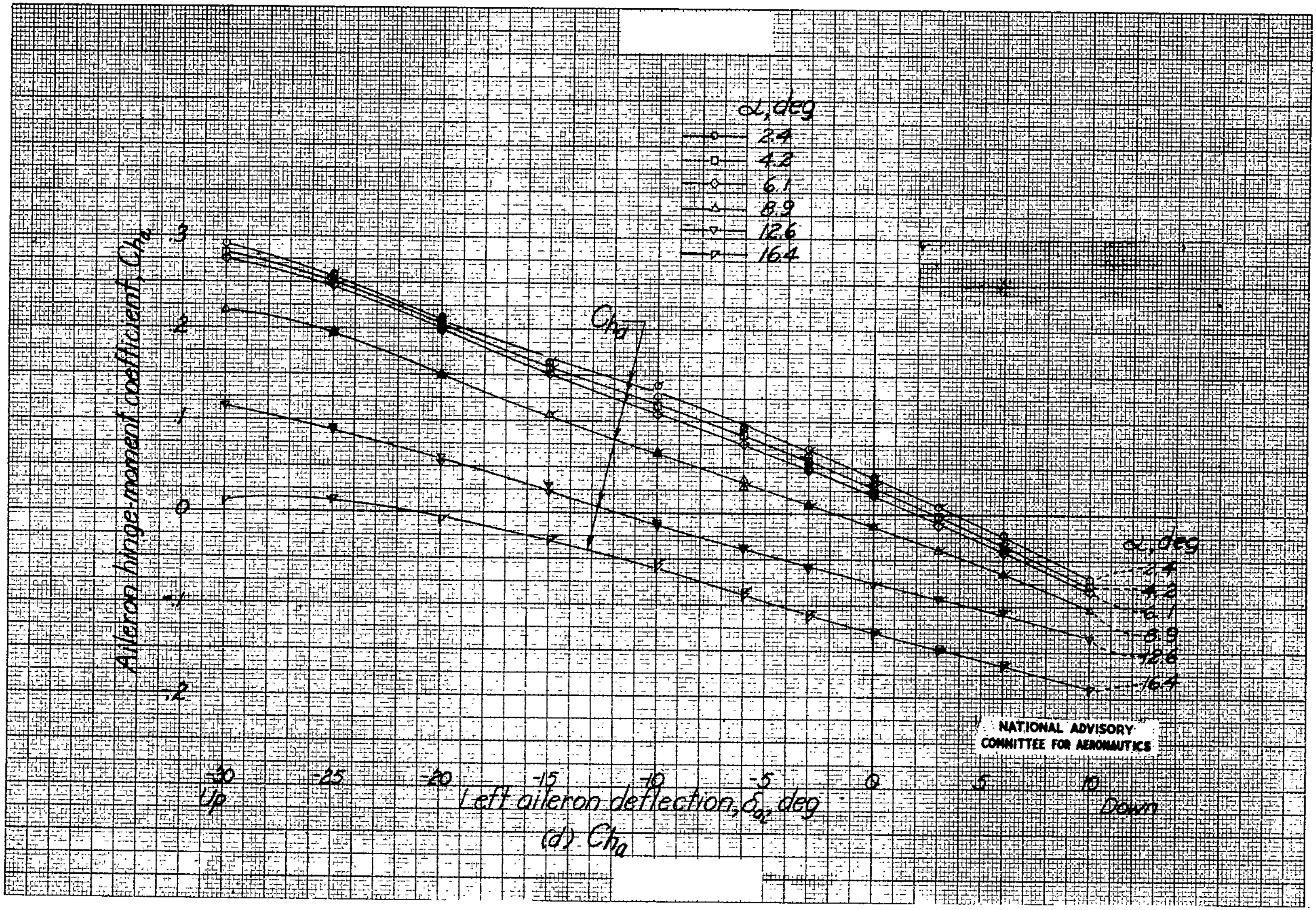

Figure 27.- Concluded.

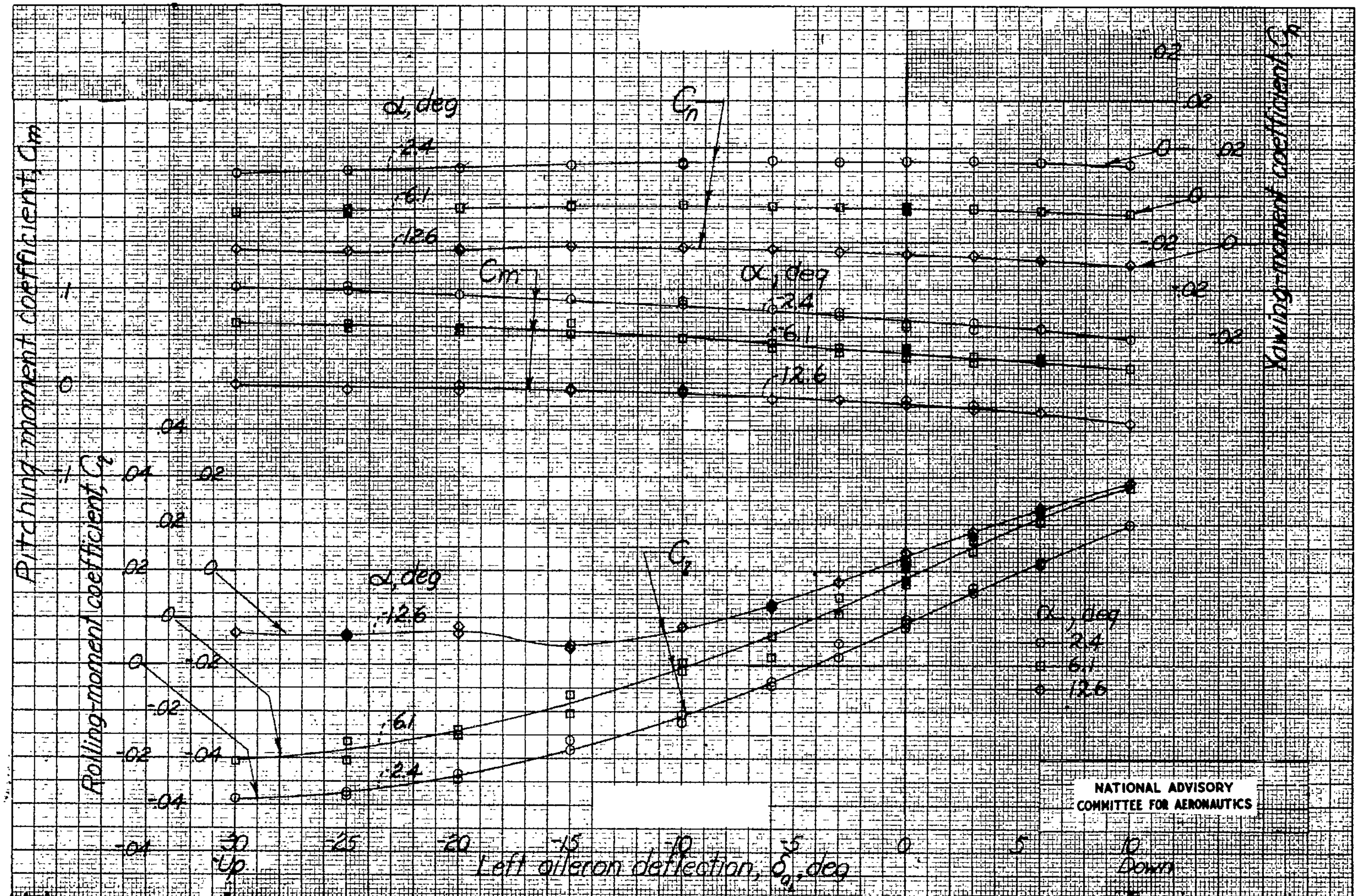

(a) ψ, 6.3°.

Figure 28.- Effect of aileron deflection on the aerodynamic characteristics of the model in yaw. Propellers windmilling; δ_e, 0°; δ_r, 0°.

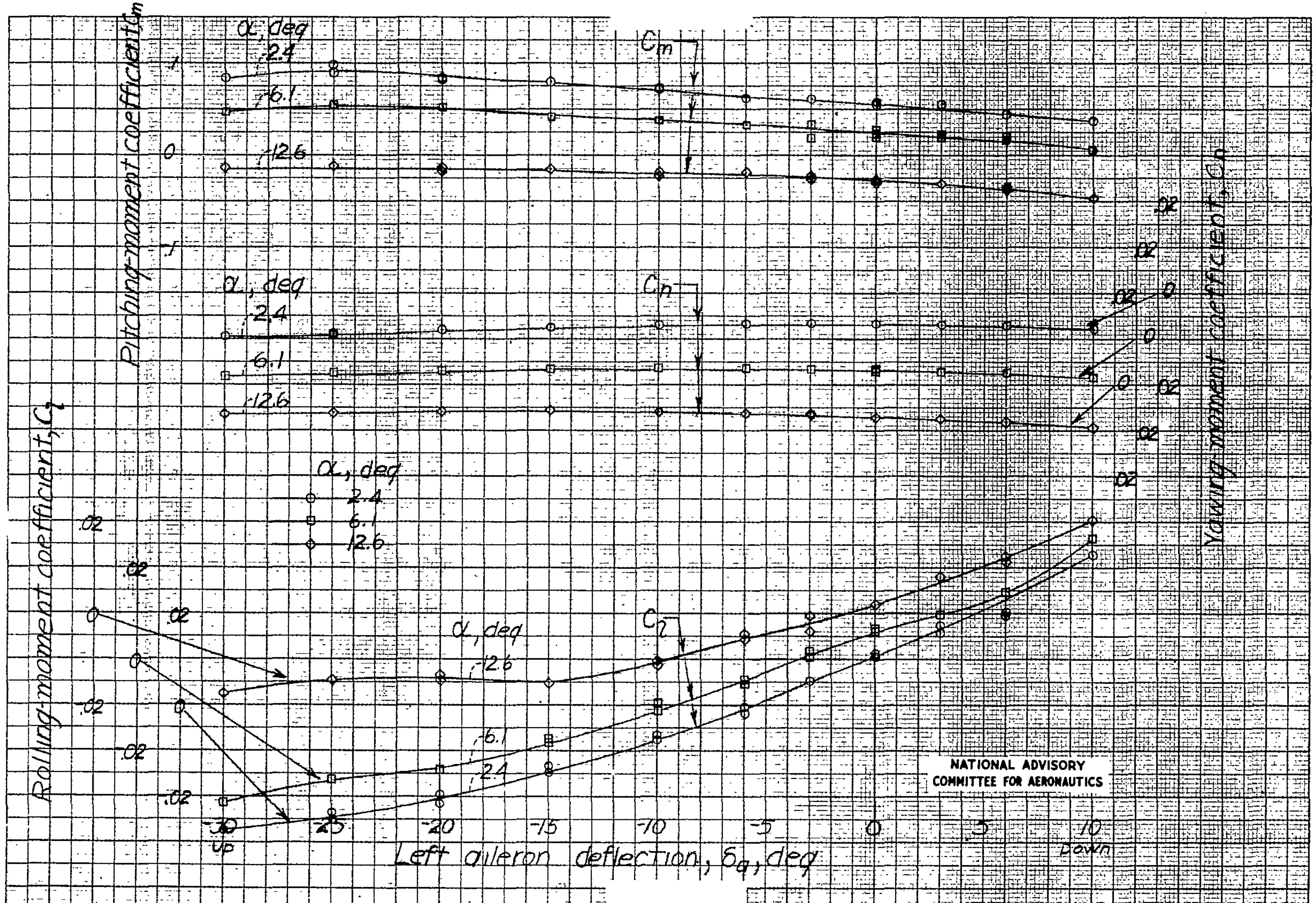

(c) ψ, 15.4°.

Figure 28.- Continued.

MR No. L6C13

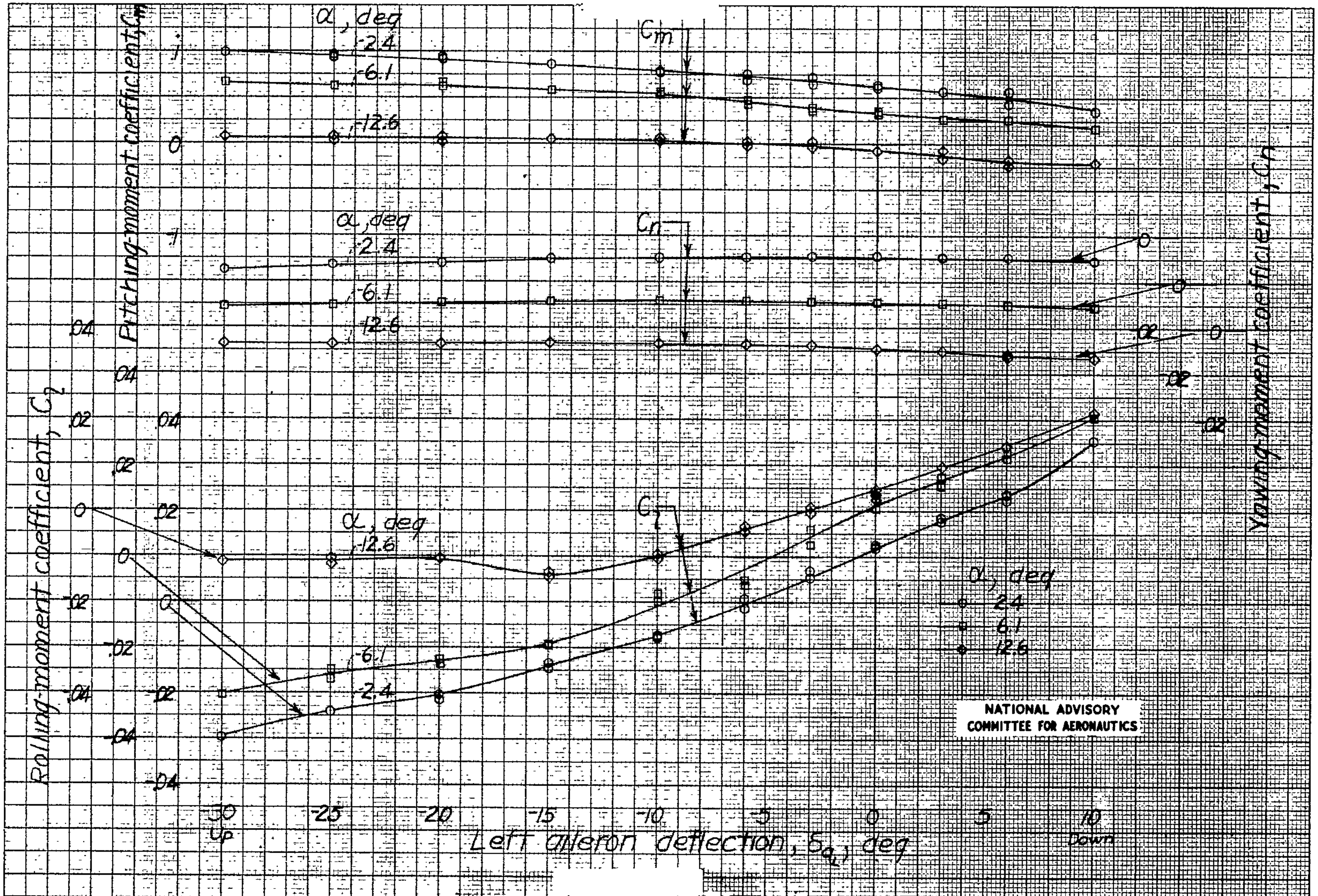

(b) ψ, 10.6°.

Figure 28.- Continued.

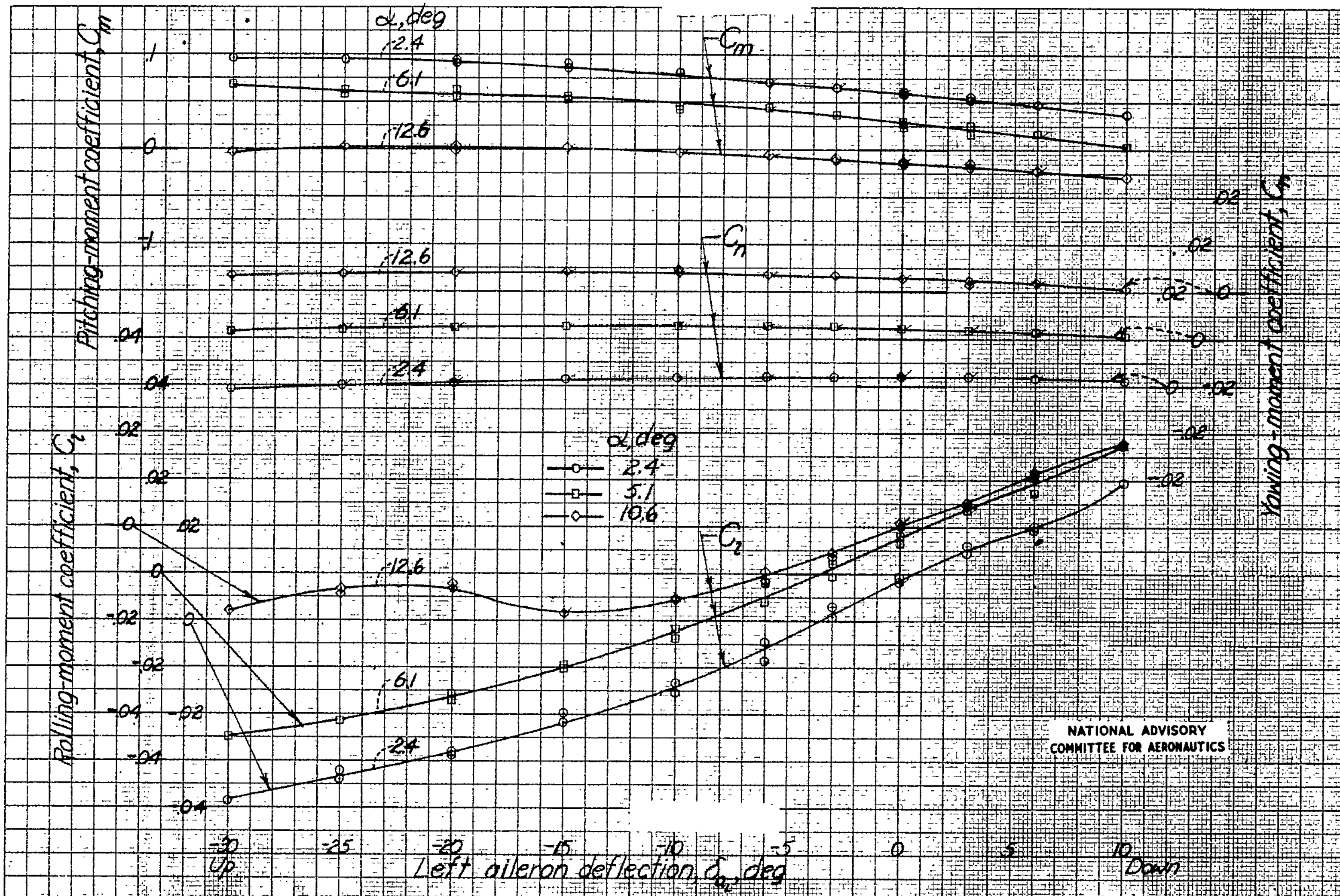

(d) ψ, -6.4°.

Figure 28.- Continued.

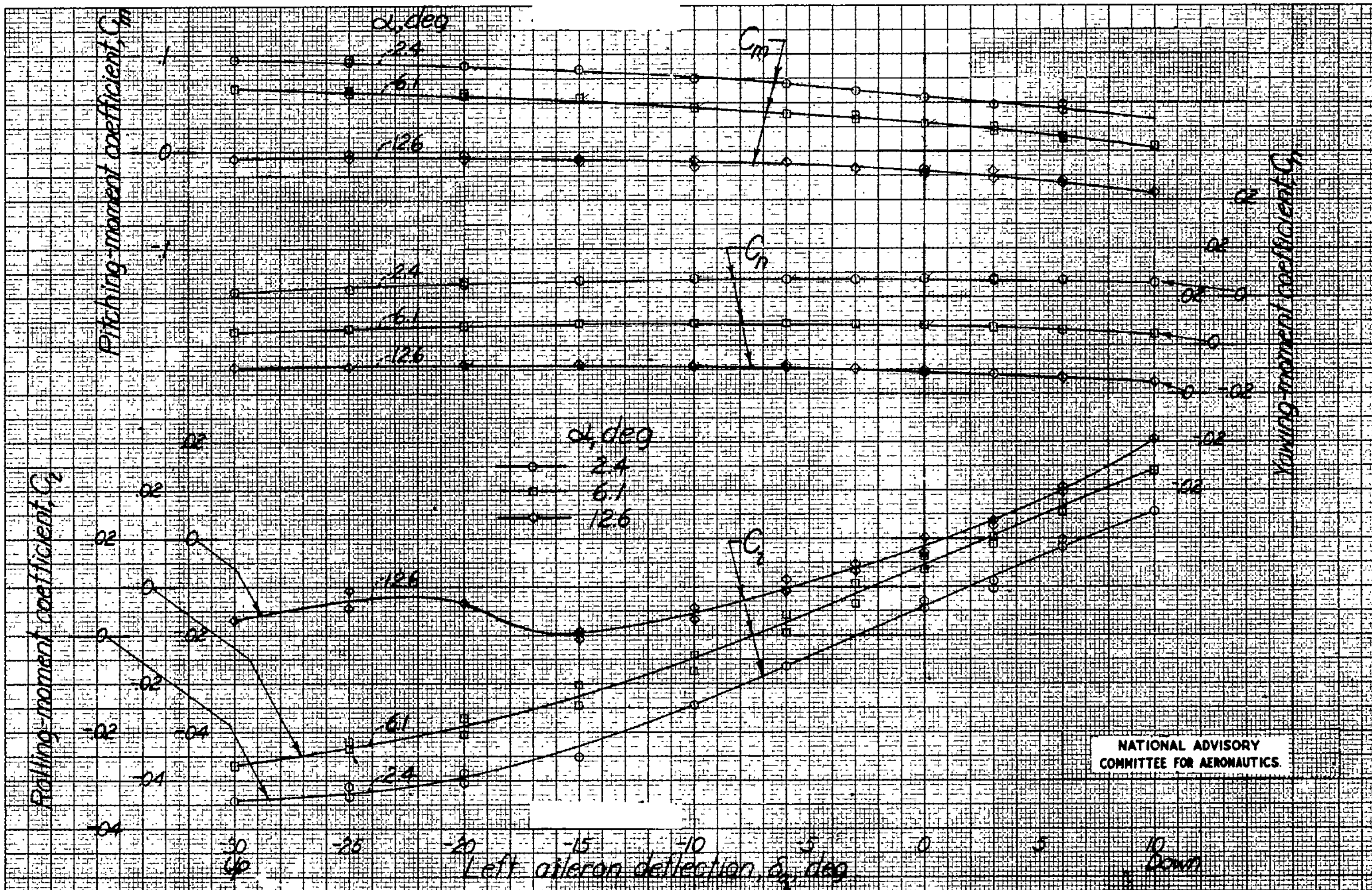

(e) ψ, -10.6°.

Figure 28.- Concluded.

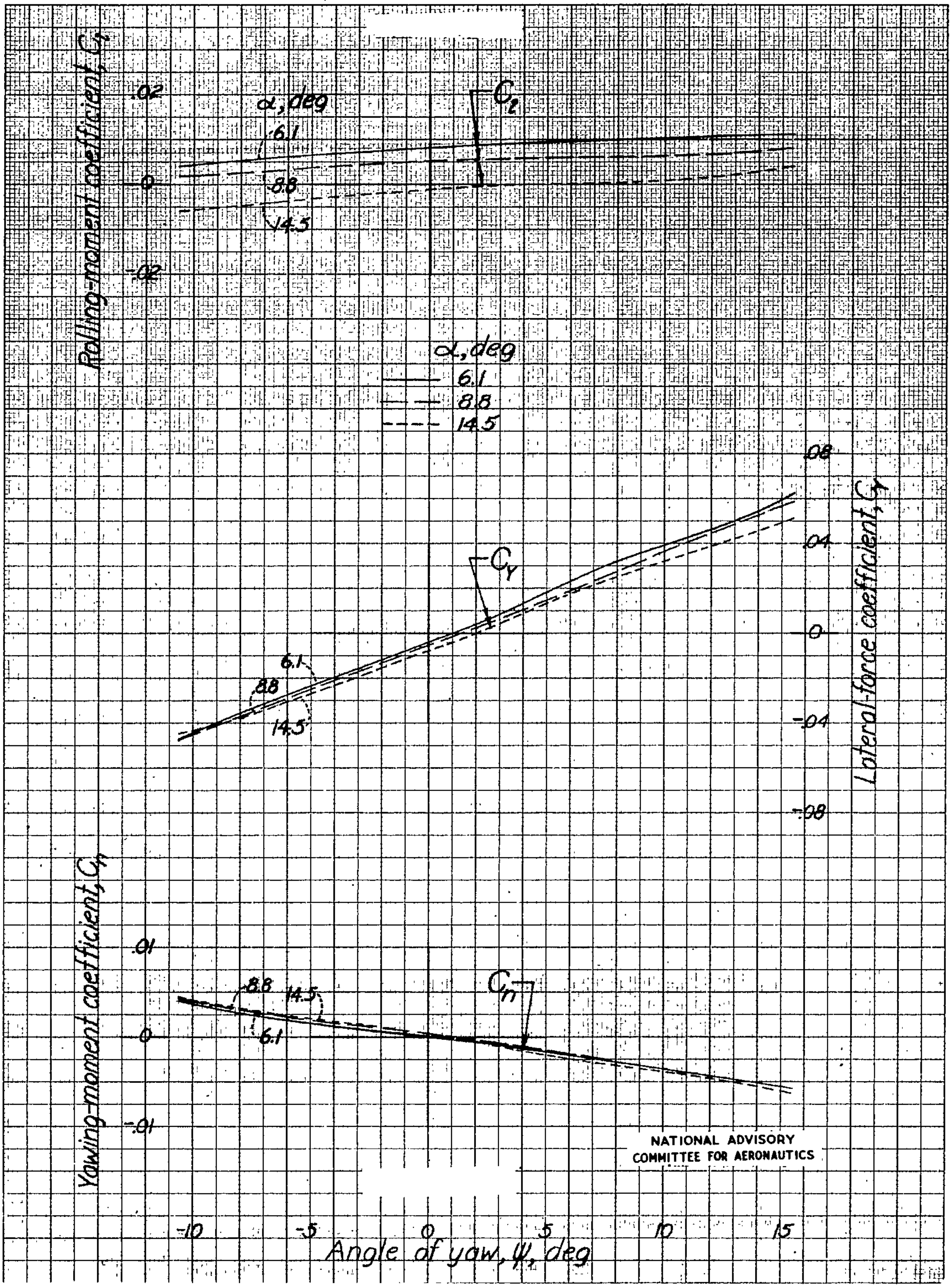

(a) Propellers windmilling.

Figure 29.- Variation of C_n, C_Y, and C_l with angle of yaw for varied power conditions. δ_r, 0°; δ_a, 0°; δ_e, 0°.

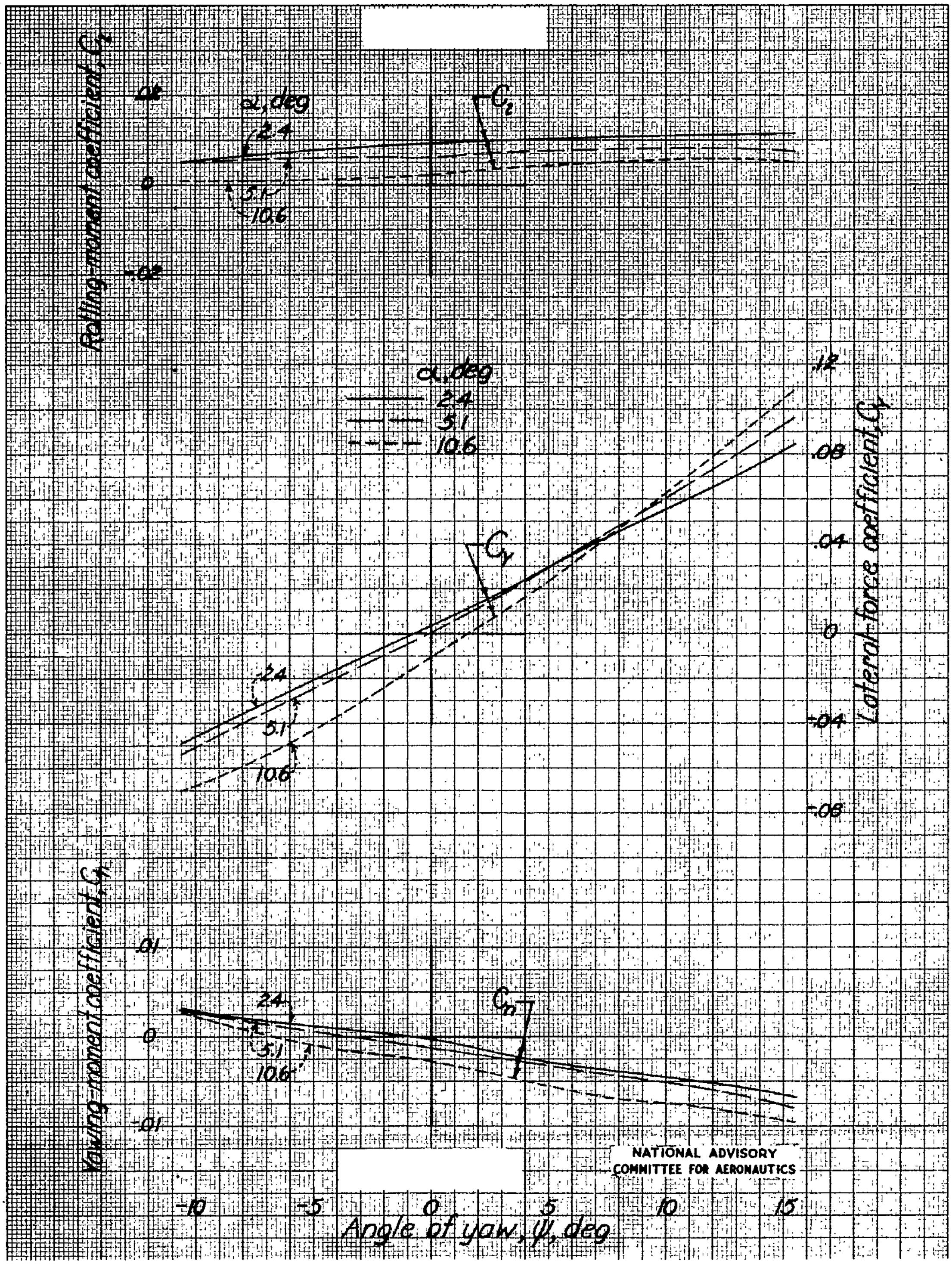

(b) Normal-rated power.

Figure 29.- Continued.

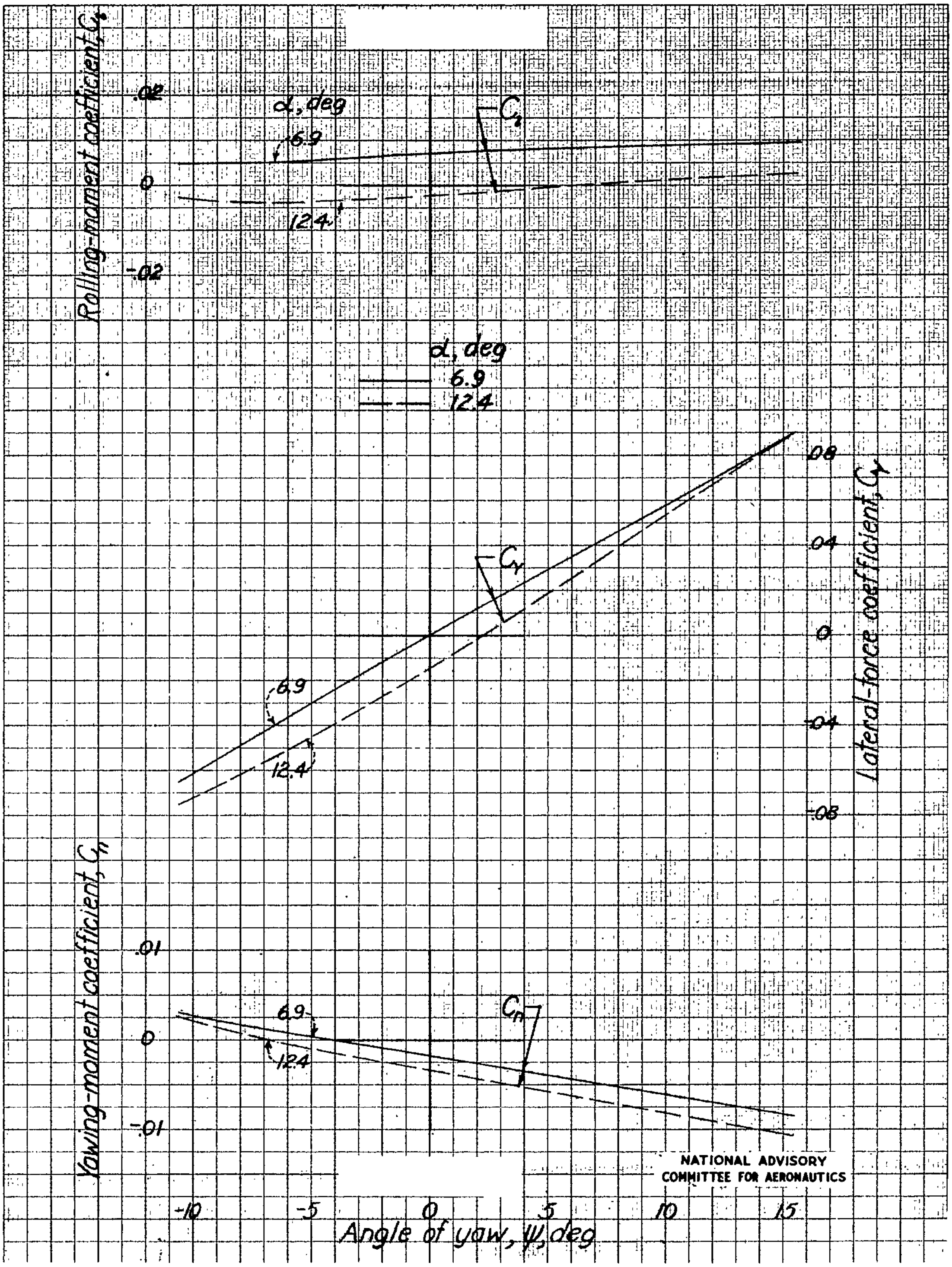

(c) Military-rated power.

Figure 29.- Continued.

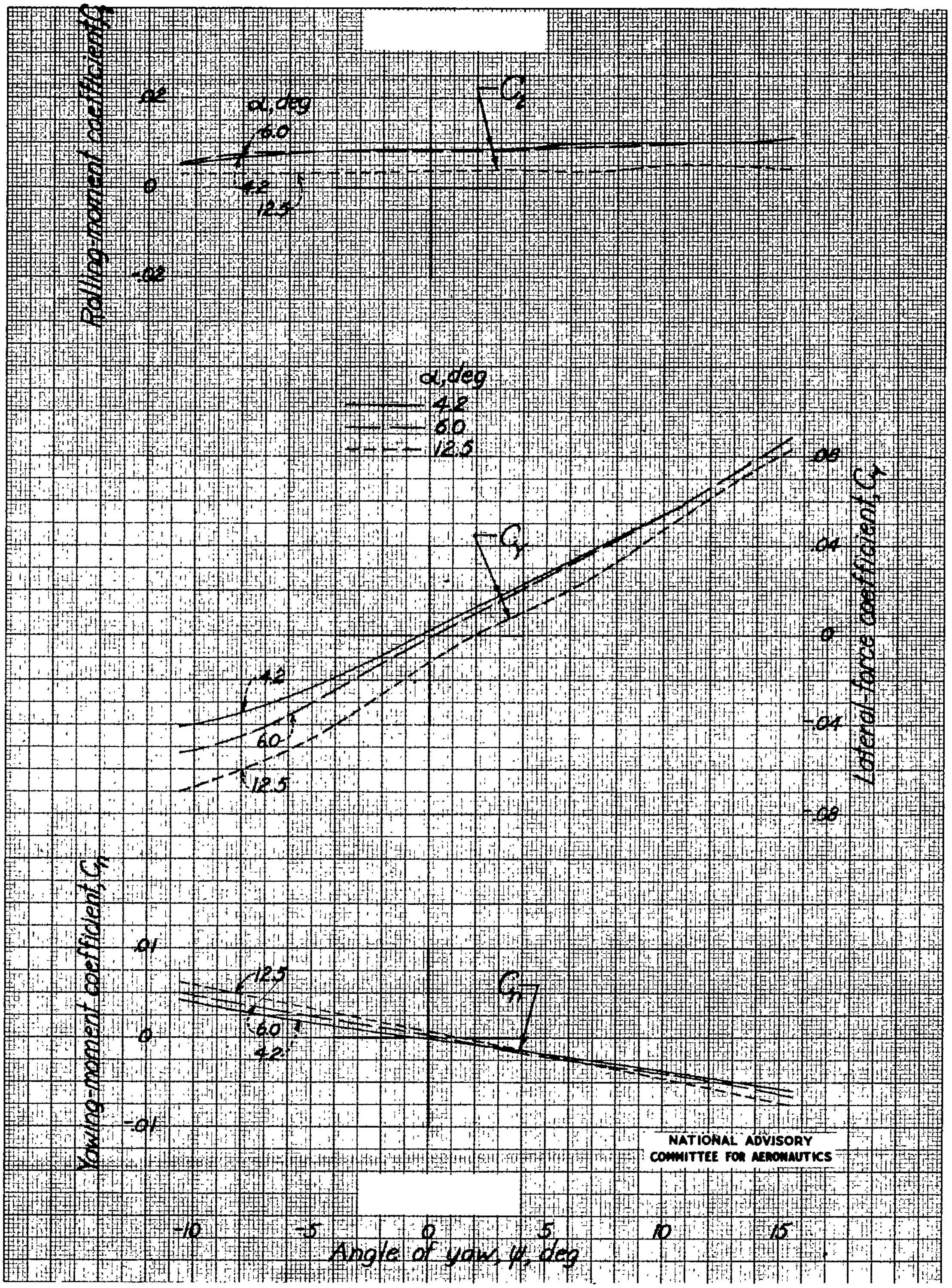

(d) Asymmetric power.

Figure 29.- Concluded.

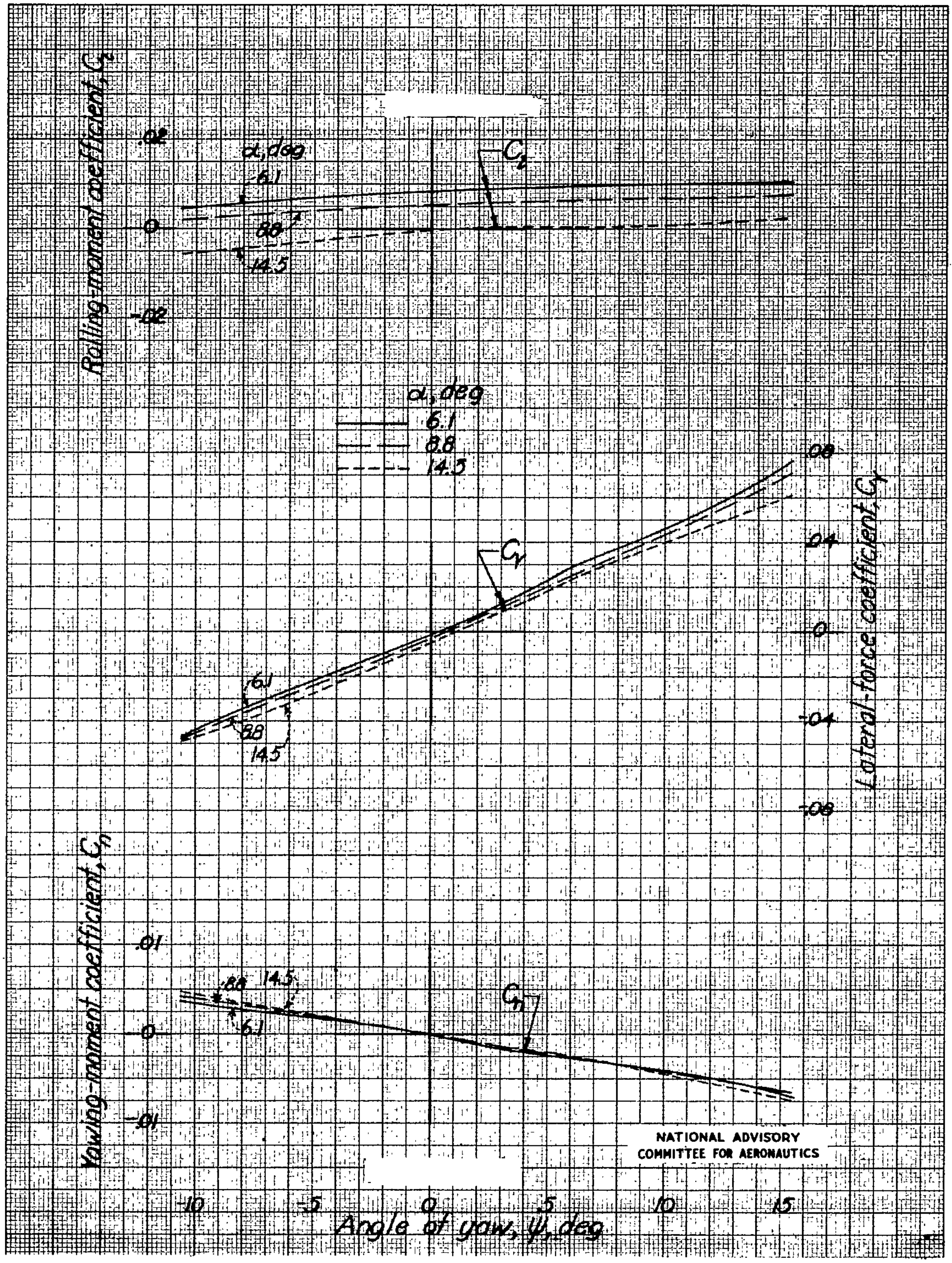

(a) Propellers windmilling.

Figure 30.- Variation of C_n, C_Y, and C_l for $C_{h_r} = 0$ with angle of yaw for varied power conditions. δ_a, 0°; δ_e, 0°.

L-531

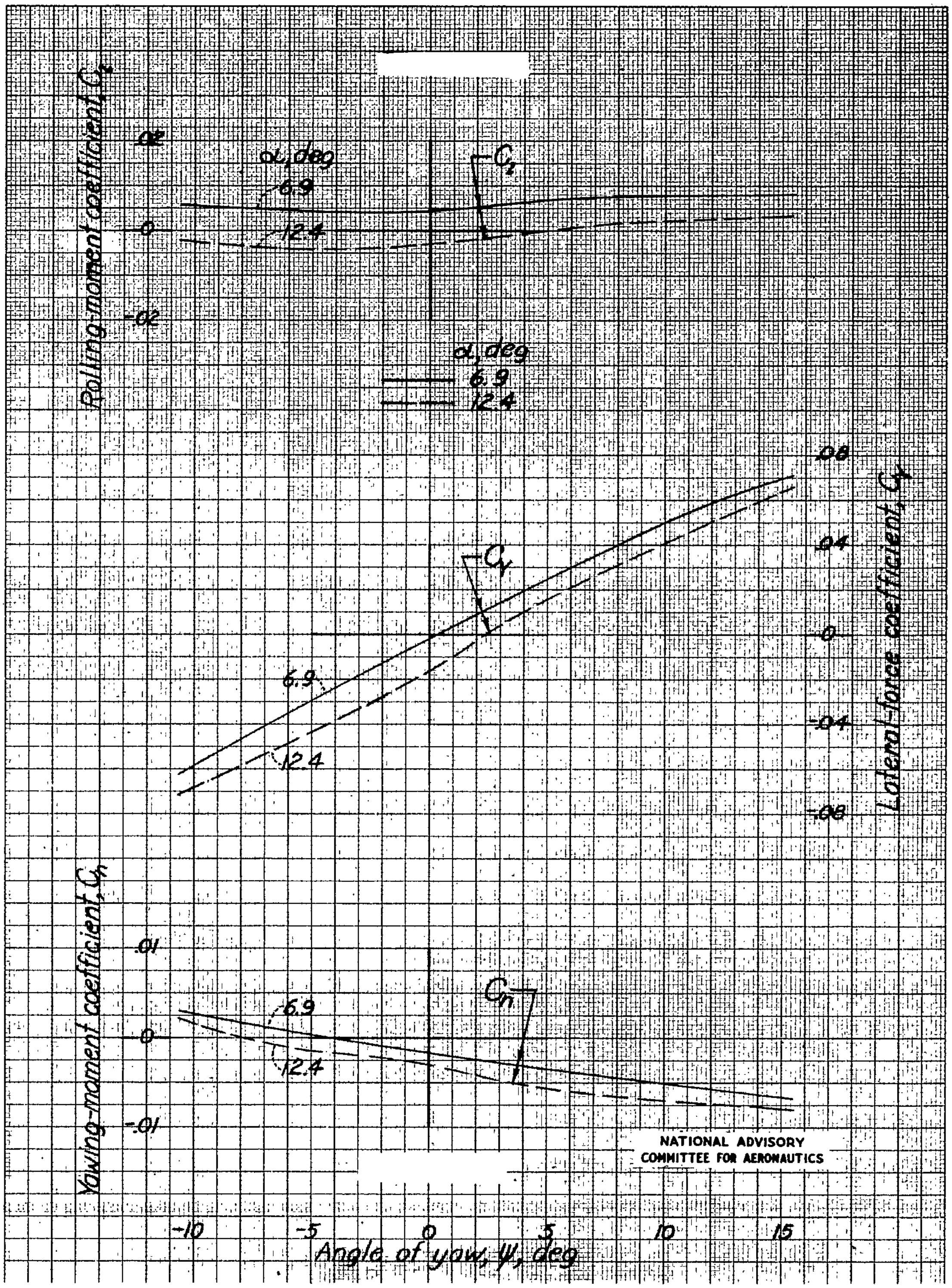

(c) Military-rated power.

Figure 30.- Continued.

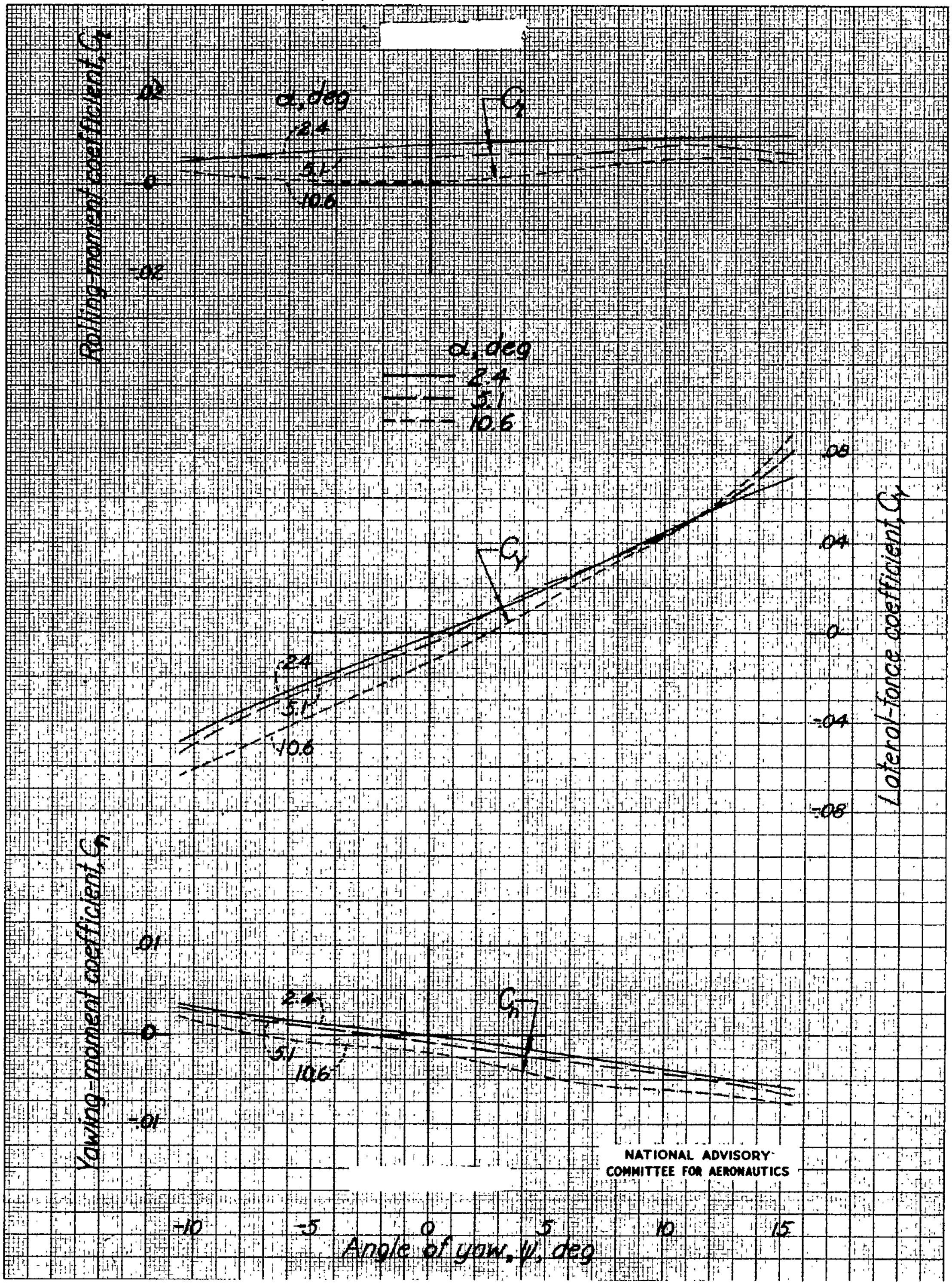

(b) Normal-rated power.

Figure 30.- Continued.

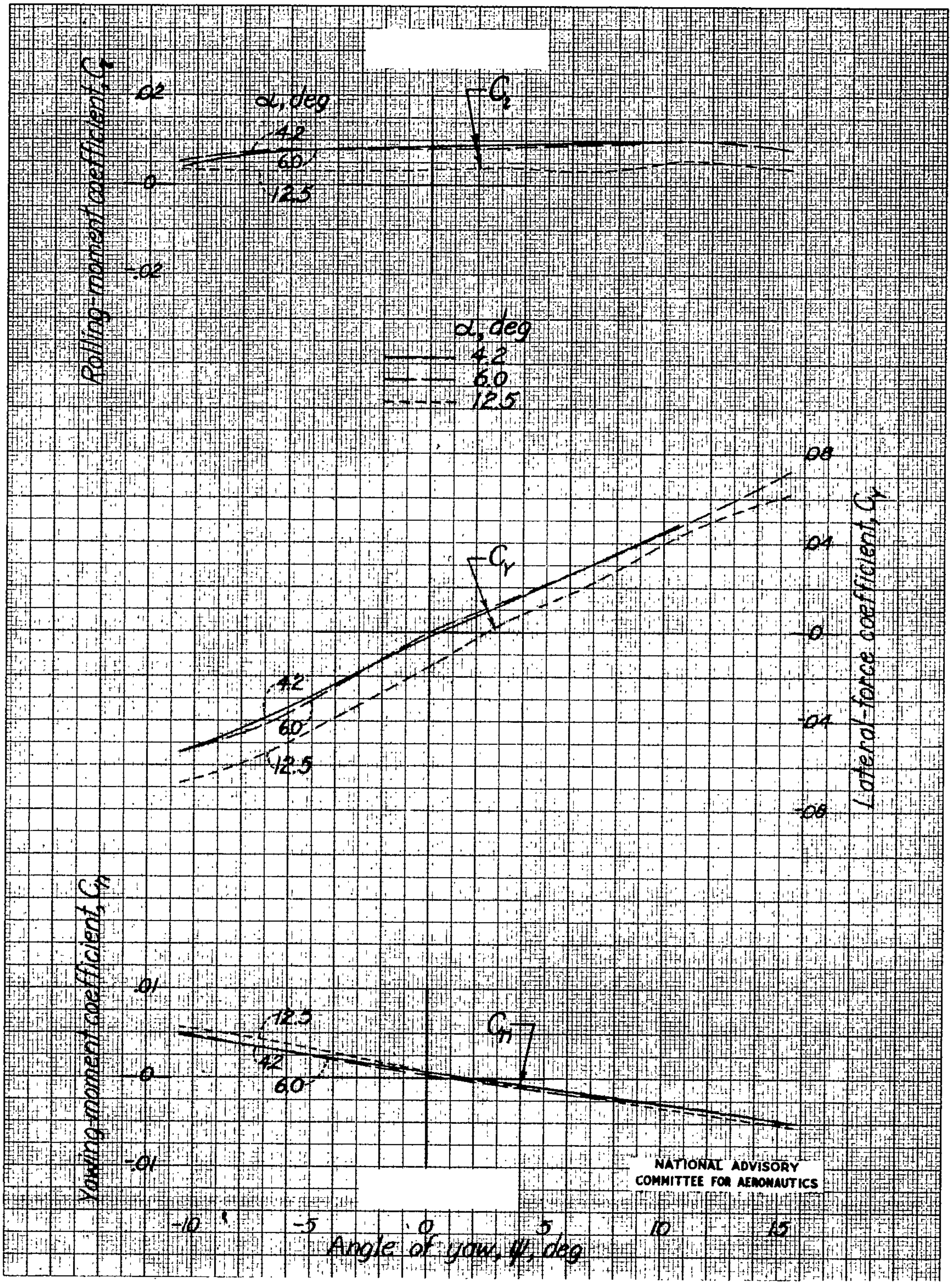

(d) Asymmetric power.

Figure 30.- Concluded.

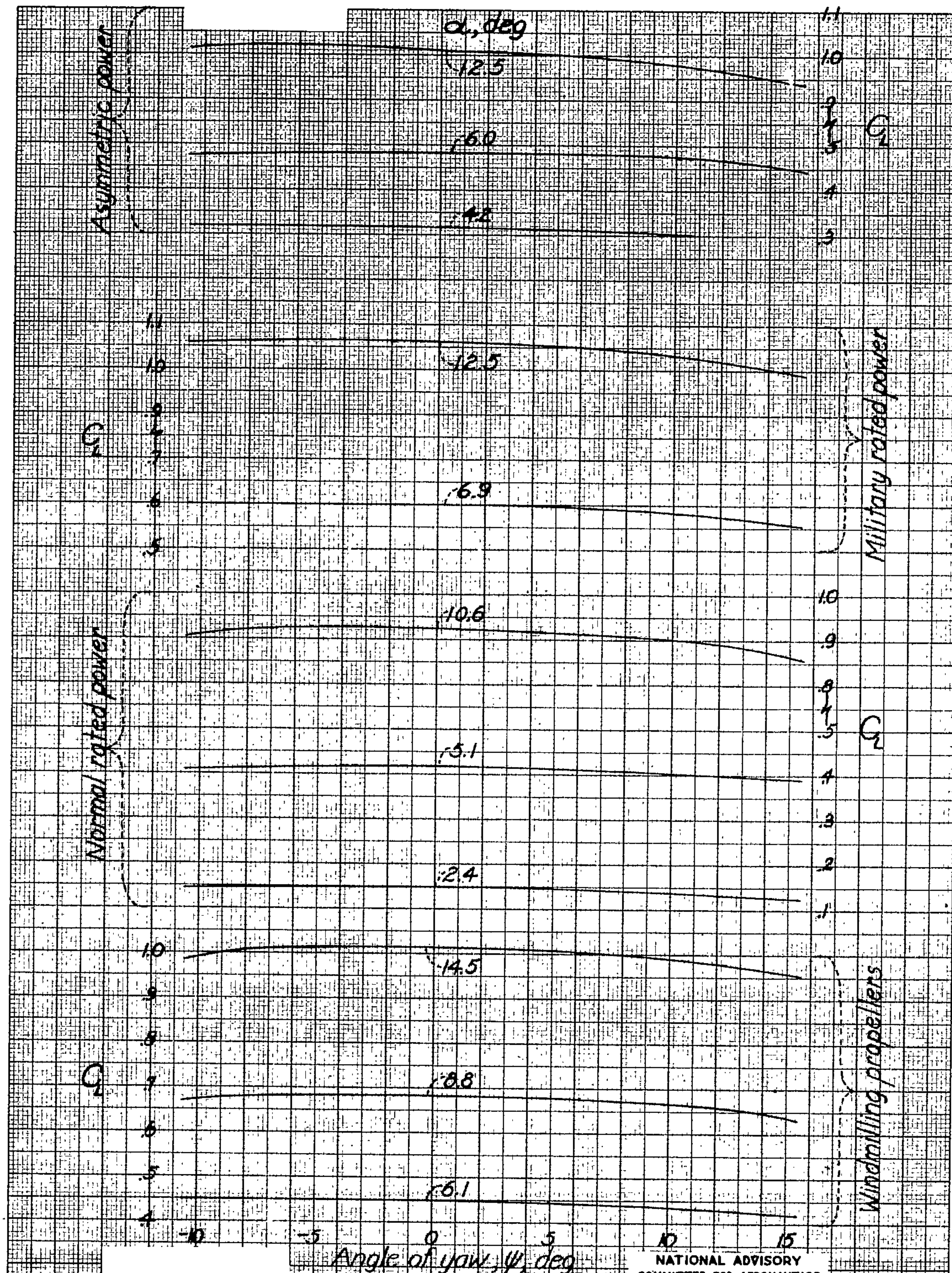

Figure 31.- Variation of lift coefficient with angle of yaw for a range of angles of attack and power conditions.